2011

The Development of Silver Nanoparticles as Antiviral Agents

John Christopher Trefry
Wright State University

THE DEVELOPMENT OF SILVER NANOPARTICLES AS ANTIVIRAL AGENTS

A dissertation submitted in partial fulfillment of the
requirements for the degree of
Doctor of Philosophy

By

JOHN CHRISTOPHER TREFRY
B.S., The Ohio State University, 2005

2011
Wright State University

AMERICAN CHEMICAL SOCIETY LICENSE
TERMS AND CONDITIONS

May 13, 2011

This is a License Agreement between John Trefry ("You") and American Chemical Society ("American Chemical Society") provided by Copyright Clearance Center ("CCC"). The license consists of your order details, the terms and conditions provided by American Chemical Society, and the payment terms and conditions.

All payments must be made in full to CCC. For payment instructions, please see information listed at the bottom of this form.

License Number: 2667130790220

License Date: May 13, 2011

Licensed content publisher: American Chemical Society

Licensed content publication: Journal of the American Chemical Society

Licensed content title: Size Selection and Concentration of Silver Nanoparticles by Tangential Flow Ultrafiltration for SERS-Based Biosensors

Licensed content author: John C. Trefry et al.

Licensed content date: Aug 1, 2010

Volume number: 132

Issue number: 32

Type of Use: Thesis/Dissertation

WRIGHT STATE UNIVERSITY

SCHOOL OF GRADUATE STUDIES

May 31, 2011

I HEREBY RECOMMEND THAT THE DISSERTATION PREPARED UNDER MY SUPERVISION BY John Christopher Trefry ENTITLED The Development of Silver Nanoparticles as Antiviral Agents BE ACCEPTED IN PARTIAL FULFILLMENT OF THE REQUIREMENTS FOR THE DEGREE OF Doctor of Philosophy.

Dawn P. Wooley Ph.D., Dissertation Director

Gerald M. Alter, Ph.D., Director, Biomedical Sciences Ph.D. Program College of Science and Mathematics and the School of Medicine

Andrew Hsu, Ph.D, Dean, School of Graduate Studies

Committee on Final Examination

Dawn P. Wooley, Ph.D.

Gerald M. Alter Ph.D.

Steven R. Higgins Ph.D.

Barbara E. Hull Ph.D.

Mill W. Miller Ph.D.

ABSTRACT

Trefry, John Christopher. Ph.D. Biomedical Sciences Ph.D. Program, Wright State University, 2011. The Development of Silver Nanoparticles as Antiviral Agents.

Silver nanoparticles (AgNPs) have received tremendous attention for their antimicrobial properties; however, many gaps in knowledge exist. To address these issues, three research objectives were examined. The first objective hypothesized AgNPs can be size selected and concentrated via tangential flow ultrafiltration. The second objective hypothesized a high-throughput method could be developed to screen nanoparticle antiviral-activity and cytotoxicity simultaneously. The third objective hypothesized AgNPs inhibit viruses by preventing viral entry.

For objective one, a tangential flow ultrafiltration scheme was tested on AgNPs synthesized via the Creighton Colloid method. AgNPs were analyzed via transmission electron microscopy. In objective two, an HIV-1 vector was adapted to 96-well format and modified to utilize 3-(4,5-dimethylthiazol-2-yl)-2,5-diphenyltetrazolium bromide (MTT) for simultaneous cytotoxicity and antiviral measurement. The third objective was investigated using *Vaccinia virus* (VACV). AgNP effects on VACV entry were monitored through β-galactosidase reporter assay and confocal microscopy. Western blots detected AgNP/VACV interaction. Plaque assays monitored AgNP inhibition over the entire VACV replication cycle. MTT and trypan blue exclusion measured AgNP cytotoxicity.

In objective one, tangential flow ultrafiltration demonstrated size selection and concentration of AgNPs. Filtered AgNPs were uniform and unaggregated with average 11 nm diameters. A high-throughput, standardized assay was developed in objective two. AgNPs had antiviral-activity at non-cytotoxic concentrations (IC_{50}=16 μg mL^{-1}). In the third objective, AgNPs prevented VACV entry in both cytoprotective and virucidal capacities at non-cytotoxic concentrations (IC_{50}=48 μg mL^{-1}). In the absence of macropinocytosis, AgNPs retained virucidal-activity but not cytoprotective effects. AgNPs bound to viral entry proteins. Plaque assays demonstrated that AgNPs inhibited the entire VACV replication cycle. Cytotoxicity assays demonstrated AgNPs were non-cytotoxic at antiviral concentrations.

Objective one's size selection and concentration method permits accurate investigation into nanoparticle antimicrobial activity by eliminating size and reagent incompatibility problems inherent to AgNP synthesis. In objective two, the traditional viral titering assay was replaced with a standardized assay measuring simultaneously antiviral activity and cytotoxicity, permitting faster and cheaper antiviral screening of nanoparticles. In the third objective, AgNP-mediated antiviral-activity was pinpointed to viral entry. Multiple mechanisms of entry inhibition were observed. These data suggest that AgNPs can be potent and broad-spectrum antiviral agents and therapeutics.

Table of Contents

Table of Contents Continued

Table of Contents Continued

Table of Contents Continued

List of Figures

List of Tables

Abbreviations

3-(4,5-dimethylthiazol-2-yl)-2,5-diphenyltetrazolium bromide (MTT)

50 nm ultrafiltered concentrate (50c)

50 nm ultrafiltered filtrate (50f)

100kD ultrafiltered concentrate (100c)

β-galactosidase (β-gal)

chlorophenol red β-D-galactopyranoside (CPRG)

colony-forming unit (CFU)

cytopathic effects (CPE)

entry fusion complex (EFC)

flame atomic absorption spectroscopy (FAAS)

Glycosaminoglycans (GAGs)

Hepatitis B virus (HBV)

Herpes simplex virus 1 (HSV-1)

Herpes simplex virus 2 (HSV-2)

Human immunodeficiency virus 1 (HIV-1)

hygromycin-B (Hyg)

inhibitory concentration 50% (IC_{50})

lethal dose 50% (LD_{50})

mature virion (MV)

Monkeypox virus (MPV)

multiplicity of infection (MOI)

multiplicity of nanoparticles (MON)

non-silencing control (NSC)

optical density (OD)

original (Ori)

p21 activated kinase 1 (Pak1)

plaque forming unit (PFU) (pfu)

polyvinylidene fluoride membrane (PVDF)

radio-immuno-precipitation-assay (RIPA)

reactive oxygen species (ROS)

rhodamine 6G (R6G)

Rhodamine B-isothiocyanate (RITC)

silver nanoparticles (AgNPs)

surface-enhanced Raman spectroscopy (SERS)

surface plasmon resonances (SPRs)

Tacaribe virus (TCRV)

tissue culture infectious dose 50% ($TCID_{50}$)

transmission electron microscopy (TEM)

ultracentrifuged pellet (Cpl)

ultracentrifuged supernatant (Csu)

UV-Vis absorption spectrophotometry (UV-Vis)

vaccinia immune globulin (VIG)

Vaccinia virus (VACV)

Vesicular stomatitis virus (VSV)

Western Reserve (WR)

CHAPTER I:

INTRODUCTION

Silver

Silver has been used for millennia as an antimicrobial agent. The Phoenicians used it to line pottery as it preserved potable goods stored within these containers (6). In Victorian England, silver salts were used in the treatment of sexually transmitted diseases and silver nitrate saw continued use as a disinfectant through the end of World War II (54). After the discovery of antibiotics, however, silver was relegated to very few uses as an antimicrobial agent. Antibiotics became preferable over silver salts because they were significantly less toxic to the host and more effective for systemic use (6).

Silver Nanoparticles

Due to the discovery of nanotechnology, silver is making a comeback in a variety of ways. Nanotechnology relies on the fabrication and manipulation of materials with at least one dimension between 1 and 100 nm. Having dimensions within this particular size window gives the material unique physical qualities. At this size, the material is too large to be considered on the atomic/ionic scale, yet far too small to be considered bulk material and, as a consequence, nanomaterials exhibit characteristics unlike their bulk or ionic counterparts. For example, nanomaterials exhibit less toxicity as compared to their ionic counterparts, yet they retain their antimicrobial activity. Compared to the bulk materials, nanoparticles exhibit greater antimicrobial effects.

In the case of silver nanoparticles (AgNPs), the unique characteristics associated with the nanotechnology size window are reviving interests in developing silver as an antimicrobial agent, in addition to more non-traditional applications. Having one dimension between 1 and 100 nm means “naked” AgNPs, those without surface modifications or capping agents, have an extremely large surface area to volume ratio, thus resulting in a very low coordination number and very highly polarized surfaces (67). Naked AgNPs bind to biological material non-specifically through their inherent need for steric and electrostatic stabilization as a result of their highly polarized surfaces and empty S orbital at its zero valent state (8, 46). Covalent bonds are thus easily established with complexes containing nitrogen (amines/protein), phosphorus (phosphates/DNA) and sulfur (thiols/protein) being common electron donors (8).

The physical traits of AgNPs can be fine-tuned using different methods to fabricate AgNPs. Each method can impart different sizes, shapes, and surface elements, which change AgNP reactivity (14, 50). There are many methods of AgNP synthesis, but these methods can be broadly classified as wet or dry processes. One of the earliest examples of wet AgNP synthesis can be found in medieval cathedrals that contain stained glass. Although historic stained glass makers were unaware, their reduction of silver salts created AgNPs. Different reduction techniques created AgNPs of different sizes and thus different colors due to a property called Surface Plasmon Resonance (26). Modern wet synthesis techniques rely on the same basic properties with much greater precision. For example, the Creighton Colloid Synthesis method, in which sodium borohydride is used to reduce silver nitrate into AgNPs in a water matrix, is one of the most common methods

in use (30). Wet synthesis methods are commonly referred to as “bottom-up” synthesis methods because AgNPs are constructed atom by atom through a nucleation process.

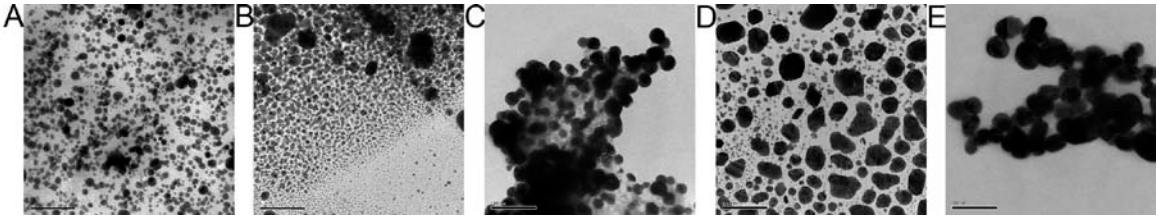

Figure 1. Preliminary characterization of different AgNPs. Each frame is a sample of many images taken to characterize the AgNPs. Bar = 100 nm. A) Commercially available bottom-up biosynthetic AgNPs with low concentration, high aggregation and high polydispersity. B) Ultraviolet radiation-based bottom-up AgNP synthesis with high polydispersity and very low concentration C) “50 nm” commercially available top-down synthesis AgNPs with high aggregation and possible stabilizing agent contamination D) “80 nm” commercially available top-down synthesis AgNPs with high polydispersity and amorphous shapes. E) “10 nm” commercially available bottom-up synthesis AgNPs with observed aggregation and average 60 nm in diameter, not the advertised 10 nm.

Dry synthesis methods of creating AgNPs are typically referred to as “top-down” methods because they involve breaking down bulk silver into AgNPs. One common method used today is laser ablation, where lasers are pulsed on a bulk piece of silver to break down the large starting material into AgNPs. With current manufacturing techniques, AgNPs synthesized in either a wet or dry synthesis demonstrate a high level of polydispersity (16). This polydispersity was documented in preliminary data acquired from transmission electron micrographs and subsequent particle analysis from a variety of AgNP synthesis methods (Figure 1). These commonly used AgNP synthesis methods were found to be too low in concentration, have high levels of polydispersity, have high levels of aggregation and/or have highly amorphous shapes as evidenced by the images

above (Figure 1). Each of these factors presents a problem in controlling effects of AgNPs on a biological system. The AgNPs sampled in the preliminary characterization were commercially available or synthesized "in-house" in efforts to find small, naked, uniform, and monodisperse AgNPs for studies involving their antiviral properties. None of the AgNPs in Figure 1 met these criteria. However, one commercially available AgNP preparation, NovaCentrix 25 nm AgNPs, was small, uniform and monodisperse, so it was chosen to carry out the research in Chapters III and IV while a technique to address the polydispersity present in other commercially available and "in-house" AgNP preparations is addressed in Chapter II.

Currently, commercially available AgNPs are produced, through both wet and dry synthesis methods, and licensed for use in consumer products at an exponential rate. Applications utilizing AgNPs have multiplied over 1,000% since 2006, with AgNPs representing 313 of the 1317 licensed nanotechnology products (73). Most of the commercial applications for AgNPs are antimicrobial. For example, AgNPs are commercially available as preservatives (*i.e.* clothing and cosmetics), medical devices (*i.e.* coatings for catheters and wound dressings), and as water treatment agents with no defined mechanisms for their antimicrobial properties (21).

Common to all AgNP synthesis methods is the problem of generating a uniform set of AgNPs, as shown in Figure 1 and discussed in the literature (16). Eliminating AgNP polydispersity has been shown to increase its antimicrobial properties, possibly as a consequence of increasing surface area and thus AgNP reactivity (3, 6). Current technologies using both wet and dry synthesis methods produce AgNPs with a broad size distribution, meaning the standard deviation of particle diameters is greater than 30% of

the average diameter measurement (14). To correct for this problem, many of the techniques used to produce AgNPs have been adapted to use additional materials during AgNP synthesis that function to restrict particle size to a narrow distribution in the final product. Examples of common additional agents, referred to as capping agents or stabilizers, added to naked AgNPs, are polyvinylpyrrolidone, citrate and polyethylene glycol. These agents have been proven biologically compatible; however, they posses their own antimicrobial properties, which would make the identification of inherent AgNP antiviral activity difficult (6, 39). These capping agents may even enhance toxicity to host cells by allowing greater distribution of AgNPs in tissues, extending their half life within the host cell or organism, or enhancing AgNP surface charges and reactivity to augment cytotoxicity over "naked," un-capped AgNPs (1, 22). Other organic and chemically aggressive reagents currently used to control AgNP size, shape and dispersity are incompatible with biological systems precluding their use in the manufacture of antimicrobial agents (14, 50, 59, 60). To overcome the limitations of current AgNP synthesis techniques and further investigate AgNPs as antimicrobials, a method of purifying, size selecting, and concentrating naked nanoparticles is needed.

Silver Nanoparticles as Antiviral Agents

Very few drugs are approved as therapies for viral infection. Most of the approved drugs are specifically designed for one species of virus and would not work in a broad-spectrum capacity. The most common examples of these types of drugs are the nucleoside analogs specific for Herpes virus infection and the neuraminidase inhibitors available for Influenza virus infection. While extremely effective, these drugs require the accurate identification of invading virus before prescriptions can be filled (45). Also

associated with these drugs is an emerging pattern of antiviral drug resistance due to the specificity in their mechanisms of action and natural selection for resistant strains (9, 56). The pattern of antiviral drug resistance is most exemplified by chronic infections with *Human immunodeficiency virus* 1 (HIV-1) and Hepatitis viruses. Current HIV-1 therapy, highly active anti-retroviral therapy, utilizes multiple drugs to specifically inhibit different proteins in viral replication such as the viral protease, reverse transcriptase and integrase. Even with multiple targets, resistant viral strains still emerge due to the high mutation rate of HIV-1 and the resultant mutants resistant to the specific inhibitors (9). For Hepatitis virus infection, treatments were designed using broad-spectrum, non-specific inhibitors in hopes to waylay the development of drug resistance. Interferon α, an innate immunity protein responsible for generating antiviral responses in the body, and Ribavirin, a suspected nucleoside analog, are used in conjunction for the treatment of Hepatitis C virus infection (10, 13). These drugs are broad-spectrum antivirals but they are not without their shortcomings. Interferon α therapy is associated with flu-like symptoms, hepatotoxicity, depression, and overtime interferon resistance (13). Ribavirin is a purine analog, not found in nature, originally synthesized in 1970. A wide range of RNA and DNA viruses have demonstrated susceptibility to Ribavirin despite the unknown mechanism(s) of activity. Ribavirin therapy has shown less instances of resistance but it is also associated with high levels hemotoxocity, differences in viral species/strain tolerance levels, and is a documented tetratogen (10). A new, broad spectrum antiviral therapy, with no existing viral resistance is desperately needed (56).

The best defense available to viral infection was, and still is, vaccination. However, vaccination may not be possible in cases of emerging infectious diseases, the

deployment of biological weapons, diseases that have proven difficult for development of vaccines, and the continued antigenic drift that can render current vaccines useless (9). Vast amounts of time and resources are required to identify viruses and generate vaccines with the best protection generated from pre-exposure prophylaxis (36). When a vaccine is unavailable one could rely on the use of the previously mentioned drugs; however, due to their specificity or associated toxicity, an accurate diagnosis must be made which takes time. A true broad-spectrum antiviral agent, effective against many viral species/strains, that does not require a diagnosis is greatly needed in the antiviral agent arsenal.

The antimicrobial properties of AgNPs have been evaluated for a wide range of bacteria, viruses, and fungi (6, 53, 55). Various mechanisms for the antimicrobial properties of AgNPs have been proposed; most of these mechanisms are based on the suggested mechanisms for silver ion toxicity due to the same elemental composition of AgNPs and Ag+. These proposed mechanisms include reactive oxygen species (ROS) production, disruption of membrane potential, depletion of intracellular ATP, inactivation of proteins, DNA damage and the production of silver ions from the AgNP surface, which would then mediate the previously listed mechanisms (53, 55). However, each of these mechanisms has been suggested based on evidence from AgNPs with different characteristics such as size, shape, capping agent, and level of dispersity. No solidly defined mechanism for AgNP antimicrobial activity is currently available.

This manuscript will focus on the antiviral aspects of AgNPs. Very little is known concerning the mechanisms by which AgNPs exert their antiviral properties. However, AgNPs have demonstrated antiviral activity against a number of viruses for both prokaryotic and eukaryotic organisms, making them a true broad-spectrum antiviral

agent. Inhibition of infection by AgNPs has been well documented for the UZ1, MS2 and M13 bacteriophages (4, 21, 34, 68). The eukaryotic pathogens HIV-1, Herpes simplex virus 1 (HSV-1), Herpes simplex virus 2 (HSV-2), Monkeypox virus (MPV), Hepatitis B virus (HBV) and Tacaribe virus (TCRV) have also demonstrated a susceptibility to AgNPs (4, 23, 32, 35, 49, 57, 58). Such broad ranges of susceptible viral species indicate that AgNPs are an ideal candidate to be developed as a broad-spectrum antiviral agent.

In each case of viral inhibition there has been documentation of a dependence on AgNP size for antiviral activity. One such study demonstrated that only small AgNPs, of 25 nm or less, were able to bind to the external membrane glycoprotein 120 knobs of HIV-1, which are responsible for receptor binding (23). The mechanism for this inhibition was proposed to be prevention of HIV-1 entry into the host cell based on observations that AgNPs prevented syncytia formation, a late stage indicator of HIV-1 infection.

Additional studies indicated that early infection might be the general time frame where AgNPs exert their antiviral activity which then impacts the rest of the viral replication cycle. AgNPs are able to prevent HIV-1 CD4/gp120 mediated cell fusion, indicating that AgNPs have the potential to inhibit virus entry; however, this study was performed in a HIV-1 free manner where CD4 and gp120 were over-expressed in target cells (32). HBV virus-like particles with bound AgNPs were also directly observed via transmission electron microscopy (35). Furthermore, AgNPs inhibited MPV and HSV-2 infection as determined by plaque assay, a measurement that includes the entire viral replication cycle (49, 57). TCRV inhibition by AgNPs was observed via quantification of progeny genomes, an endpoint that encompasses the entire replication cycle of the virus

(58). Generally, smaller AgNPs, less than or equal to 25 nm, have demonstrated the greatest antiviral potential. Furthermore, each study suggested that early steps in the infection process are the likely general time point for AgNP-mediated antiviral activity. However, a precise mechanism of AgNP antiviral activity and precise stage of infection at which AgNPs exert antiviral activity have yet to be determined. If a mechanism(s) could be identified, further studies are possible regarding the antiviral development of AgNPs to fill the vital niche of a broad-spectrum antiviral agent.

Mechanisms suggested for the antibacterial effects of AgNPs, such as ROS production, disruption of membrane potential, depletion of ATP and DNA damage, are downstream, long-term events that require an active metabolism that is not present in viruses. Silver ion leaching, the suggested mechanism by which the antibacterial activities occur, as a method of antiviral activity is unlikely as all leached ions would quickly complex with free chlorine ions in the cellular growth medium (17). Furthermore, Navarro *et al.* demonstrated that less than 1% of the silver in culture media containing AgNPs was in the ionic form after 8 days of AgNP exposure to a synthetic growth medium (41). While the previously mentioned mechanisms might affect host cells, these mechanisms are unlikely to be the cause of early viral infection inhibition due to the long exposure times required for these events. The most likely mechanism of antiviral activity, as suggested by the literature, is AgNPs binding to viral or host proteins and inactivating or decreasing their function at an early stage of infection.

With no specific time point identified as the target of AgNP-mediated antiviral activity, more precise and mechanistic studies of where and when AgNPs exert their antiviral activity are necessary. Additionally, new methods of examining AgNP-mediated

antiviral activity are in great need. Traditional antiviral testing methods such as plaque assays are subjective and costly due to the personnel and resources required. High-throughput methods of detecting antiviral activity are also currently unable to distinguish between antiviral effects, cytotoxicity and inherent characteristics of AgNPs that may interfere with automation, such as surface plasmon resonances. Furthermore, these assays measure the entire course of viral infection so, if viral inhibition is recorded, there is little to no indication of how or when this inhibition might occur.

It is critical that new methods of producing and screening for antiviral activity of AgNPs be developed because AgNPs could have significant benefits over traditional antiviral agents. Because they are a metal they are resistant to extremes in temperature, unlike current antiviral agents and vaccines that require temperature regulation. This resiliency could also favor multiple methods of deployment, oral, inhalation, topical application and even possible injection. Since AgNPs' proposed mechanism of antiviral activity is non-specific binding of biological molecules such as proteins, theoretically all known viral species would be susceptible since no known viral species is devoid of protein. While cellular proteins would also be impacted by AgNP binding, viruses could be uniquely susceptible to AgNP binding as they are unable to regenerate damaged proteins. The broad-spectrum activity of AgNPs would be useful for those situations were a treatment is needed prior to a diagnosis being made or in the absence of a working vaccine (9, 45). Traditional antivirals are demonstrating a fast emerging resistance, but since the proposed mechanism of AgNP antiviral activity is interaction with viral proteins, the probability of AgNP resistant viruses developing is low.

Silver Nanoparticle Cytotoxicity

In addition to the studies performed concerning antimicrobial activities of AgNPs, there is a growing body of research concerning their toxicity. Drawing specific conclusions from sources of literature concerning the general toxicity of AgNPs is difficult. Most studies utilize different sets of AgNPs with differences in size, shape, surface elements, distribution, and synthesis methods with poor particle characterization being a common issue. Differences in AgNP characteristics can cause markedly different reactive properties, especially in biological systems (40). *In vitro* cytotoxicity values for lethal dose 50% (LD_{50}) in the literature range from 0.7 μg mL^{-1} to greater than 449 μg mL^{-1} with no LD_{50} values reached for *in vivo* studies (2, 31). These differences in the literature make the question of AgNP toxicity a difficult one to answer. A precise mechanism responsible for AgNP cytotoxic observations has not been proposed due to the lack of standard assays to accurately assess AgNP cytotoxicity and the lack of experimental controls that exclude possible contamination of AgNPs with the toxic chemicals used in their synthesis. Gaps in knowledge surrounding AgNP cytotoxicity are critical questions to address in the development of a broad-spectrum antiviral agent as they could potentially mask antiviral activity.

Viral Vectors

Viral vectors offer a unique platform upon which the antiviral activity of a material such as AgNPs might be examined. At their most basic level, viral vectors are tools for delivering genetic information into a host cell (24). What makes a viral vector different from a wild type virus is its genetic modification to render the virus replication deficient. This modification allows the virus to successfully infect a cell and deliver its

genetic payload, but prevents the virus from reproducing. This functionality could be adapted to test AgNPs and other nanomaterials for antiviral activity in high-throughput fashion by determining whether or not AgNPs prevent the previously mentioned genetic transfer, a measure of infection.

The most popular viral vector system is based on the Lentivirus HIV-1 (24). HIV-1 is a single stranded RNA virus of the family *Retroviridae*. Typical wild type infection with HIV-1 follows classical type I viral entry kinetics via specific virus/host interaction at the plasma membrane of the cell, followed by the reverse transcription of viral RNA and subsequent integration of proviral DNA (18). At this point the transcription of proviral genes may then facilitate the production of progeny virions. In the viral vector system, the genes required to produce progeny virions are not incorporated into the viral genome, instead they are replaced with the genes to be delivered to the host cell. Additionally, the specific HIV-1/host cell interaction required for wild type viral infection is replaced by a viral receptor of choice. This envelope protein replacement permits the production of viral vector particles that can simulate the infection of many different viral species simply by utilizing their envelope proteins responsible for entry. For example, a common envelope protein replacement for an HIV-1 vector is the switch from HIV-1 wild type gp120 envelope protein to the Vesicular stomatitis virus G glycoprotein (28). This swap confers broad tropism onto the vector virions instead of the gp120/CD4 specific reaction of wild type HIV-1, which limits tropism to only those cells expressing CD4 and appropriate co-receptors. The ability to simulate many different viral species by interchanging the viral entry proteins would be a standardizing measure that would greatly benefit a screening assay for nanoparticle antiviral activity.

Vaccinia Virus

As a result of the bioterrorism attacks in 2001, the Department of Health and Human Services has named broad-spectrum antimicrobial discovery and development a top priority (66). The National Institute of Allergy and Infectious Disease also lists discovery and development of therapeutics for Category A pathogens a top priority. *Variola major*, an Orthopoxvirus and the causative agent of smallpox, is a Category A pathogen and a growing concern for use in a potential biological weapon due to decreased population immunity as a result of the cessation of vaccination.

Study of *Variola major* virus is highly restricted to only one location within the United States. However, an accurate analog for the study of *Variola major* is available in the form of the virus used as the vaccine for smallpox, *Vaccinia virus*. *Vaccinia virus* (VACV), also an Orthopoxvirus, is similar enough to *Variola major* that exposure to VACV offers immunity to *Variola major*. Due to their similarities, VACV has become the gold standard for research on Orthopoxviruses and also for this reason, would make a great system for the development of a rapid-response antiviral agent in the event of the re-emergence of smallpox or the emerging disease monkeypox.

VACV is a double stranded DNA virus of about 200 kb. VACV replicates solely in the host cell cytoplasm. The large genome encodes almost all of the structural proteins and enzymes required to complete its replication process (19).

The infection process typically begins with VACV adsorption to the membrane of a permissible host cell (Figure 2). This binding to the cell surface is accomplished through VACV membrane proteins A27 and H3, D8, L1 and A26, which bind heparan sulphate, chondroitin sulphate, and laminin respectively (15, 25, 27, 33, 47, 70). At this

stage in the infection process the virion is bound to the cell surface but entry has not yet occurred.

There are discrepancies in reports on the process of adsorption. Observations exist for strain differences at the adsorption step prior to VACV entry into the host cell. Certain strains, IHD-J, Elstree, and Copenhagen, show a high level of dependence on the presence of glycosainoglycans (GAGs) such as heparan sulphate, while other strains, such as Western Reserve (WR) and Wyeth, show tolerance to the absence or interference of cellular binding factors (5). Non-GAG dependent adsorption may occur through laminin or could be completely bypassed by virions contacting the vesicle membrane as a result of a macropinocytotic mechanism. This variation in viral adsorption makes VACV an ideal candidate for the development of a broad-spectrum viral entry inhibitor.

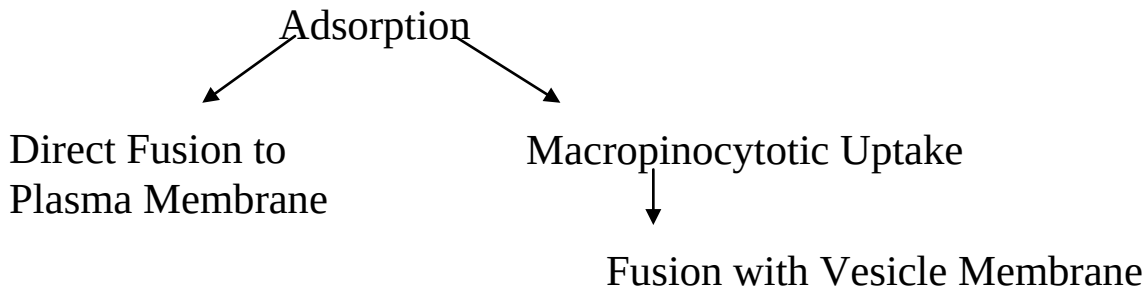

Figure 2. Ouline of VACV Infection. VACV once absorbed to its host cell can proceed via two routes to gain access to the host cell cytoplasm. As indicated above these methods are either direct fusion to the plasma membrane or macropinocytotic uptake, followed by fusion with the macropinocytotic vesicle.

VACV entry is dependent on a set of entry fusion complex proteins. Entry of VACV via the entry fusion complex (EFC) has been demonstrated at both neutral and low pH corresponding to direct fusion and macropinocytosis-dependent fusion respectively. These differences demonstrate that VACV is capable of two distinct entry

methods (7, 52, 69). Identified as a complex of proteins, the EFC is composed of A16, A21, A28, F9, G3, G9, H2, I2, J5, L1, L5, and O3 with nine out of twelve of these proteins considered integral members of the EFC as their disruption or removal destabilizes the complex (7, 11, 29, 42, 43, 43, 44, 51, 62, 63, 65, 72). The EFC proteins are highly conserved among all poxviruses and mutation of any of these components yields non-infectious virions (52). The stoichiometry of the complex and its precise mechanism of action have yet to be classified or determined (71). The EFC is theorized to be the facilitator of virion membrane fusion with the host cell membranes for both methods of VACV entry.

Entry into the host cell is broadly characterized as the delivery of the virion core to the cytoplasm, regardless of how the virions are adsorbed or gain access to the host cell cytoplasm. The viral core comes equipped with all the enzymes necessary to begin early transcription (48). Once the viral core has entered the cytoplasm it immediately begins to transcribe early genes (12). This process has been well documented and is easily assayed within the first 6 hours of VACV infection via β-galactosidase expression driven by a constitutive early/late promoter (29, 70).

One mode of VACV entry is acid mediated and dependent on viral uptake into a macropinocytotic vesicle. VACV entry through macropinocytosis has been proposed based on evidence that low pH treatment of bound VACV increased entry ten-fold (64). Electron microscopy has also demonstrated VACV occupying macropinocytotic vesicles (20). Furthermore, inhibitors of acidification drastically reduce VACV entry (61, 64). Also, an 83% reduction in viral entry has been observed upon dominant negative expression of Pak1, a vital component of macropinocytosis. Without this component

there is little to no macropinocytotic uptake of virions, and the virus is not exposed to the acidic environment of the macropinosome. The decreased infectivity as a result of Pak1 inactivation was recovered by brief acid-buffer treatment of virions attached to the surface of the cell, supporting Pak1's role in mediating macropinocytosis and VACV's macropinocytosis-dependent fusion upon exposure to the low pH environment of the macropinosome (37).

The other mode of VACV entry is direct fusion with the plasma membrane. This method of entry has been shown experimentally by VACV indifference to a variety of endosomal acidification inhibitors (64). Furthermore, direct observation via electron microscopy has shown that strains WR and Modified Ankara Virus fuse directly with the plasma membrane (15). Also, viral membrane proteins examined via transmission electron microscopy after immuno-labeling were found to be part of the plasma membrane immediately after core delivery (47). This finding is indicative of the viral membrane, and its incorporated proteins, fusing with the plasma membrane without macropinocytotic uptake.

Based on the evidence, it seems the preferred entry method, like adsorption method, varies from strain to strain and that each strain is capable of utilizing both methods of entry to a certain extent. Viral strains that are highly dependent on GAGs for adsorption could compensate by using Laminin for adsorption or instead depend more on direct fusion with the plasma membrane. Generally, VACV strains that are tolerant to a lack of cellular attachment factors generally depend more on macropinocytotic uptake. However, WR, a popular research strain, has been observed directly fusing with the plasma membrane, while other reports claim this strain is dependent on macropinocytotic

uptake for subsequent entry into the cell cytoplasm (15, 38, 64). This discrepancy could be the result of cell type dependent entry but suggests that this viral strain uses both entry methods to gain access to the host cell cytoplasm. The ability to enter cells in a variety of methods makes VACV an ideal candidate for the development of a broad-spectrum antiviral agent.

Research Objectives and Rationale

In order to address the previously mentioned gaps in knowledge surrounding the biological applications of AgNPs, three research objectives were identified. Each objective was designed around a central hypothesis. Furthermore, each objective's hypothesis was investigated via a set of specific aims designed to fully explore the gaps in knowledge of each respective field.

The first objective hypothesized that highly concentrated, highly homogenous, non-aggregated AgNPs can be size selected and concentrated via tangential flow ultrafiltration. This hypothesis manifested from the lack of accurate methods capable of producing AgNPs free of contaminants from their synthesis, with limited polydispersity and without the use of capping or stabilizing agents. To test this hypothesis specific research aims were established.

The first aim sought to develop a tangential flow ultrafiltration scheme capable of size selecting and concentrating AgNPs synthesized via Creighton method. This aim addressed the issues surrounding the production of AgNPs with limited polydispersity in the absence of capping or stabilizing agents that may interfere with the use of AgNPs as antimicrobial agents. The second aim examined the relative size selection and concentration effectiveness between the newly developed tangential flow ultrafiltration

scheme and the commonly used ultracentrifugation method for the size selection and concentration of AgNPs.

The development of more precise and higher-throughput methods for examining the antiviral activity of AgNPs was the focus of the second research objective. Because traditional plaque assays are subjective and require large amounts of time and money, a quicker high-throughput format for screening antiviral activity is desirable. Additionally, current techniques rely on performing cytotoxicity assays separately from the antiviral testing. This separation can result in the masking of antiviral activity by cytotoxicity. This objective also addressed the need for standardization of antiviral testing between viral species, since current methods require separate assays for different viral species.

To address the issues surrounding the second objective, three research aims were developed. The first aim sought to adapt a large scale screening technique for HIV-1 mutation rate, utilizing a viral vector system, to a small-scale, high-throughput format designed to assess viral titer. Aim two of this objective characterized the ability the novel assay format to accurately assess viral titer compared to the original colony forming unit assay. The third aim of the second objective was to determine the assay's ability to simultaneously chart antiviral activity and cytotoxicity.

The third objective hypothesized that AgNP mediated antiviral activity was the result of AgNPs preventing viral entry. This objective would pinpoint the stage of viral infection at which AgNP antiviral activity occurs and illuminate possible mechanisms behind this inhibition, a vital gap in knowledge concerning AgNP antiviral activity. VACV was chosen as the viral system to examine AgNP-mediated antiviral activity and

its possible mechanisms due to the call to research by various governmental agencies and the growing concern for the use of *Variola major* as a potential bioweapon.

The third objective's hypothesis would be investigated through three specific aims. The first aim sought to investigate the effects of AgNPs on the adsorption of VACV to host cells. Determination of AgNP effects on overall VACV entry was addressed in the second aim of this objective. Finally, the third aim examined the effects of AgNPs on the direct fusion entry pathway of VACV, in the absence of macropinocytosis.

REFERENCES

1. **Allen, H. J., C. A. Impellitteri, D. A. Macke, J. L. Heckman, H. C. Poynton, J. M. Lazorchak, S. Govindaswamy, D. L. Roose, and M. N. Nadagouda.** 2010. Effects from filtration, capping agents, and presence/absence of food on the toxicity of silver nanoparticles to Daphnia magna. Environ. Toxicol. Chem. **29:**2742-2750. doi: 10.1002/etc.329; 10.1002/etc.329.

2. **Arora, S., J. Jain, J. M. Rajwade, and K. M. Paknikar.** 2009. Interactions of silver nanoparticles with primary mouse fibroblasts and liver cells. Toxicol. Appl. Pharmacol. **236:**310-318. doi: 10.1016/j.taap.2009.02.020.

3. **Asharani, P. V., M. P. Hande, and S. Valiyaveettil.** 2009. Anti-proliferative activity of silver nanoparticles. BMC Cell Biol. **10:**65. doi: 10.1186/1471-2121-10-65.

4. **Baram-Pinto, D., S. Shukla, N. Perkas, A. Gedanken, and R. Sarid.** 2009. Inhibition of herpes simplex virus type 1 infection by silver nanoparticles capped with mercaptoethane sulfonate. Bioconjug. Chem. **20:**1497-1502. doi: 10.1021/bc900215b.

5. **Bengali, Z., A. C. Townsley, and B. Moss.** 2009. Vaccinia virus strain differences in cell attachment and entry. Virology. **389:**132-140. doi: 10.1016/j.virol.2009.04.012.

6. **Bhattacharya, R., and P. Mukherjee.** 2008. Biological properties of "naked" metal nanoparticles. Adv. Drug Deliv. Rev. **60:**1289-1306. doi: 10.1016/j.addr.2008.03.013.

7. **Bisht, H., A. S. Weisberg, and B. Moss.** 2008. Vaccinia virus l1 protein is required for cell entry and membrane fusion. J. Virol. **82:**8687-8694. doi: 10.1128/JVI.00852-08.

8. **Bönnemann, H., and R. M. Richards.** 2001. Nanoscopic Metal Particles, Synthetic Methods and Potential Applications. Eur. J. Inorg. Chem. 2455.

9. **Boriskin, Y. S., I. A. Leneva, E. I. Pecheur, and S. J. Polyak.** 2008. Arbidol: a broad-spectrum antiviral compound that blocks viral fusion. Curr. Med. Chem. **15:**997-1005.

10. **Brillanti, S., G. Mazzella, and E. Roda.** 2010. Ribavirin for chronic hepatitis C: And the mystery goes on. Dig. Liver Dis. doi: 10.1016/j.dld.2010.10.007.

11. **Brown, E., T. G. Senkevich, and B. Moss.** 2006. Vaccinia virus F9 virion membrane protein is required for entry but not virus assembly, in contrast to the related L1 protein. J. Virol. **80:**9455-9464. doi: 10.1128/JVI.01149-06.

12. **Broyles, S. S., and M. Kremer.** 2004. An *in vitro* transcription system for studying vaccinia virus early genes. Methods Mol. Biol. **269:**135-142. doi: 10.1385/1-59259-789-0:135.

13. **Burke, J. D., and E. N. Fish.** 2009. Antiviral strategies: the present and beyond. Curr. Mol. Pharmacol. **2:**32-39.

14. **Canamares, M. V., J. V. Garcia-Ramos, S. Sanchez-Cortes, M. Castillejo, and M. Oujja.** 2008. Comparative SERS effectiveness of silver nanoparticles prepared by different methods: a study of the enhancement factor and the interfacial properties. J. Colloid Interface Sci. **326:**103-109. doi: 10.1016/j.jcis.2008.06.052.

15. **Carter, G. C., M. Law, M. Hollinshead, and G. L. Smith.** 2005. Entry of the vaccinia virus intracellular mature virion and its interactions with glycosaminoglycans. J. Gen. Virol. **86:**1279-1290. doi: 10.1099/vir.0.80831-0.

16. **Chaloupka, K., Y. Malam, and A. M. Seifalian.** 2010. Nanosilver as a new generation of nanoproduct in biomedical applications. Trends Biotechnol. **28:**580-588. doi: 10.1016/j.tibtech.2010.07.006.

17. **Choi, O., K. K. Deng, N. J. Kim, L. Ross Jr, R. Y. Surampalli, and Z. Hu.** 2008. The inhibitory effects of silver nanoparticles, silver ions, and silver chloride colloids on microbial growth. Water Res. **42:**3066-3074. doi: 10.1016/j.watres.2008.02.021.

18. **Colman, P. M., and M. C. Lawrence.** 2003. The structural biology of type I viral membrane fusion. Nat. Rev. Mol. Cell Biol. **4:**309-319. doi: 10.1038/nrm1076.

19. **Condit, R. C., N. Moussatche, and P. Traktman.** 2006. In a nutshell: structure and assembly of the vaccinia virion. Adv. Virus Res. **66:**31-124. doi: 10.1016/S0065-3527(06)66002-8.

20. **Dales, S., and L. Siminovitch.** 1961. The development of vaccinia virus in Earle's L strain cells as examined by electron microscopy. J. Biophys. Biochem. Cytol. **10:**475-503.

21. **De Gusseme, B., T. Hennebel, E. Christiaens, H. Saveyn, K. Verbeken, J. P. Fitts, N. Boon, and W. Verstraete.** 2011. Virus disinfection in water by biogenic silver

immobilized in polyvinylidene fluoride membranes. Water Res. **45:**1856-1864. doi: 10.1016/j.watres.2010.11.046.

22. **El Badawy, A. M., R. G. Silva, B. Morris, K. G. Scheckel, M. T. Suidan, and T. M. Tolaymat.** 2011. Surface charge-dependent toxicity of silver nanoparticles. Environ. Sci. Technol. **45:**283-287. doi: 10.1021/es1034188.

23. **Elechiguerra, J. L., J. L. Burt, J. R. Morones, A. Camacho-Bragado, X. Gao, H. H. Lara, and M. J. Yacaman.** 2005. Interaction of silver nanoparticles with HIV-1. J. Nanobiotechnology. **3:**6. doi: 10.1186/1477-3155-3-6.

24. **Escors, D., and K. Breckpot.** 2010. Lentiviral vectors in gene therapy: their current status and future potential. Arch. Immunol. Ther. Exp. (Warsz). **58:**107-119. doi: 10.1007/s00005-010-0063-4.

25. **Foo, C. H., H. Lou, J. C. Whitbeck, M. Ponce-de-Leon, D. Atanasiu, R. J. Eisenberg, and G. H. Cohen.** 2009. Vaccinia virus L1 binds to cell surfaces and blocks virus entry independently of glycosaminoglycans. Virology. **385:**368-382. doi: 10.1016/j.virol.2008.12.019.

26. **Hossain, M. K., Y. Kitahama, G. G. Huang, X. Han, and Y. Ozaki.** 2009. Surface-enhanced Raman scattering: realization of localized surface plasmon resonance using unique substrates and methods. Anal. Bioanal Chem. **394:**1747-1760. doi: 10.1007/s00216-009-2762-4.

27. **Hsiao, J. C., C. S. Chung, and W. Chang.** 1999. Vaccinia virus envelope D8L protein binds to cell surface chondroitin sulfate and mediates the adsorption of intracellular mature virions to cells. J. Virol. **73:**8750-8761.

28. **Huang, K. J., and D. P. Wooley.** 2005. A new cell-based assay for measuring the forward mutation rate of HIV-1. J. Virol. Methods. **124:**95-104. doi: 10.1016/j.jviromet.2004.11.010.

29. **Izmailyan, R. A., C. Y. Huang, S. Mohammad, S. N. Isaacs, and W. Chang.** 2006. The envelope G3L protein is essential for entry of vaccinia virus into host cells. J. Virol. **80:**8402-8410. doi: 10.1128/JVI.00624-06.

30. **J. Alan Creighton, Christopher G. Blatchford and M. Grant Albrecht.** 1979. **Plasma resonance enhancement of Raman scattering by pyridine adsorbed on silver or gold sol particles of size comparable to the excitation wavelength** Journal Cover:J. Chem. Soc. , Faraday Trans. 2. **75:**790.

31. **Kim, J. S., E. Kuk, K. N. Yu, J. H. Kim, S. J. Park, H. J. Lee, S. H. Kim, Y. K. Park, Y. H. Park, C. Y. Hwang, Y. K. Kim, Y. S. Lee, D. H. Jeong, and M. H. Cho.** 2007. Antimicrobial effects of silver nanoparticles. Nanomedicine. **3:**95-101. doi: 10.1016/j.nano.2006.12.001.

32. **Lara, H. H., N. V. Ayala-Nunez, L. Ixtepan-Turrent, and C. Rodriguez-Padilla.** 2010. Mode of antiviral action of silver nanoparticles against HIV-1. J. Nanobiotechnology. **8:**1. doi: 10.1186/1477-3155-8-1.

33. **Law, M., G. C. Carter, K. L. Roberts, M. Hollinshead, and G. L. Smith.** 2006. Ligand-induced and nonfusogenic dissolution of a viral membrane. Proc. Natl. Acad. Sci. U. S. A. **103:**5989-5994. doi: 10.1073/pnas.0601025103.

34. **Liga, M. V., E. L. Bryant, V. L. Colvin, and Q. Li.** 2011. Virus inactivation by silver doped titanium dioxide nanoparticles for drinking water treatment. Water Res. **45:**535-544. doi: 10.1016/j.watres.2010.09.012.

35. **Lu, L., R. W. Sun, R. Chen, C. K. Hui, C. M. Ho, J. M. Luk, G. K. Lau, and C. M. Che.** 2008. Silver nanoparticles inhibit hepatitis B virus replication. Antivir Ther. **13:**253-262.

36. **Magden, J., L. Kaariainen, and T. Ahola.** 2005. Inhibitors of virus replication: recent developments and prospects. Appl. Microbiol. Biotechnol. **66:**612-621. doi: 10.1007/s00253-004-1783-3.

37. **Mercer, J., and A. Helenius.** 2008. Vaccinia virus uses macropinocytosis and apoptotic mimicry to enter host cells. Science. **320:**531-535. doi: 10.1126/science.1155164.

38. **Mercer, J., M. Schelhaas, and A. Helenius.** 2010. Virus entry by endocytosis. Annu. Rev. Biochem. **79:**803-833. doi: 10.1146/annurev-biochem-060208-104626.

39. **Mergemeier, S.** 2010. Polyvinylpyrrolidone as a Therapeutically Active Compound for the Treatment and Prevention of Diseases Involving Bacterial, Viral and Fungal Pathogens. Patent # WO/2010/054858.

40. **Monteiro-Riviere, N. A., A. O. Inman, and L. W. Zhang.** 2009. Limitations and relative utility of screening assays to assess engineered nanoparticle toxicity in a human cell line. Toxicol. Appl. Pharmacol. **234:**222-235. doi: 10.1016/j.taap.2008.09.030.

41. **Navarro, E., F. Piccapietra, B. Wagner, F. Marconi, R. Kaegi, N. Odzak, L. Sigg, and R. Behra.** 2008. Toxicity of silver nanoparticles to *Chlamydomonas reinhardtii*. Environ. Sci. Technol. **42:**8959-8964.

42. **Nichols, R. J., E. Stanitsa, B. Unger, and P. Traktman.** 2008. The vaccinia virus gene I2L encodes a membrane protein with an essential role in virion entry. J. Virol. **82:**10247-10261. doi: 10.1128/JVI.01035-08.

43. **Ojeda, S., A. Domi, and B. Moss.** 2006. Vaccinia virus G9 protein is an essential component of the poxvirus entry-fusion complex. J. Virol. **80:**9822-9830. doi: 10.1128/JVI.00987-06.

44. **Ojeda, S., T. G. Senkevich, and B. Moss.** 2006. Entry of vaccinia virus and cell-cell fusion require a highly conserved cysteine-rich membrane protein encoded by the A16L gene. J. Virol. **80:**51-61. doi: 10.1128/JVI.80.1.51-61.2006.

45. **Oxford, J. S., S. Balasingam, C. Chan, A. Catchpole, and R. Lambkin.** 2005. New antiviral drugs, vaccines and classic public health interventions against SARS coronavirus. Antivir. Chem. Chemother. **16:**13-21.

46. **Pavel, I., E. McCarney, A. Elkhaled, A. Morrill, K. Plaxco, and M. Moskovits.** 2008. Label-Free SERS Detection of Small Proteins Modified to Act as Bifunctional

Linkers. J. Phys. Chem. C. Nanomater Interfaces. **112:**4880-4883. doi: 10.1021/jp710261y.

47. **Pedersen, K., E. J. Snijder, S. Schleich, N. Roos, G. Griffiths, and J. K. Locker.** 2000. Characterization of vaccinia virus intracellular cores: implications for viral uncoating and core structure. J. Virol. **74:**3525-3536.

48. **Roberts, K. L., and G. L. Smith.** 2008. Vaccinia virus morphogenesis and dissemination. Trends Microbiol. **16:**472-479. doi: 10.1016/j.tim.2008.07.009.

49. **Rogers, J. V., C. V. Parkinson, Y. W. Choi, J. L. Speshock, and S. M. Hussain.** 2008. A Preliminary Assessment of Silver Nanoparticle Inhibition of Monkeypox Virus Plaque Formation. Nanoscale Res Lett. **3:**129. doi: 10.1007/s11671-008-9128-2.

50. **Samberg, M. E., P. E. Orndorff, and N. A. Monteiro-Riviere.** 2010. Antibacterial efficacy of silver nanoparticles of different sizes, surface conditions and synthesis methods. Nanotoxicology. . doi: 10.3109/17435390.2010.525669.

51. **Senkevich, T. G., and B. Moss.** 2005. Vaccinia virus H2 protein is an essential component of a complex involved in virus entry and cell-cell fusion. J. Virol. **79:**4744-4754. doi: 10.1128/JVI.79.8.4744-4754.2005.

52. **Senkevich, T. G., S. Ojeda, A. Townsley, G. E. Nelson, and B. Moss.** 2005. Poxvirus multiprotein entry-fusion complex. Proc. Natl. Acad. Sci. U. S. A. **102:**18572-18577. doi: 10.1073/pnas.0509239102.

53. **Sharma, V. K., R. A. Yngard, and Y. Lin.** 2009. Silver nanoparticles: green synthesis and their antimicrobial activities. Adv. Colloid Interface Sci. **145:**83-96. doi: 10.1016/j.cis.2008.09.002.

54. **Silver, S., T. Phung le, and G. Silver.** 2006. Silver as biocides in burn and wound dressings and bacterial resistance to silver compounds. J. Ind. Microbiol. Biotechnol. **33:**627-634. doi: 10.1007/s10295-006-0139-7.

55. **Silvestry-Rodriguez, N., E. E. Sicairos-Ruelas, C. P. Gerba, and K. R. Bright.** 2007. Silver as a disinfectant. Rev. Environ. Contam. Toxicol. **191:**23-45.

56. **Song, J. M., and B. L. Seong.** 2010. Viral membranes: an emerging antiviral target for enveloped viruses? Expert Rev. Anti Infect. Ther. **8:**635-638. doi: 10.1586/eri.10.51.

57. **Sopova, E. A., V. I. Baranov, O. A. Gankovskaia, V. F. Lavrov, and V. V. Zverev.** 2010. Effects of silver and silicon dioxide nanopowders on the development of herpesvirus infection *in vitro*. Gig. Sanit. **(4):**89-91.

58. **Speshock, J. L., R. C. Murdock, L. K. Braydich-Stolle, A. M. Schrand, and S. M. Hussain.** 2010. Interaction of silver nanoparticles with Tacaribe virus. J. Nanobiotechnology. **8:**19. doi: 10.1186/1477-3155-8-19.

59. **Sun, Y., and Y. Xia.** 2002. Shape-controlled synthesis of gold and silver nanoparticles. Science. **298:**2176-2179. doi: 10.1126/science.1077229.

60. **Tolaymat, T. M., A. M. El Badawy, A. Genaidy, K. G. Scheckel, T. P. Luxton, and M. Suidan.** 2010. An evidence-based environmental perspective of manufactured

silver nanoparticle in syntheses and applications: a systematic review and critical appraisal of peer-reviewed scientific papers. Sci. Total Environ. **408:**999-1006. doi: 10.1016/j.scitotenv.2009.11.003.

61. **Townsley, A. C., and B. Moss.** 2007. Two distinct low-pH steps promote entry of vaccinia virus. J. Virol. **81:**8613-8620. doi: 10.1128/JVI.00606-07.

62. **Townsley, A. C., T. G. Senkevich, and B. Moss.** 2005. The product of the vaccinia virus L5R gene is a fourth membrane protein encoded by all poxviruses that is required for cell entry and cell-cell fusion. J. Virol. **79:**10988-10998. doi: 10.1128/JVI.79.17.10988-10998.2005.

63. **Townsley, A. C., T. G. Senkevich, and B. Moss.** 2005. Vaccinia virus A21 virion membrane protein is required for cell entry and fusion. J. Virol. **79:**9458-9469. doi: 10.1128/JVI.79.15.9458-9469.2005.

64. **Townsley, A. C., A. S. Weisberg, T. R. Wagenaar, and B. Moss.** 2006. Vaccinia virus entry into cells via a low-pH-dependent endosomal pathway. J. Virol. **80:**8899-8908. doi: 10.1128/JVI.01053-06.

65. **Turner, P. C., B. P. Dilling, C. Prins, S. G. Cresawn, R. W. Moyer, and R. C. Condit.** 2007. Vaccinia virus temperature-sensitive mutants in the A28 gene produce non-infectious virions that bind to cells but are defective in entry. Virology. **366:**62-72. doi: 10.1016/j.virol.2007.03.060.

66. **U.S. Department of Health and Human Services.** 2007. HHS Public Health Emergency Medical Countermeasure Enterprise Imlpementation Plan for Chemical, Biological, Radiological and Nuclear Threats.

67. **V. V. Kopeikin and E. F. Panarin.** 2001. Water-Soluble Nanocomposites of Zerovalent Metallic Silver with Enhanced Antimicrobial Activity. Doklady Chemistry. **380:**277.

68. **Vijayakumar, P. S., and B. L. Prasad.** 2009. Intracellular biogenic silver nanoparticles for the generation of carbon supported antiviral and sustained bactericidal agents. Langmuir. **25:**11741-11747. doi: 10.1021/la901024p.

69. **Wagenaar, T. R., and B. Moss.** 2007. Association of vaccinia virus fusion regulatory proteins with the multicomponent entry/fusion complex. J. Virol. **81:**6286-6293. doi: 10.1128/JVI.00274-07.

70. **Whitbeck, J. C., C. H. Foo, M. Ponce de Leon, R. J. Eisenberg, and G. H. Cohen.** 2009. Vaccinia virus exhibits cell-type-dependent entry characteristics. Virology. **385:**383-391. doi: 10.1016/j.virol.2008.12.029.

71. **White, J. M., S. E. Delos, M. Brecher, and K. Schornberg.** 2008. Structures and mechanisms of viral membrane fusion proteins: multiple variations on a common theme. Crit. Rev. Biochem. Mol. Biol. **43:**189-219. doi: 10.1080/10409230802058320.

72. **Wolfe, C. L., and B. Moss.** 2011. Interaction between the G3 and L5 proteins of the vaccinia virus entry-fusion complex. Virology. **412:**278-283. doi: 10.1016/j.virol.2011.01.014.

73. **Woodrow Wilson International Center for Scholars and the Pew Charitable Trusts.** 2011. The Project on Emerging Nanotechnologies. The Silver Nanotechnology Commercial Inventory. **2011**. http://www.nanotechproject.org/inventories/silver/

CHAPTER II

Size Selection and Concentration of Silver Nanoparticles by Tangential Flow Ultrafiltration for Use as SERS-Based Biosensors

John C. Trefry,[ǂ] Jennifer L. Monahan,[†] Kent M. Weaver,[†] Allie J. Meyerhoefer,[†] Marjorie M. Markopolous,[†] Zachary S. Arnold,[†] Dawn P. Wooley[ǂ]* and Ioana E. Pavel[†]*

Department of Chemistry[†] and Department of Neuroscience, Cell Biology and Physiology[ǂ], Wright State University, 3640 Colonel Glenn Highway, Dayton, OH 45435

J Am Chem Soc. 2010 Aug 18;132(32):10970-2

Summary of Involvement

John C. Trefry was responsible for writing the manuscript, editing the manuscript, transmission electron microscopy, AgNP size analysis, ultracentrifugation, tangential flow ultrafiltration development/implementation and photography.

ABSTRACT

A proposed tangential flow ultrafiltration method was compared to the widely-used ultracentrifugation method for efficiency and efficacy in concentrating, size selecting and minimizing the aggregation state of a silver nanoparticle (AgNP) colloid while probing the AgNPs' SERS-based sensing capabilities. The ultrafiltration method proved to be more efficient, more effective and was found to tremendously boost the SERS-based sensing capabilities of these AgNPs through the increased number of homogenous SERS hot spots available for a bio-target molecule within a minimal focal volume. Future research studies and applications that address the physiochemical properties or biological impact of AgNPs would greatly benefit from ultrafiltration for its ability to generate monodisperse colloidal nanoparticles, to eliminate excess toxic chemicals from nanoparticle synthesis and to generate minimum levels of aggregation during nanoparticle concentration.

INTRODUCTION

Silver nanoparticle (AgNP) preparation and manipulation is an extremely active research area due to the numerous applications of these nanomaterials to catalysis, photonics, electronics, biosensing, drug delivery, pharmaceuticals, etc.[1] One of the most exciting and demanding applications of AgNPs is their surface-enhanced Raman spectroscopy (SERS)-based biosensing capability. SERS is a powerful analytical technique used to detect specific molecular vibration modes, which has experienced an explosive interest due to its strong molecular specificity and its extremely low detection limits, down to the single-molecule level.[2a,b] Theory predicts[2c,d] and experiments confirm[2a,b, 1c] that exceptionally large increases in Raman cross-section, or signals attained through Raman spectroscopy, are associated with molecules located in the nano-sized interstitial sites of interacting colloidal AgNPs (*i.e*. hot spots).

Significant challenges remain for the preparation and isolation of colloidal AgNPs with controlled polydispersity, toxicity and aggregation. Limiting AgNP polydispersity (*i.e*., narrow size and shape distribution)[3a] improves the optical/electronic properties,[2c,d, 3a] SERS enhancement factors, or increases in Raman signals corresponding to the presence of an enhancement material,[2c,d] and antimicrobial properties.[1e 3f] Reducing AgNP toxicity by eliminating chemically aggressive reagents or organic solvents[3a,c] significantly lowers the impact to biological systems, while facilitating the identification of novel activities and mechanisms.[1e, 3c-e] Minimizing AgNP aggregation at higher concentrations[1c, 3a,c] allows the assessment of SERS nanostructure-function relationship,[2c,d] improves the cellular uptake of AgNPs[1c, 3d-f] and maintains the number of potentially active catalytic sites.[1a] Additionally, use of methods such as centrifugation,[4a] size exclusion

chromatography,[4a,b] gel electrophoresis,[4c] diafiltration,[4d] size-dependent solubility[4e] and fractional crystallization[4f] have been reported for the size-based separation and/or concentration of NPs. These approaches may lead to issues with aggregation,[4a] instability,[4a] cost,[4b, 4e] undesired coatings,[4c 4f] and less effective protocols for NPs of smaller size.[4f] As a result, these methods are time intensive, expensive, toxic or inefficient.[4] These limitations were overcome in this study by using a tangential flow ultrafiltration method, commonly used for weight-based separation of proteins, but not yet tested on silver or polydisperse colloids.[4d] This method relies on passing a fluid through a hollow fiber with specific pore sizes, allowing the solvent to pass through the pores and retaining solutes possessing sizes larger than the pore size within the hollow fiber. Tangential flow ultrafiltration is a single pass procedure to size select and to concentrate a target species using a series of membrane-modules with pores ranging from 1 nm to 100 μm. The proposed method was compared to the widely-used ultracentrifugation method for efficiency and efficacy in concentrating, size selecting and minimizing the aggregation state of an AgNP colloid while probing the AgNPs' SERS-based sensing capabilities.

RESULTS AND DISCUSSION

Colloidal AgNPs were synthesized according to a well-known, inexpensive Creighton method by the simple reduction of silver nitrate with sodium borohydride. Once synthesized, the 600 mL original colloid (Ori) product was divided into two aliquots for the comparative analysis. Ultracentrifugation was performed at 7.8 x 10^3 g and 10°C for 90 min to separate the colloid into a supernatant (Csu) and a pellet (Cpl) of AgNPs. Cpl was resuspended in 10 mL of supernatant. For ultrafiltration, the colloid was

pumped through a 50 nm filter yielding a concentrate (50c; AgNPs > pore size) and a filtrate (50f; AgNPs < pore size) sample. The 50f sample was then pumped through a 100 kD filter to produce a concentrated (100c) sample (Figure S1).

Visual inspection, transmission electron microscopy (TEM), UV-Vis absorption, and flame atomic absorption spectrophotometry (FAAS) measurements on each sample revealed corroborating data that the ultrafiltration method was more efficient at specific size selection and concentration of AgNPs with minimal aggregation than ultracentrifugation (Fig. 1A, Table 1). The dramatic color change between Ori, Cpl, and 100c confirms that darker, more opaque solutions contain larger particles with high levels of AgNP aggregation (Fig. 1A, column 1).[5a,] TEM micrographs (Fig. 1A, column 1) show that Ori is characteristic of moderately dispersed, lowly concentrated AgNPs. Cpl contains high concentrations of massive, heterogeneous AgNP-aggregates. 100c consists of highly concentrated yet lowly aggregated and homogenous AgNPs. The UV-Vis spectra show both Ori and 100c samples had surface plasmon resonance (SPR) absorption maximums at 400 nm, but 100c had a 10-fold higher intensity. This sharp, symmetrical peak is characteristic of small (10-20 nm diameter) and spherical AgNPs of low aggregation.[5c,d] The spectra for Cpl had a broader SPR peak with a clear shoulder, showing the ultracentrifugation process leads to the formation of polydisperse AgNP-aggregrates.

Size histograms (Fig. 1A, column 2) were prepared by analyzing the TEM micrographs of each sample (number of AgNPs = 500). The differences in size distribution and maximum diameters for the Ori and Cpl samples are significant (e.g., more than twice for Cpl) in comparison to the 100c sample. Most of the aggregates larger

than 20 nm were eliminated in 100c (Fig. 1, column 2), while Cpl had increased numbers of larger aggregates (5% of the total AgNPs have diameters 50 nm or larger). These large aggregates produced by ultracentrifugation accounted for 96% of the AgNP weight. Ultrafiltration was also 2.5-fold more efficient at concentrating the Ori colloid (from 77.4 to 198.7 μg mL^{-1} of silver). Concentration factors for Cpl and 100c were 5.1- and 13.0-fold, respectively (Table 1).

Sample	Ori	Csu	Cpl	50c	50f	100c
Ave.	10.4	8.5	11.4	18.2	3.3	11
Max.	141	54.4	161	162.5	87.3	60.5
%Dist.	100	106	162	129	127	73
Conc.	15.3	7.9	77.4	16.4	14.3	198.7

Table 1. Specific characteristics of each AgNP preparation. Average size in nm (Ave.), maximum size in nm (Max.), percent distribution (% Dist.), final concentration of silver in μg mL^{-1} (Conc.).

The SERS-sensing efficiencies, the analytical (AEF) and surface enhancement factors (SEF), of Ori, Cpl and 100c were calculated by measuring the Raman, SERS, and fluorescence spectra of a 10^{-6} M rhodamine 6G (R6G) solution as a standard (Fig. 1B; Supporting Info).[5c] The AEF and SEF for Cpl and 100c were found to have similar values (e.g., AEF of 8.1×10^7 and SEF of 7.9×10^4 for 100c). These factors are 1,000-fold larger than those calculated for Ori. Recent studies[5c] showed that a SEF of 10^7 is sufficient to observe single-molecule SERS events for a R6G concentration of 10^{-9} M, at 632.8 nm, and with an integration time of 1s. The fluorescence data indicate that 100c and Cpl have comparable, improved R6G absorption abilities. Over 96% of the R6G molecules

effectively complexed to the AgNP surface and contribute to the SERS signal in 100c and Cpl (70% of the R6G probes for Ori). The enormous increase in signal for 100c is due to the highly concentrated, uniform colloidal AgNPs available for creating dimers or small AgNP-aggregates. Although the amount of silver is 2.5-fold less in Cpl, similar enhancement factors are achieved due to the large, heterogeneous AgNP-aggregates. However, the Cpl aggregates are formed in an uncontrolled manner and may impede cellular uptake and assessment of nanostructure-function relationship.

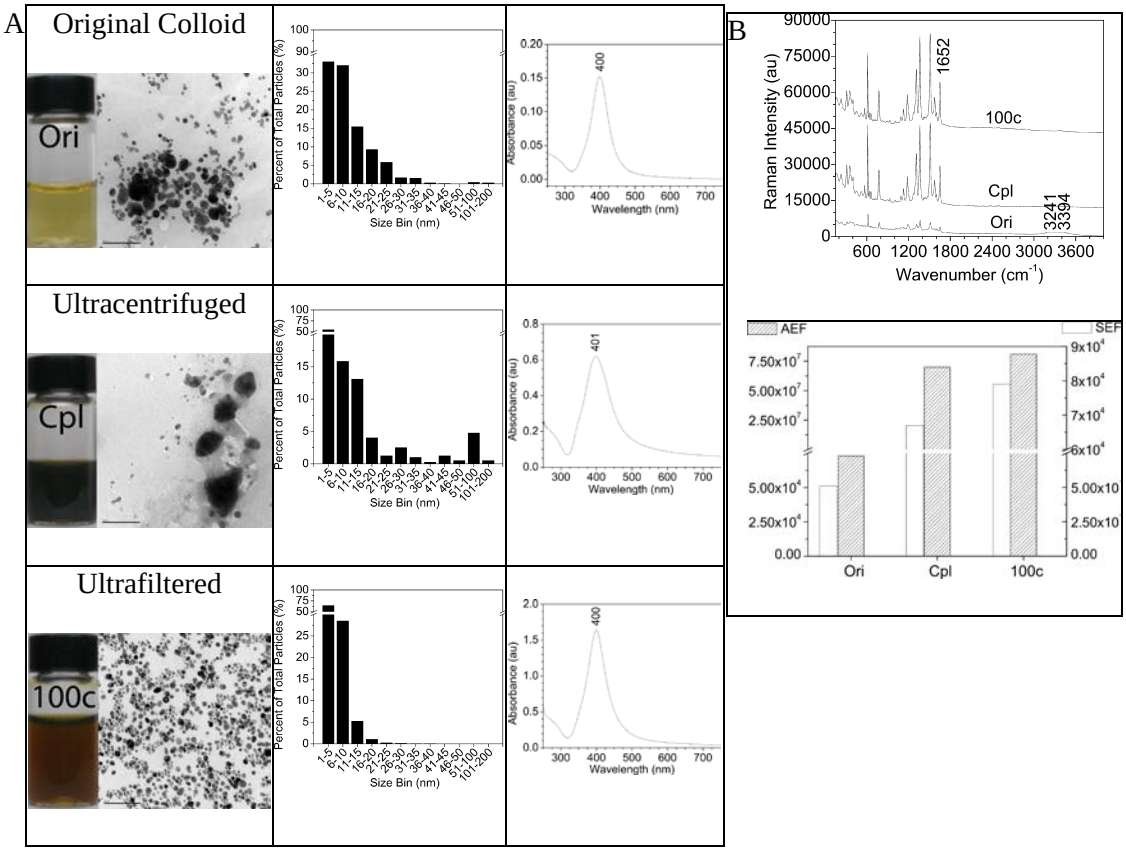

Figure 1. AgNPs were characterized at each step in the isolation and concentration process. A) Each row represents a distinct preparation: column 1) visual and TEM inspection photos, bar = 100 nm, column 2) size analysis from TEM data, and column 3) UV-Vis absorption spectra. B top) SERS spectra of R6G dye (10^{-6} M) for each colloid. B bottom) Estimated analytical (AEF) and surface enhancement factors (SEF) for each colloid.

The data presented here demonstrate that ultrafiltration permits greater control over AgNP size, concentration and aggregation state than conventional methods of isolation such as ultracentrifugation. Future research studies and applications addressing the physiochemical properties or biological impact of AgNPs would greatly benefit from ultrafiltration for its ability to generate monodisperse colloidal NPs, to eliminate excess toxic chemicals from NP synthesis, and to obtain minimum levels of aggregation during NP concentration. The ultrafiltration method for AgNP isolation could tremendously boost the SERS-based sensing capabilities of these nanomaterials through the increased number of homogenous SERS hot spots available for a bio-target molecule within a minimal focal volume. Additionally, ultrafiltration could easily be implemented at various volume scales, for both research and industrial purposes.

Supporting information available: Experimental methods and AEF/SEF calculations are available at http://pubs.acs.org.

Acknowledgment. We thank Dr. Gerald M. Alter for the use of the fluorescence spectrophotometer in his research laboratory. Dr. I. Pavel gratefully acknowledges the WSU Women in Science Giving Circle Award.

REFERENCES for MAIN TEXT CHAPTER 1

1. (a) Jana, N.R.; Sau, T.K.; Pal, T. J. Phys. Chem. B 1999, 103, 115-121. (b) Li, Y.; Wu, Y.; Ong, B.S. J. Am. Chem. Soc. 2005, 127, 3266-3267. (c) Willets, K.A. Anal. Bioanal. Chem. 2009, 394, 85-94. (d) Jain, J.; Arora, S.; Rajwade, J.M.; Omray, P.; Khandelwal, S.; Paknikar, K.M. Mol. Pharm. 2009, 6, 1388-1401. (e) Bhattacharya, R.; Mukherjee, P. Adv. Drug. Deliver. Rev. 2008, 60, 1289-1306.

2. (a) Nie, S.; Emory, S.R. Science 1997, 275, 1102-1106. (b) Xu, H.; Bjerneld, E.J.; Käll, M.; Börjesson, L. Phys. Rev. Lett. 1999, 83, 4357-4360. (c) Xu, H.; Aizpurua, J.; Käll, M.; Apell, P. Phys. Rev. E 2000, 62, 4318-4324. (d) Aravind, P.K.; Nitzan, A.; Metiu, H. Surf. Sci. 1981, 110, 189-204.

3. (a) Sun, Y.; Xia, Y. Science 2002, 298, 2176-2179. (b) Jana, N.R.; Peng, X.G. J. Am. Chem. Soc. 2003, 125, 14280-14281. (c) Tolaymat, T.M.; El Badawy, A.M.; Genaidy, A.; Scheckel, K.G.; Luxton, T.P., Suidan, M. Sci. Total Environ. 2010, 408, 999-1006. (d) Miura, N.; Shinohara, Y. Biochem. Bioph. Res. Co. 2009, 390, 733-737. (e) Auffan, M.; Rose, J.; Bottero, J.-Y.; Lowry, G.V., Jolivet, J.-P., Wiesner, M.R., Nat. Nanotechnol. 2009, 4, 634-641. (f) AshaRani, P.V.; Mun, G.L.K.; Hande, M.P., Valiyaveettil, S. ACS Nano 2009, 3, 279-290. (g) Scown, T.M.; Santos, E.M.; Johnston, B.M.; Gaiser, N.; Baalousha, M.; Mitov, S.; Lead, J.R.; Stone, V.; Fernandes, T.S.; Jepson, M.; van Aerle, R.; Tyler, C.R. Toxicol. Sci. 2010, e-pub

4. (a) Novak, J.P.; Nickerson, C.; Franzen, S.; Feldheim, D.L. Anal. Chem. 2001, 73, 5758-5761. (b) Al-Somali, A,M.; Krueger, K.M.; Falkner, J.C.; Colvin, V.L. Anal. Chem. 2004, 76, 5903-5910. (c) Hanauer, M.; Pierrat, S.; Zins, I.; Lotz, A., Sönnichsen, C. Nano Lett. 2007, 7, 2881-2885. (d) Sweeny, S.F.; Woehrle, G.H.; Hutchison, J.E. J. Am. Chem.

Soc. 2006, 128, 3190-3197. (e) Clarke, N.Z.; Waters, C.; Johnson, K.A.; Satherley, J.; Schiffrin, D.J. Langmuir 2001, 17, 6048-6050. (f) Schaaff, T.G.; Shafigullin, M.N.; Khoury, J.T.; Vezmar, I.; Whetten, R.L.; Cullen, W.G.; First, P.N. J. Phys. Chem. B. 1997, 101, 7885-7891.

5. (a) Sönnichsen, C.; Reinhard, B.M.; Liphardt, J.; Alivisatos, A.P. Nat. Biotechnol. 2005, 23, 741-745. (b) Ciou, S.H; Cao, Y.W.; Huang, H.C.; Su, D.Y.; Huang, C.L. J. Phys. Chem. C 2009, 113, 9529-9525. (c) Le Ru, E.C.; Blackie, E.; Meyer, M.; Etchegoin, P.G. J. Phys. Chem. C. 2007, 111, 13794-13803.

MATERIALS AND METHODS

Abbreviations

R6G – rhodamine 6G; Colloidal Samples: Ori – Original, Csu – Ultracentrifuged supernatant, Cpl – Ultracentrifuged, 50f – 50 nm Ultrafiltered filtrate, 50c – 50 nm Ultrafiltered concentrate, and 100c –100kD Ultrafiltered.

Experimental section

All starting materials were purchased from commercial sources as analytical pure reagents.

Chemicals and procedures

Colloidal silver nanoparticles (AgNPs) synthesis

A slightly modified Creighton[1] colloid was produced by the borohydride reduction ($NaBH_4$, Fisher Scientific) of silver nitrate ($AgNO_3$, Fisher Scientific). Briefly, an $AgNO_3$ solution (1.70 mg in 10.0 mL of highly purified water) cooled to approximately 10±2°C was added drop wise, with constant stirring, to a $NaBH_4$ solution (4.53 mg in 60.0 mL of highly purified water) pre-cooled to 2±1°C. Stirring was continued for another 50 min in the ice bath. The colloid was then stored in refrigerator at 4±1°C until use.

Theoretical estimate of the amount of colloidal AgNPs

In preparing the colloid, 1.70 mg of $AgNO_3$, corresponding to 10^{-5} mols, were added to 10.0 mL of water and slowly mixed with 60.0 mL of a $NaBH_4$ solution. Therefore, the final volume of colloid (70.0 mL) had a total silver mass of 1.08×10^{-3} g. Thus, the amount of silver per milliliter of colloid is 15.42 μg mL^{-1}.

Instrumentation

Sample Preparation

Freshly synthesized AgNP suspensions were passed through 0.2 μm filters prior to purification (Nalgene Labware). A 300 mL volume of these pre-filtered AgNPs, which was obtained by combining several batches, was then used for processing by ultracentrifugation and tangential flow filtration methods.

Ultracentrifugation

All centrifugation was performed in a L8M-70 ultracentrifuge using a 45-Ti fixed angle rotor and a 70 mL bottle with cap assembly (Beckman Coulter). Samples were centrifuged at 10 °C, for 90 minutes at 7.8 x 10^3 g (10,000 rpm). Supernatants were removed using serological pipets. While decanting the supernatant, 10 mL were left within the centrifuge bottle. This remaining supernatant was used to resuspend the AgNP pellet. The ultracentrifugation scheme is represented in Figure S1.

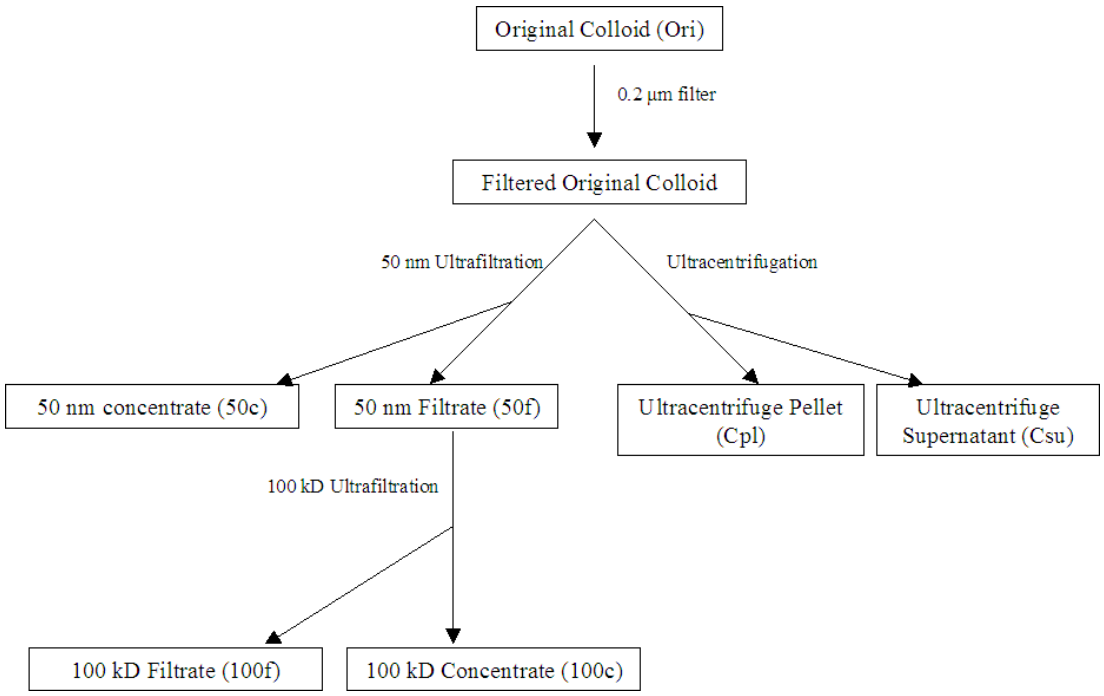

Figure S1. A schematic representation of the overall size selection and concentration processes. Samples taken at each step in the process are represented in boxes. Labeled arrows indicate the specific size selection and concentration step.

Tangential Flow Filtration

The filtering apparatus and equipment was assembled according to the manufacturer's recommendations (Spectrum Laboratories, Rancho Dominguez, CA). Samples were filtered through a 50 nm Midi Kros module at a steady flow rate of 300 mL min^{-1} using the KrosFlo II Research System. The resulting filtrate's volume, containing particles smaller than 50 nm (50f), was further filtered through a 100 kD Midi Kros module, while the concentrate volume (system holdup volume of 10 mL) was saved for analysis. The 100 kD filtrate, containing particles smaller than 100 kD (100f), and concentrate, containing particles larger than 100 kD (100c), volumes were likewise

retained for analysis. The filtering scheme is represented in Figure S1. Tubing and reservoirs were replaced or cleaned by washing three times with de-ionized water and 7x detergent (MP Bio), followed by three flushes of de-ionized water, between each filtering step.

UV-Vis absorption spectrophotometry

The absorption spectra, corresponding to innate surface plasmon resonances of AgNPs which indicate AgNP size and dispersity in solution, were recorded using an 8453 UV-VIS-NIR (Hewlett Packard Inc.) spectrophotometer and a Cary 50 UV-VIS-NIR spectrophotometer (Varian Inc.) at 1 nm intervals. Each colloidal AgNPs sample was diluted with highly purified water (1:10 volume ratio) before measurement. A cell (Fisher Scientific) of a path length of 10.0 mm and a capacity of 4.5 mL was used for all measurements.

Transmission Electron Microscopy (TEM)

Samples were diluted in highly purified water when necessary. Twenty microliters of each sample were then deposited on 300-mesh formvar-coated gold grids (Electron Microscopy Sciences). Grids were left to dry in a desiccator and viewed within one day. A Phillips EM 208S transmission electron microscope operating at an accelerating potential of 70kV was used to visualize the nanoparticle samples before and after each step of the purification process. Electron micrographs were captured using a high resolution Gatan Bioscan camera.

TEM image analysis

Tagged image files were analyzed by ImagePro software (Media Cybernetics Inc.). Automated count settings were used to distinguish the light background from the

dark perimeter of the AgNPs. One particle was defined by a complete and enclosed perimeter. A minimum of 500 particles per sample were analyzed. The Microsoft Excel software was then used to bin and analyze the average particle diameter data collected from the micrographs. The Origin 8 software was then used to graphically represent the data.

The average particle diameters for 50f and 100c were 3.3 nm and 11 nm, respectively. (Table 1 of the manuscript) This corresponding increase in average particle diameter is due to the increased counting frequency of particles with sizes between the upper and lower filter limits and the reduction in frequency of the smaller particles due to their passage through the filter. The larger particle frequency is increased due to large particle retention within the lumen of filter module. Concurrently there is a decrease in small particle frequency from their passage through the membrane and into the eluent or filtrate. Additionally, the maximum diameter of 60.5 nm for 100c was unexpected for the filter limit of 50 nm. In theory, all of the particles with diameters larger than 50 nm should have been removed from the 50f sample by their retention in the 50 nm filter. However, particles with maximum diameters larger than 50 nm can still exist in the 50f sample because they may be slightly non-spherical and have other dimensions less than 50 nm allowing them to pass through the filter in the first filtering scheme (50 nm filter), but be retained in the second step (100 kD filter). This explanation applies to the 50f sample as well.

Flame Atomic Absorption Spectroscopy (FAAS)

An AA reference silver standard solution of 1.0 x 10^3 µg mL^{-1} was purchased from Fisher Scientific (Lot Number: CL4-132AG) and used for the preparation of six

silver standards of 0.1, 0.2, 0.5, 1.0, 2.0, and 4 μg mL^{-1}. The FAAS calibration curve is depicted in Figure S2. Each sample contained 2% nitric acid (Optima grade, Fisher Scientific, Catalog #A467-500). Samples were diluted 100x (Ori, Csu, 50f) or 200x (Cpl, 50c, 100c).

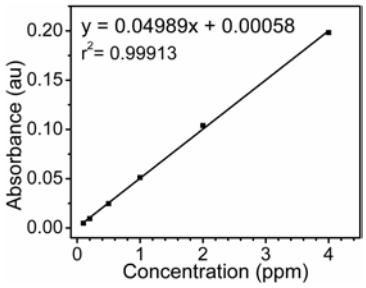

Figure S2: Flame atomic absorption spectroscopy calibration curve constructed by using six silver standards of 0.1, 0.2, 0.5, 1.0, 2.0, and 4 ppm.

A fast sequential atomic absorption spectrometer (model AA240 FS, Varian Inc.) equipped with an air-acetylene burner and a silver hollow cathode lamp (5 mA) was used for the determination of silver content within samples. The operating conditions were set as recommended by manufacturer: wavelength - 328.1 nm, slit width – 0.5 nm, air flow rate – 13.50 L min^{-1}, and acetylene flow rate 2.00 L min^{-1}. The acquisition time of each measurement was 5 s, and a delay time of 3 s was introduced in between measurements. Each sample was measured three times and the absorbance values were averaged before extrapolating the silver concentration from the calibration curve. A blank solution was introduced between each sample.

Raman and SERS Spectroscopy

A 10^{-3} M stock solution of the rhodamine 6G dye (R6G, Fisher Scientific) was prepared in water and further diluted to the desired concentrations. The SERS samples were obtained by adding 0.9 x 10^{2} μL of the 2.22 x 10^{-6} M R6G solution and 0.1 x 10^{2} μL

of the 1 M KBr (Fisher Scientific) solution to 1 mL of each of the colloidal samples (i.e, Ori, Csu, Cpl, 50c, 50f, and 100c). The final concentrations of KBr and R6G in the colloidal suspension were approximately 0.5 x 10^{-1} M and 10^{-6} M, respectively.

The Raman and SERS measurements were performed using a LabRamHR 800 system (Horiba Jobin Yvon Inc.) equipped with 1800 and 600 grooves/mm holographic gratings. The 633 nm output of a He-Ne laser was used as an excitation line. The laser output was 17 mW. The laser beam spot had a diameter of about 1 μm and was focused on the colloidal samples placed in cuvettes with the help of a high resolution confocal Raman microscope (high stability BX41) and a long working distance Olympus objective (50x). The confocal hole was set at 300 μm and the backscattered Raman signal was recorded using an open electrode thermo-electric cooled CCD detector (1024x526 pixels). The spectral resolution was 1 cm^{-1}. The acquisition times were a) 30 s for normal Raman measurements and b) 3 s (all samples except for 100c and Cpl) or 0.5 s (100c and Cpl) for SERS spectra. Each Raman and SERS spectral window was averaged over 3 and 5 cycles, respectively. The Raman data were then analyzed and processed using the LabSpec 5 and Origin 8 software. A comparative graph showing the SERS spectra of Ori, Cpl, and 100c was prepared for Figure 1 of the manuscript after rescaling the intensities in the SERS spectrum of the original colloid (Ori) to compensate for the different acquisition times (3s for Ori and 0.5 s for 100c and Cpl). In this graph, the SERS spectra of Cpl and 100c were shifted on the Y scale (Raman Intensity) to allow for a direct comparison of peak intensities.

Fluorescence Spectroscopy

The fluorescence emission spectra of all SERS samples and R6G solution (0.75 x 10^{-6} M) were recorded in a fluorescence quartz cuvette using a Cary Eclipse fluorescence spectrophotometer (Varian Inc.). The 10^{-6} M solution of R6G caused detector saturation and could not be recorded. The excitation wavelength was 532 nm and the emission spectra were collected in the 540-700 nm range using a PMT detector voltage of 600 V at a scan rate of 600 nm min^{-1}.

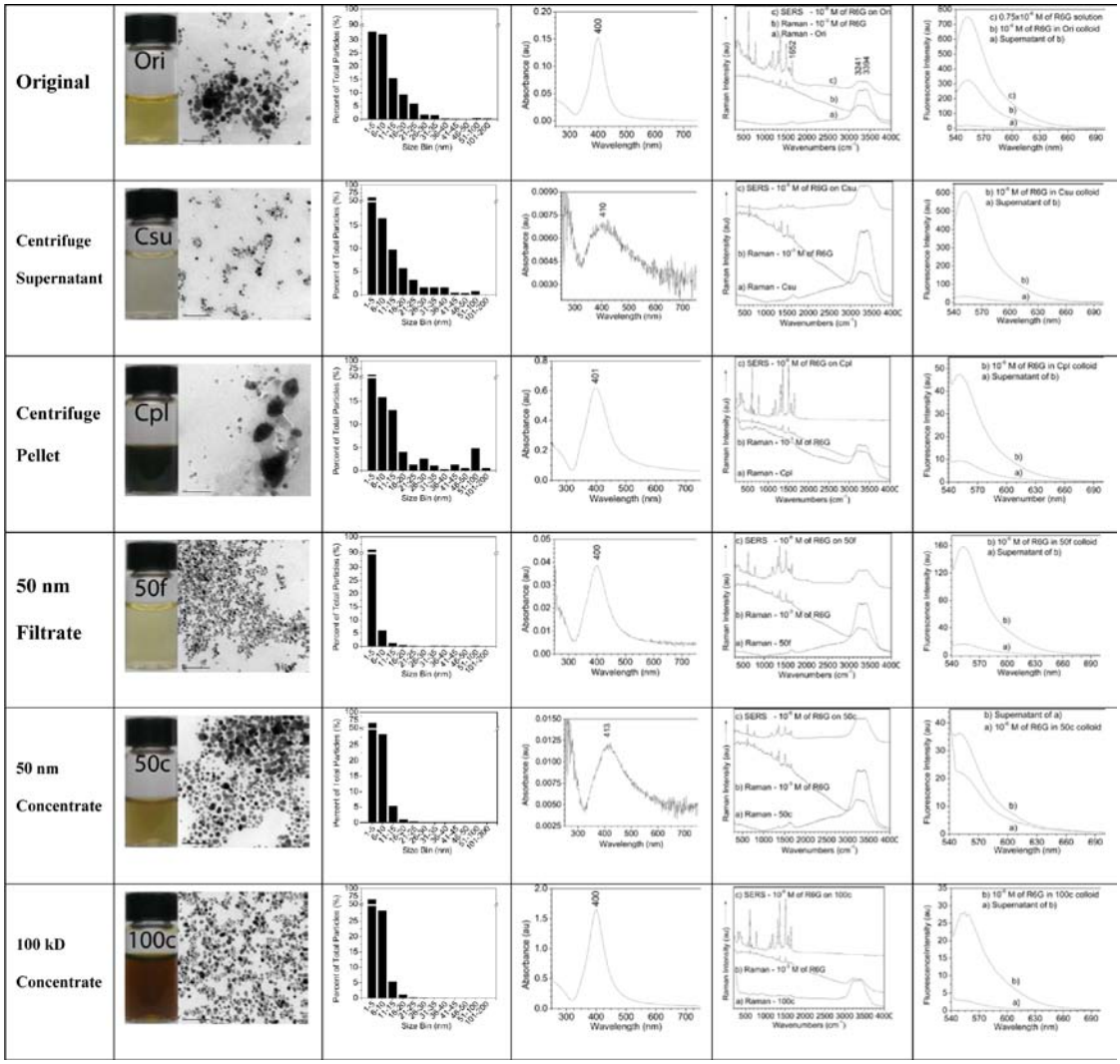

Figure S3. Overview of colloidal AgNP processing and characterization. AgNPs were characterized at each step in the ultracentrifugation (Csu and Cpl) and ultrafiltration (50c, 50f, and 100c) process, and compared with the original colloid (Ori). Each row represents a distinct preparation step: column 1) sample name, column 2) visual and TEM inspection photos, bar = 100 nm, column 3) size analysis of AgNPs from TEM data, column 4) UV-Vis absorption spectra, column 5) Raman (at 10^{-3} M) and SERS (at 10^{-6} M) spectra of R6G (The ordinary Raman spectrum of each colloidal sample was inserted as a control), and column 6) fluorescence emission spectra of each colloidal sample incubated with R6G at 10^{-6} M before and after centrifugation (supernatant) at 7.8 x 10^3 g and 10°C for 90 min (The fluorescence emission spectrum of R6G at 0.75 x 10^{-6} M was inserted for comparison reasons).

Analytical Enhancement Factor (AEF) and Surface Enhancement Factor (SEF) Estimates

The AEF and SEF are the most important values for characterizing the SERS effect. The peaks at 1652 cm^{-1} of R6G (*i.e.*, a streching of the R6G xanthine ring) and 3250-3420 cm^{-1} of H_2O (*i.e.*, two broad bands corresponding to the symmetric and asymmetric water stretching modes) were chosen to estimate these factors using an excitation line of 632.8 nm.[2,3] After a baseline correction (User defined baseline anchor points: 10 points, Interpolation method: Bspline), the ratio of the integrated peak areas at 1652 cm^{-1} and at 3380 cm^{-1} was determined for both, the Raman and SERS spectra of R6G (e.g., $\text{Int.area}_{\text{R6G, Raman}} / \text{Int.area}_{\text{H}_2O,\ \text{Raman}} = 2.26\times10^4 / 2.06\times10^6$ for the normal Raman spectrum of the 10^{-3}M R6G solution). The non-SERS differential Raman cross-section of R6G ($d\sigma_{\text{R6G, Raman}} / d\Omega$) was included to obtain reliable and realistic enhancement factors. This aspect has often been ignored and is partially responsible for the unrealistically large enhancement factors sometimes reported in literature. Dyes such as R6G can have notably large differential Raman-cross sections[2] even in non-resonance conditions due to pre-resonance effects[2,3]. The R6G dye has an absorption maximum at 528 nm and the excitation wavelength employed in this study was 632.8 nm.

The non-SERS differential Raman cross section of R6G ($d\sigma_{\text{R6G,\ Raman}} / d\Omega$) was determined using the following formula:

$$\frac{d\sigma_{\text{R6G, Raman}} / d\Omega}{d\sigma_{H_2O,\text{Raman}} / d\Omega} = \frac{\text{Int.area}_{\text{R6G, Raman}} / C_{R6G,\text{Raman}}}{\text{Int.area}_{\text{H}_2O,\ \text{Raman}} / C_{H_2O,\text{Raman}}} \quad (1)$$

where $d\sigma_{\mathrm{R6G,\ Raman}}/d\Omega$ and $d\sigma_{\mathrm{H_2O,\ Raman}}/d\Omega$ $(2.2\,x\,10^{-30}\ \mathrm{cm^2 sr^{-1}})^3$ are the differential normal Raman cross-sections of R6G and H_2O, respectively, excited at 632.8 nm. $C_{R6G,\,\mathrm{Raman}}$ (10^{-3} M) and $C_{H_2O,\,\mathrm{Raman}}$ (55.5 M) denote the molar concentrations of R6G and water, respectively.

In this study, a non-SERS differential Raman cross section of $1.3\,\mathrm{x}\,10^{-27}\ \mathrm{cm^2 sr^{-1}}$ was obtained for the peak at 1652 $\mathrm{cm^{-1}}$ of R6G which agrees well with the one reported in literature.[3] Although this cross-section is much larger than the value which Nie et al. had estimated in his single-molecule SERS study,[4] it is similar to the experimental results in the literature ($4.4\,\mathrm{x}\,10^{-27}\ \mathrm{cm^2 sr^{-1}}$).[2,3] The differential Raman cross-section of R6G at resonance was recently predicted to be on the order of $10^{-25}\ \mathrm{cm^2 sr^{-1}}$.[3,4] The large differential Raman cross section of R6G at $\lambda_0 = 632.8\,\mathrm{nm}$ is partially due to the relatively large size of the R6G molecule, but above all, it is the result of the pre-resonance Raman effect (the excitation wavelength is close to the resonance wavelength).[2,3]

A similar approach was used to calculate the differential SERS cross-section of R6G (e.g., $d\sigma_{\mathrm{R6G,\ SERS}}/d\Omega = 9.746\,\mathrm{x}\,10^{-24}\ \mathrm{cm^2 sr^{-1}}$ for Ori) at an analyte concentration, $C_{R6G,\,\mathrm{SERS}}$, of 10^{-6} M foreach colloidal suspension (i.e., Ori, Cpl, and 100c). The water concentration, $C_{H_2O,\,\mathrm{Raman}}$, was maintained the same as for the normal Raman experiments.

The AEF factor indicates how much more signal can be expected from SERS as compared to the normal Raman under the given conditions.

$$AEF = \frac{d\sigma_{R6G,\,SERS}/d\Omega}{d\sigma_{R6G,\,Raman}/d\Omega} \text{ x } \frac{\text{acq. time}_{\text{Raman}}}{\text{acq. time}_{\text{SERS}}}$$

(2)

The different acquisition times for the Raman and SERS measurements of Ori, Cpl, and 100c were also factored into the above formula (e.g., 30s/3s for Ori). All other experimental conditions were identical (i.e., microscope objective, lenses, spectrometer, cuvette, etc.) The values obtained for each colloidal sample are listed in Table S1.

Although $C_{R6G,\,\text{SERS}}$ does not fully characterize the number of R6G molecules adsorbed AEF is useful for specific practical applications (e.g., colloidal solutions). The AEF factor strongly depends on many parameters, in particular, on the adsorption properties and surface coverage of the dye probe. The AEF formula ignores that only the adsorbed probe molecules contribute to the SERS signal and that the enhancement effect is distance-dependent. Hence, the AEF factor does not offer a good characterization of the SERS substrate itself and it cannot be used to an absolute comparison term for the performance of different SERS substrates. AEF does represent a simple figure for SEF provided that submonolayer coverage is ensured.

The absorption ability of the Ori, Cpl, and 100c colloidal samples towards the R6G probes were estimated in this study using fluorescence quenching experiments. It should be mentioned here that only the free R6G molecule in the colloidal suspension are able to contribute to the fluorescence intensity. The colloidal samples alone and their corresponding supernatants after the centrifugation process exhibited the same fluorescence intensities.

The fluorescence emission spectra in Figure S3 show that the Ori, Cpl, and 100c colloidal samples incubated with R6G at a 10^{-6} M concentration present a significant

decrease in fluorescence intensity ($I_{R6G\text{ in colloid}}$) in comparison with their corresponding supernatants collected after ultracentrifugation ($I_{R6G\text{ in colloid supernatant}}$). The decreased intensity is due to the inability of R6G molecules to fluoresce because of their absorption on the AgNP surface. As expected, dramatic fluorescence intensity reductions were noticed for Cpl and 100c due to the increased number of AgNPs available to adsorb the R6G dye molecules within the same volume when compared to Ori. The actual number of R6G molecules ($C_{R6G\text{ on }AgNP\ surface}$) contributing to the observed SERS enhanced signal (Table 1) was calculated using equation (3) based on the observed changes in intensity and the fluorescence intensity of the R6G bulk solution ($I_{R6G\,bulk\text{ solution}}$) as a reference. The difference in concentration for the R6G solution in the bulk solution (0.75 x 10^{-6} M) and the colloid (10^{-6} M) was also factored in.

$$C_{R6G\text{ on }AgNP\ surface} = 10^{-6}\text{ M x (100\% - }\frac{I_{R6G\text{ in colloid}} - I_{R6G\text{ in colloid supernatant}}}{I_{R6G\,bulk\text{ solution}}}\text{ x }\frac{0.75\text{x}10^{-6}\text{ M}}{10^{-6}\text{ M}}\text{ x 100\%)} \quad (3)$$

The SEF factors were then determined according to the following equation:

$$\frac{SEF}{C_{R6G\text{ on }AgNP\ surface}} = \frac{AEF}{C_{R6G\text{ in }bulk\text{ solution}}} \quad (4)$$

where $C_{R6G\text{ on }AgNP\ surface}$ and $C_{R6G\text{ in }bulk\text{ solution}}$ are the number of R6G molecules on the AgNP surface and in the bulk solution, respectively.

Sample	% of R6G molecules contributing to SERS signal	AEF	SEF
Ori	70	7.3×10^4	5.1×10^1
Cpl	97	7.0×10^7	6.7×10^4
100c	96	8.1×10^7	7.9×10^4

Table S1. Analytical (AEF) and surface (SEF) enhancement factors estimated at an R6G analyte concentration of 10^{-6} M and an excitation wavelength of 632.8 nm.

REFERENCES for MATERIALS AND METHODS

1. Creighton, J.A.; Blatchford, C.G.; Albrecht, M.G. Plasma resonance enhancement of Raman scattering by pyridine adsorbed on silver or gold sol particles of size comparable to the excitation wavelength *J. Chem. Soc., Faraday T. 2*, 1979, *75*, 790-798.
2. Ru, E.C.; Blackie, E.; Meyer, M.; Etchegoin, P.G. Surface Enhanced Raman Scattering Enhancement Factors: A Comprehensive Study *J. Phys. Chem. C.* 2007, *111*, 13794-13803.
3. Ciou, S.H.; Cao, Y.W.; Huang, H.-C.; Su, D.Y.; Huang, C.L. SERS Enhancement Factors Studies of Silver Nanoprism and Spherical Nanoparticle Colloids in The Presence of Bromide Ions. *J. Phys.Chem*. C 2009, *113*, 9520-9525.
4. Nie, S.; Emory, S. R. Probing Single Molecules and Single Nanoparticles by Surface-Enhanced Raman Scattering. *Science* 1997, *275*, 1102-1106.

CHAPTER III

A High-throughput Screen for Nanotechnology-based Antiviral Agents as Demonstrated with Silver Nanoparticles

ABSTRACT

Nanotechnology offers untapped potential into the development of novel antiviral agents; however, no technology exists to screen these new materials for antiviral activity in a high-throughput format. To address this issue a new assay was developed that combines a cellular proliferation assay with a viral vector system to simultaneously measure antiviral activity and cytotoxicity of nanomaterials. Silver nanoparticles, currently generating broad interest and increasing commercial presence as antimicrobials, were chosen to test the new assay's ability to measure antiviral activity in addition to charting the new assays sensitivity in parallel with traditional methods. This new assay was sensitive to viral inhibition spanning 99% of the infectious titer generated with the viral vector system. Significant antiviral activity of silver nanoparticles was observed at doses as low as 2 μg mL^{-1}, while cytotoxicity was found only at doses ≥ 500 μg mL^{-1}, without reaching the LD_{50}. These results reveal a sensitive and innovative method for determining the antiviral activity of nanomaterials in a small-scale, high-throughput manner.

INTRODUCTION

Nanotechnology is currently a hotbed of interest for the development of commercial applications, in particular the discovery of novel antimicrobial agents. Many different nanomaterials have demonstrated innate antibacterial activity but little research exists on their antiviral potential. An explanation for the understudied antiviral properties of nanomaterials stems from the lack of established methods to screen the antiviral activity of nanomaterials, especially in a high-throughput format.

Defined as having one dimension between 1 and 100 nm, nanomaterials are characteristically distinct from their bulk and ionic counterparts due to their large surface-to-volume ratios and unique reactivities. Silver nanoparticles (AgNPs), in particular, were chosen for the current study because they have demonstrated antimicrobial properties (5, 15, 21, 22). Silver, in its ionic form, has been used as an antimicrobial for millennia with little known resistance, and the emergence of nanotechnology has generated new interest in the development of silver as a potent antimicrobial in the post-antimicrobial resistance era. AgNPs are gaining critical attention due to their ever-increasing commercial presence, despite the unknown mechanisms for their antimicrobial action and potential for cytotoxic effects (7, 10, 17, 23).

In order to accurately gauge the potential of nanomaterials as an antiviral agent, a new assay was successfully developed to measure inhibition of viral infection while simultaneously charting the toxicity of the nanomaterial itself. Traditional colony forming unit (CFU) assays for viruses, based on the transduction of a selective marker through a non-lytic virus, are cumbersome and impractical for screening large numbers of drugs at multiple doses. The new assay, based on the standard 3-(4,5-dimethylthiazol-2-

yl)-2,5-diphenyltetrazolium bromide (MTT) cytotoxicity assay employs a high-throughput, small-scale format that will be more efficient and economical, thus enabling more in depth investigations of nanomaterials as antiviral agents.

MATERIALS AND METHODS

Nanoparticle Characterization

Spherical, 25 nm diameter AgNPs were used (NovaCentrix, Austin, TX). The AgNPs were 99.9% pure silver as determined by induction-coupled plasma spectroscopy performed by NovaCentrix. Transmission electron microscopy (TEM) was conducted to confirm size and morphology using a Philips EM 208S operating at 70kV (Royal Philips Electronics, NL; Fig. 1A). AgNPs were negatively stained with 3% uranyl acetate to test for organic capping agents or impurities bound to the particles' surfaces (Fig. 1B). Analysis of TEM images was accomplished using Image-Pro 6.2 software (Media Cybernetics, Inc., Bethesda, MD). Specifically, size measurements were performed by allowing the software to automatically define the perimeter of each nanoparticle, and then calculate the average of multiple diameter measurements for each particle. Prior to use in viral inhibition assays or particle characterization, AgNPs were sonicated for 30 seconds using a Misonix S-4000 ultrasonic liquid processor, with a 419 microtip probe attachment (Misonix, Inc., Farmingdale, NY).

Antiviral Assay

An assay originally developed for measuring HIV-1 mutation rate was modified for high-throughput screening of nanoparticle antiviral activity (8). This assay uses an HIV-1 vector system that measures a single cycle of viral replication through the point of proviral gene expression. The HIV-1 particle carries the hygromycin-B resistance gene

for selection and the envelope protein of *Vesicular stomatitis virus* (VSV), a species of virus from the *Rhabdoviridae* family that enters cells by a pH-dependent fusion mechanism mediated by the envelope protein. This viral pseudotype was produced by transient transfection of three separate plasmids as previously described (8). Briefly, 3 μg of the viral vector backbone (Δgag -pol), 1 μg of the VSV-glycoprotein and 3 μg of the helper plasmid containing gag-pol were transfected via Lipofectamine2000™ (Invitrogen, Carlsbad, CA) into 293T/17 cells (ATCC, Manassas, VA) following the Invitrogen's protocol. 293T/17 cells were plated at 2 x 10^5 cells in 60 mm^2 dishes 24 hours prior to transfection. Forty-eight hours post transfection the supernatant containing the infectious yet replication deficient viral vector, was harvested and used immediately for infections.

Infections for the nanoparticle screen were modified from the previous study by using a quantity of virus equal to or greater than 2.5 times the tissue culture infectious dose 50% ($TCID_{50}$) as determined by the Karber method (11). Infections were performed in 96-well microtiter plates containing Vero76 cells (ATCC, Manassas, VA) at a density of 1 x 10^4 cells per well, plated 24 hours prior to infection. Varying AgNP concentrations, prepared in serum-free cell medium, were mixed 1:1 with fresh, not previously frozen, virus stock for one hour at 37°C. After one hour, medium was aspirated from each well and a 50 μL volume of the virus-AgNP mixture was applied to the appropriate wells. The infection mixture was incubated at 37°C for one hour and removed from the monolayer by aspiration. A final volume of 200 μL of medium was added to each well. Twenty-four hours post-infection, a 200 μL volume of medium containing 400 μg mL^{-1} hygromycin-B (Hyg) was added to each infected well and to the

uninfected selective medium positive control wells. Negative control wells, containing uninfected cells incubated with each AgNP concentration, were given 200 μL of normal, non-selective medium. The medium was replaced in this manner every four days for two weeks to allow for the selective effects of Hyg.

A cytotoxic assay was conducted after the two-week Hyg selection period to quantify viral infection using the chemical MTT as the colorimetric reagent and 0.04 N HCl in isopropanol as the stop solution (16). Trypsin was used as part of the protocol to disrupt colonies and allow cell exposure to the MTT chemical. The optical density (OD) was measured at 570 nm using a Dynatech Laboratories MRX automated plate reader (Dynex, Richfield MN). A One-way ANOVA statistical analysis of the MTT results from three independent experiments was performed using SigmaPlot 11.0 software comparing each dose to the untreated control (Systat Software, Inc., San Jose, CA). P-values of less than 0.050 were considered statistically significant. For each experiment, traditional colony-forming unit (CFU) assays were performed in parallel as previously described to quantify the viral titer and ensure sensitivity in the new assay (8). Briefly, the freshly harvested virus was serially diluted 10-fold, from the undiluted stock down to a dilution of 10^{-4}, and each 10-fold dilution was used to infect Vero 76 cells, which were plated out at 5×10^5 cells in 60 mm^2 dishes 24 hours prior to infection. The infection took place for one hour then infection dilutions were aspirated and replaced with non-selective medium and incubated at 37°C overnight. After 24 hours the medium was changed to selective media containing Hyg. The medium was aspirated and replaced every four days for two weeks, at which time the plates were stained with a solution of 0.1 % Crystal violet in 100% ethanol.

RESULTS

Nanoparticle Characterisitics

AgNPs were evaluated via TEM for size, morphology, and surface coatings (Fig. 1A). Multiple TEM images selected at random from separate preparations were analyzed and over 200 particles were measured to confirm the AgNPs were generally spherical with an average diameter of 25 nm ± 10 nm. Negative staining of AgNPs with uranyl acetate demonstrated that the particles were completely surrounded by the heavy metal stain, gradual darkening up to the perimeter of the nanoparticle, indicating that there were no organic surface modifications such as surfactants or capping agents (Fig. 1B). If organic surface modifications were present the gradual darkening surrounding each nanoparticle would be interrupted by a relatively white-colored halo superficial to the dark nanoparticles' perimeter.

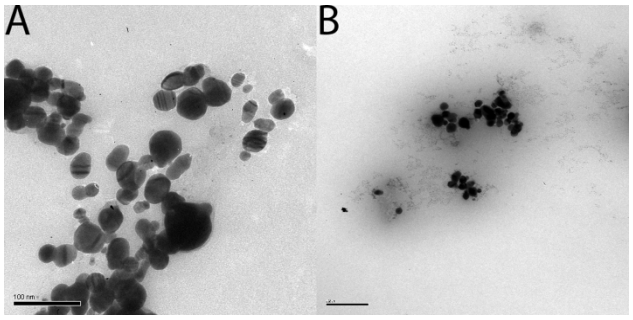

Figure 1. Transmission electron micrographs of AgNPs. A) Unstained AgNPs applied to Formvar coated grid were analyzed for morphology and size, bar = 100 nm. B) AgNPs negatively stained with 3% uranyl acetate to detect organic surface modifications, bar = 0.2 μm.

Antiviral Assay Validation

Viral titers obtained from the new assay were compared to those obtained from the traditional CFU assay in order to validate the new drug-screening platform. As can be seen in Fig. 2, the OD readings from the new assay correlated well with the CFU output of the traditional assay. Two representative fresh virus stocks harvested immediately after the transfection period (one high and one low titer) were chosen for the comparison. The titers of these virus stocks were 10-fold apart as measured by the traditional CFU assay (1 x 10^4 and 1 x 10^3 CFU mL^{-1} for the high and low titer stocks, respectively), which made for a convenient comparison. In agreement with theoretical prediction, when the high-titer virus stock was diluted by 10-fold, it yielded a similar OD reading to that of the undiluted low-titer stock, (compare open circle at dilution 10^{-1} with closed circle at undiluted, Fig. 2). Similarly, when diluted by 100-fold, the high-titer stock gave a similar OD reading to that of the 10-fold dilution of the low titer stock (compare open circle at dilution 10^{-2} with closed circle at dilution 10^{-1}, Fig. 2). The 100-fold dilution of the low-titer stock reached the cut-off OD value of 0.3 for the MTT assay, *i.e.* it was out of the linear range on the lower end (closed circle at dilution 10^{-2}, Fig. 2), and did not follow the same correlation trend. The new assay accurately detected changes in infectious virus over 99 % of the total infectious viral titer generated. The uninfected cell control (closed triangle at undiluted, Fig. 2) showed a similar OD as compared with the undiluted high titer virus stock (open circle, Fig. 2), suggesting that both conditions had reached confluence in their respective wells and attained the upper limit of the assay's linear range.

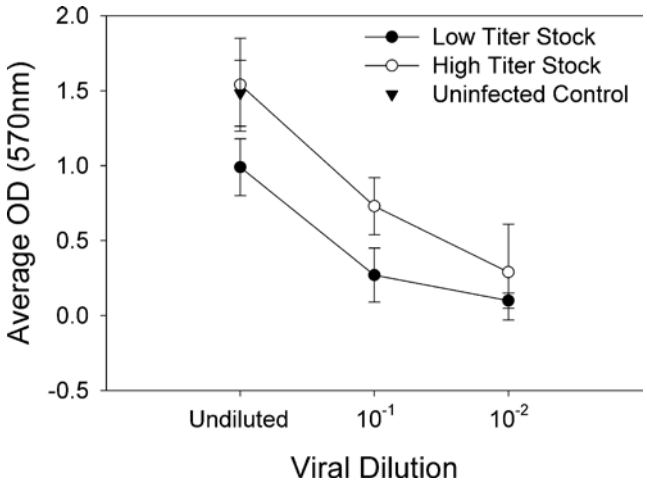

Figure 2. Correlation of viral titers obtained by optical density and colony forming unit readout. Fresh virus stocks were measured in parallel using the new MTT-based assay versus the traditional CFU-based assay.

Nanoparticle Antiviral Activity

The antiviral activity of individual AgNP preparations was measured using the MTT-based assay with three independent, fresh virus stocks (n = 3, Fig. 3). A cytotoxicity assay was performed simultaneously with the antiviral measurement in the same microtiter plate wherein cells were incubated in a non-selective medium with the same doses of AgNPs without the addition of virus (Fig. 3). The AgNPs exhibited statistically significant antiviral activity at doses as low as 2 μg mL^{-1} ($p = 0.005$). The minimum inhibitory concentration 50% (IC_{50}) of AgNPs against the virus was 16 μg mL^{-1}. No false OD readings produced by AgNP reduction of MTT were observed in control experiments where MTT was incubated with various AgNP concentrations (data not shown). Cytotoxicity was insignificant, as demonstrated by one-way ANOVA, at all doses up through 250 μg mL^{-1}($p \geq 0.340$ at 250 μg mL^{-1}). Significant AgNP cytotoxicity was observed beginning at 500 μg mL^{-1} ($p = 0.020$). The increasing variation

associated with the higher concentrations of AgNPs was a consequence of cells reacting differently to these AgNP concentrations between experiments. However, even at the highest dose tested (1,000 μg mL^{-1}, data not shown), toxicity against the cells did not reach the lethal dose 50% (LD_{50}). Thus, the therapeutic index for the AgNPs is greater than 63 as calculated by dividing the LD_{50} by the IC_{50}.

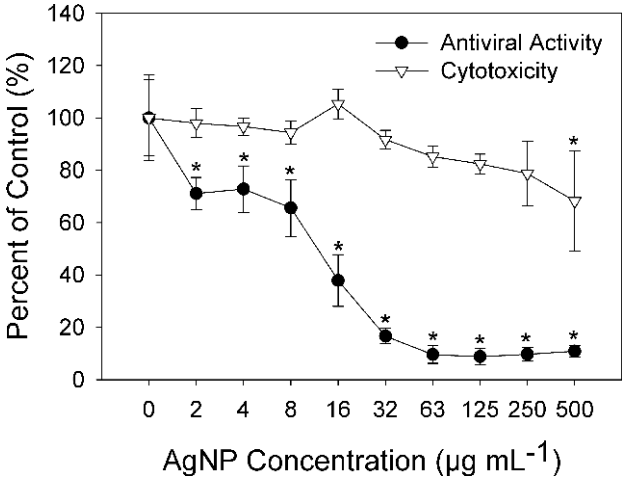

Figure 3. AgNP antiviral activity and cytotoxicity. The new MTT-based assay was used to assess antiviral activity and cytotoxicity across a range of AgNP concentrations. Data are represented as percent of infected, untreated controls. Asterisks above the symbols represent values that were statistically significant compared to the untreated control, as measured by one-way ANOVA for either the antiviral measurements or the cytotoxicity measurements separately (n = 3).

DISCUSSION

Many different tetrazolium-based assays exist for determining cell viability based on metabolic activity. The assay described here utilizes MTT, which has been shown to have advantages over other cytotoxicity assays due to its decreased evaporation errors, low variability, and high sensitivity in 14-day cultures (4, 9, 18, 20). Since MTT is reduced in the cytoplasm instead of at the plasma membrane surface, the chances that nanomaterials bound to the cell surface will interfere with the chemical reduction of the salt or the uptake of other dyes, such as neutral red (1).

Another advantage of MTT-based screening methods for AgNPs and other metallic nanomaterials is the lack of interference with surface plasmon resonances (SPRs), an innate physical property of metal nanoparticles responsible for their characteristic colors, which can interfere with the OD readings of other cytotoxicity assays, typically performed in the 400-500 nm range. The OD reading of the MTT assay is performed at a wavelength of 570 nm, well past the characteristic SPR absorbance of AgNPs (~400 nm) and unaggregated AgNPs less than 30 nm should not demonstrate significant absorbances via SPR at 570 nm (6, 13). This new antiviral assay would also be adaptable for nanoparticles with SPRs around 570 nm as it would be easy to simply utilize a relative of MTT, such as MTS, XTT or WST-1, which absorb at different wavelengths. Dye-based cytoxicity assays, including MTT and its chemical relatives, have been shown to be problematic for certain carbon-based nanoparticles, particularly carbon nanotubes (2, 14, 25). However, a recent study showed that the MTT assay performed well with a non-carbon, metallic nanomaterial (quantum dots) indicating that tetrazolium based assays are a legitimate means for detecting cellular viability and thus

antiviral activity of nanomaterials when coupled with this method (14). The multiple media changes that occur over the course of the new assay further reduce the chance that nanomaterials will interfere with the OD readings because unbound nanomaterials are washed away. MTT has also been shown to be superior to lactate dehydogenase and trypan blue exclusion assays for determining cell viability, and thus antiviral activity when coupled with this new method (3).

MTT-based assays have been used for determining cytotoxicity, viral titers, and antiviral activity through cytopathic effects (CPE) for over 20 years (19). In fact, the National Cancer Institute lists an MTT-based assay as a standard method for characterizing nanomaterial cytotoxicity (24). Utilizing this standard tetrazolium based assay to detect antiviral activity, in addition to cytotoxicity, eliminates the possibility of translating cytotoxic effects of the nanomaterial as antiviral activity during traditional plaque forming unit (PFU) or CFU methods with replication competent viruses. To the authors' knowledge this assay is the first of its kind to replicate the traditional CFU assay, or reduction/neutralization tests, in high-throughput, 96-well plate format for the purposes of screening antiviral activity. The widespread use of the MTT platform, in general, suggests that many laboratories have the required automation capabilities, tools, and reagents to carry out the new assay described within this communication.

Multiple concentrations of AgNPs incubated with the virus were used to determine their antiviral activity. Existing technology, such as the traditional CFU and PFU assays, are labor intensive and as a result do not permit easy examination of various doses. This new assay serves as a preliminary screen for antiviral activity as well as a rudimentary indicator of a possible antiviral mechanism. If antiviral activity is detected

these results will then warrant further examination for the mechanism of antiviral activity, post-exposure efficacy, multiplicity of nanoparticles (MON) required to inhibit infection, cytoprotective effects of the nanomaterial and the MON required for possible cytoprotective effects.

A recent report suggests that inhibition of HIV-1 by AgNPs occurs at an early stage of infection (12). The current assay supports this data by allowing for mechanistic studies in the critical early stage of infection; later events in the viral replication cycle are intentionally blocked through genetic engineering of the virus (8). Furthermore, CPE normally associated with late-stage HIV-1 infection are eliminated, allowing for proliferation to be measured. In this way, CPE of the virus is not mistaken for nanoparticle cytotoxicity.

The viral pseudotyping system employed in the current study broadens the utility of the new assay and provides standardization. Many different viral envelope proteins can be placed on the outside of the HIV-1 particle to simulate infection for different viruses. This interchangeable envelope protein is additionally advantageous through its ability to simulate, at lower levels of biocontainment, viruses normally studied under biocontainment levels 3 and 4. This pseudotyping adaptability ensures that varying levels of CPE that might be associated with the parental viruses are not falsely interpreted as enhanced or reduced antiviral activity against the simulated virions when comparing prospective new agents.

CONCLUSIONS

A new high-throughput screening assay was successfully developed and used to simultaneously measure the antiviral activity and cytotoxicity of nanomaterials in a cell

culture-based system creating a new system by which nanomaterials can be screened for antiviral activity. Furthermore, the results of this assay can serve as a "finger in the wind," from which the direction of future mechanistic studies of nanomaterial antiviral activity. In the process of validating this new assay with a contemporary nanomaterial, silver nanoparticles showed clear-cut antiviral effects and low cytotoxicity, demonstrating a potential treatment with a high therapeutic index. The AgNPs inhibited the virus at an early stage of replication prior to assembly of new particles in the cell. Further investigation into the mechanism of nanoparticle antiviral activity is warranted.

ACKNOWLEDGEMENTS

The Ohio Board of Regents and the Biomedical Sciences Ph.D. Program at Wright State University supported this study.

REFERENCES

1. **Berridge, M. V., P. M. Herst, and A. S. Tan.** 2005. Tetrazolium dyes as tools in cell biology: new insights into their cellular reduction. Biotechnol. Annu. Rev. **11:**127-152. doi: 10.1016/S1387-2656(05)11004-7.

2. **Casey, A., E. Herzog, M. Davoren, F. M. Lyng, H. J. Byrne, and G. Chambers.** 2007. Spectroscopic analysis confirms the interactions between single walled carbon nanotubes and various dyes commonly used to assess cytotoxicity. Carbon. **45:**1425.

3. **da Costa, A. O., M. C. de Assis, A. Marques Ede, and M. C. Plotkowski.** 1999. Comparative analysis of three methods to assess viability of mammalian cells in culture. Biocell. **23:**65-72.

4. **DiStefano, D. J., S. L. Gould, S. Munshi, and D. K. Robinson.** 1995. Titration of human-bovine rotavirus reassortants using a tetrazolium-based colorimetric end-point dilution assay. J. Virol. Methods. **55:**199-208.

5. **Elechiguerra, J. L., J. L. Burt, J. R. Morones, A. Camacho-Bragado, X. Gao, H. H. Lara, and M. J. Yacaman.** 2005. Interaction of silver nanoparticles with HIV-1. J. Nanobiotechnology. **3:**6. doi: 10.1186/1477-3155-3-6.

6. **Evanoff, D. D.,Jr, and G. Chumanov.** 2005. Synthesis and optical properties of silver nanoparticles and arrays. Chemphyschem. **6:**1221-1231. doi: 10.1002/cphc.200500113.

7. **Hobson, D. W.** 2009. Commercialization of nanotechnology. Wiley Interdiscip. Rev. Nanomed Nanobiotechnol. **1:**189-202. doi: 10.1002/wnan.28.

8. **Huang, K. J., and D. P. Wooley.** 2005. A new cell-based assay for measuring the forward mutation rate of HIV-1. J. Virol. Methods. **124:**95-104. doi: 10.1016/j.jviromet.2004.11.010.

9. **Huang, K. T., Y. H. Chen, and A. M. Walker.** 2004. Inaccuracies in MTS assays: major distorting effects of medium, serum albumin, and fatty acids. BioTechniques. **37:**406, 408, 410-2.

10. **Johnston, H. J., G. Hutchison, F. M. Christensen, S. Peters, S. Hankin, and V. Stone.** 2010. A review of the in vivo and in vitro toxicity of silver and gold particulates: particle attributes and biological mechanisms responsible for the observed toxicity. Crit. Rev. Toxicol. **40:**328-346. doi: 10.3109/10408440903453074.

11. **Karber, G.** 1931. Contribution to the Collective Treatment of Pharmacological Serial Experiments. Archive for Pathology and Pharacology. .

12. **Lara, H. H., N. V. Ayala-Nunez, L. Ixtepan-Turrent, and C. Rodriguez-Padilla.** 2010. Mode of antiviral action of silver nanoparticles against HIV-1. J. Nanobiotechnology. **8:**1. doi: 10.1186/1477-3155-8-1.

13. **Lu, X., M. Rycenga, S. E. Skrabalak, B. Wiley, and Y. Xia.** 2009. Chemical synthesis of novel plasmonic nanoparticles. Annu. Rev. Phys. Chem. **60:**167-192. doi: 10.1146/annurev.physchem.040808.090434.

14. **Monteiro-Riviere, N. A., A. O. Inman, and L. W. Zhang.** 2009. Limitations and relative utility of screening assays to assess engineered nanoparticle toxicity in a human cell line. Toxicol. Appl. Pharmacol. **234:**222-235. doi: 10.1016/j.taap.2008.09.030.

15. **Morones, J. R., J. L. Elechiguerra, A. Camacho, K. Holt, J. B. Kouri, J. T. Ramirez, and M. J. Yacaman.** 2005. The bactericidal effect of silver nanoparticles. Nanotechnology. **16:**2346. doi: 10.1088/0957-4484/16/10/059.

16. **Mosmann, T.** 1983. Rapid colorimetric assay for cellular growth and survival: application to proliferation and cytotoxicity assays. J. Immunol. Methods. **65:**55-63.

17. **Oberdorster, G.** 2010. Safety assessment for nanotechnology and nanomedicine: concepts of nanotoxicology. J. Intern. Med. **267:**89-105. doi: 10.1111/j.1365-2796.2009.02187.x.

18. **Pabbruwe, M. B., K. Stewart, and J. B. Chaudhuri.** 2005. A comparison of colorimetric and DNA quantification assays for the assessment of meniscal fibrochondrocyte proliferation in microcarrier culture. Biotechnol. Lett. **27:**1451-1455. doi: 10.1007/s10529-005-1308-x.

19. **Pannecouque, C., D. Daelemans, and E. De Clercq.** 2008. Tetrazolium-based colorimetric assay for the detection of HIV replication inhibitors: revisited 20 years later. Nat. Protoc. **3:**427-434. doi: 10.1038/nprot.2007.517.

20. **Patel, M. I., R. Tuckerman, and Q. Dong.** 2005. A Pitfall of the 3-(4,5-dimethylthiazol-2-yl)-5(3-carboxymethonyphenol)-2-(4-sulfophenyl)-2H-tetra zolium

(MTS) assay due to evaporation in wells on the edge of a 96 well plate. Biotechnol. Lett. **27:**805-808. doi: 10.1007/s10529-005-5803-x.

21. **Rai, M., A. Yadav, and A. Gade.** 2009. Silver nanoparticles as a new generation of antimicrobials. Biotechnol. Adv. **27:**76-83. doi: 10.1016/j.biotechadv.2008.09.002.

22. **Sharma, V. K., R. A. Yngard, and Y. Lin.** 2009. Silver nanoparticles: green synthesis and their antimicrobial activities. Adv. Colloid Interface Sci. **145:**83-96. doi: 10.1016/j.cis.2008.09.002.

23. **Silvestry-Rodriguez, N., E. E. Sicairos-Ruelas, C. P. Gerba, and K. R. Bright.** 2007. Silver as a disinfectant. Rev. Environ. Contam. Toxicol. **191:**23-45.

24. **Stern, S. T., and T. M. Potter.** 2006. Nanotechnology Characterization Laboratory, Method GTA-1 and GTA-2, Version 1.0. Nanotechnology Characterization Laboratory, National Cancer Institute. .

25. **Worle-Knirsch, J. M., K. Pulskamp, and H. F. Krug.** 2006. Oops they did it again! Carbon nanotubes hoax scientists in viability assays. Nano Lett. **6:**1261-1268. doi: 10.1021/nl060177c.

CHAPTER IV

Silver Nanoparticles Inhibit Vaccinia Virus Infection by Preventing Viral Entry

ABSTRACT

Nanotechnology, specifically silver nanoparticles (AgNPs), have gained tremendous attention and increasing presence in consumer products for their antimicrobial properties despite defined mechanisms of activity. *Vaccinia virus* (VACV), is a common analog for the study of *Variola major*, a Category A pathogen and a high priority for the development of effective antiviral agents. This study hypothesized that AgNPs inhibit VACV infection by preventing viral entry. A VACV reporter assay, designed specifically for the viral entry window, demonstrated that AgNPs significantly prevent VACV entry at doses as low as 8 μg mL^{-1} with an IC_{50} value as low as 48 μg mL^{-1}. Confocal microscopy confirmed the anti-entry effect of AgNPs, with significant inhibition as low as 32 μg mL^{-1}. AgNPs prevented both direct fusion and macropinocytosis-dependent entry of VACV in a virucidal capacity. Western blot data suggested that AgNPs may bind directly to the entry fusion complex of VACV at anti-entry concentrations revealing a potential virucidal mechanism. Inhibition of entry was demonstrated at non-cytotoxic doses as determined by MTT and trypan-blue exclusion assay. Observations were made for an additional mechanism of AgNP antiviral activity based on the loss of AgNP anti-entry effects after knockdown of Pak1, a vital component of macropinocytosis. Furthermore, plaque assays demonstrated AgNP inhibition of the

entire VACV replication cycle. These data suggest that AgNPs could be a potent antiviral therapeutic due to their multiple mechanisms of antiviral activity.

INTRODUCTION

Nanotechnology, an emerging field of research for materials with one dimension between 1 and 100 nm, is generating a significant presence among new commercially available products with the general public recognizing it as a buzzword and the scientific community presently hard at work discovering new applications. Metal nanoparticles, particularly silver nanoparticles (AgNPs), have received tremendous attention recently for their observed antimicrobial properties. Applications utilizing AgNPs have multiplied over 1,000% since 2006 with AgNPs representing 313 of the 1317 licensed nanotechnology products (55). Most of the commercial applications for AgNPs are antimicrobial; for example, AgNPs are commercially available as preservatives (*i.e.* clothing and cosmetics), medical devices (*i.e.* coatings for catheters and wound dressings), and as water treatment agents with no defined mechanism for their antimicrobial properties (11, 17, 39).

AgNP antimicrobial activity is a rapidly expanding new field of research and development due to the benefits this technology can provide. For example, because they are a metal, AgNPs are highly resilient to changes in temperature and humidity relative to traditional antimicrobials. AgNPs also have an advantage over traditional antibiotics and antivirals in their lack of microbial resistance. In addition to the benefits over traditional antibacterial and antiviral agents, AgNPs have been observed to exert antimicrobial effects on a wide range of bacteria and viruses, making AgNPs a true broad-spectrum antimicrobial (32). Since an exponentially increasing number of products are approved for public consumption each year, this study sought to understand the mechanisms behind AgNP mediated antiviral activity, for which these products are marketed.

AgNPs exhibit large surface to volume ratio and low coordination numbers that result in enhanced catalytic and reactive abilities which lead to their antimicrobial activity (5, 50). AgNPs bind to biological material non-specifically through their inherent requirement for steric and electrostatic stabilization as a result of their highly polarized surfaces and empty S1 orbital at the zero valent state (5, 30). Covalent bonds are thus easily established, with complexes containing nitrogen (amines/protein), phosphorus (phosphanes/DNA) and sulfur (thiols/protein) being common electron donors (5).

Various mechanisms for the antimicrobial properties of AgNPs have been proposed (38, 40). However, these studies mostly examined the antibacterial properties of AgNPs. Relatively little data is available for the mechanism of AgNP antiviral activity, which could differ drastically due to the inherent differences between bacteria and viruses. The antiviral activity of AgNPs has been documented in many different viral species including the human pathogens HIV-1, HBV, MPV and TCRV (12, 21, 23, 34, 41). Each study suggested that an early event in viral infection is the likely point of AgNP antiviral activity.

Variola major, an Orthopoxvirus and the causative agent of smallpox, is a Category A pathogen and a growing concern as a potential biological weapon due to decreased population immunity as a result of the cessation of vaccination. Study of *Variola major* virus is restricted to only one location within the United States. However, an accurate analog for the study of *Variola major* is available in the form of the virus used as the vaccine for smallpox, *Vaccinia virus* (VACV). Due to the similarities with *Variola major* and its use in vaccination, VACV has become the gold standard for research on Orthopoxviruses. Multiple government agencies have listed the development

therapeutics for Category A pathogens a high priority, which makes VACV an attractive target for investigations into the antiviral activity of AgNPs (49).

VACV is a double stranded DNA virus of about 200kb and it replicates solely in the host cell cytoplasm. The large genome encodes almost all of the structural proteins and enzymes required to complete its replication process (9). There are two infectious forms of VACV: the mature virion (MV) and the extracellular virion, which differ from each other by the number of envelope membranes and a few proteins (33). This study will focus on the MV form of VACV. The infection process begins with VACV adsorption to the membrane of a permissible host cell. This binding to the cell surface is accomplished through VACV membrane proteins A27 and H3, D8, L1 and A26, which bind heparan sulphate, chondroitin sulphate, and laminin respectively (8, 13, 15, 22, 31, 52). At this stage in the infection process the virion is bound to the cell surface but has not yet entered the cell.

VACV demonstrates two methods of entry, which makes it an ideal candidate for the investigation, because these methods can be independently assessed for a better understanding of AgNP mediated anti-entry effects. Both entry methods are dependent on a set of entry fusion complex proteins. Entry of VACV via the entry fusion complex (EFC) has been demonstrated at both neutral and low pH (4, 37, 51). Identified as a complex of proteins, the EFC is composed of A16, A21, A28, F9, G3, G9, H2, I2, J5, L1, L5, and O3, with nine out of twelve of these proteins considered integral members of the EFC as their disruption or removal destabilizes the complex (4, 6, 16, 27-29, 36, 44, 45, 48, 54). The stoichiometry of the complex and its precise mechanism of action have yet to be classified or determined (53).

Entry into the host cell is broadly characterized as the delivery of the virion core to the cytoplasm. The viral core comes equipped with all the enzymes necessary to begin early transcription (33). Once the viral core has entered the cytoplasm, it immediately begins to transcribe early genes (7). This process has been documented to occur within the first six hours of infection and is measurable via reporter assay with protein expression driven by a constitutive early/late promoter (16, 52). One pathway for VACV entry is acid-mediated and dependent on macropinocytosis (10, 43, 46). Additionally, VACV adsorption induces the activation of mediators for macropinocytosis, such as the serine-threonine kinase p21 activated kinase 1 (Pak1); without this cellular signaling component there is little to no macropinocytotic uptake of VACV (25). The other mode of VACV entry is direct fusion of the virion membrane with the plasma membrane (8, 31, 46). Both methods are dependent on the correct function of the EFC.

A mechanism through which viral infection is inhibited by AgNPs has yet to be determined. This study investigates the hypothesis that AgNPs exert their antiviral activity by preventing viral entry. VACV was chosen as the viral system to test this hypothesis due to the increased concern of the use of its close relative *Variola major* in a potential bioweapon and the call for the development of therapeutics for Category A pathogens. Also, VACV demonstrates multiple methods of cellular entry, which can be analyzed separately to gather a clear picture of how AgNPs mediate broad-spectrum antiviral activity.

MATERIALS AND METHODS

Antibodies, cell lines, nanoparticles and viruses.

The BS-C-1 (CCL-26), Vero 76 (CRL-1587) and HeLa (CCL-2) cell lines were acquired form American Type Culture Collection (Manassas, VA) and grown according to manufacturer recommendations. All infections were performed with VACV in the MV form. Powdered AgNPs, certified 99.99% pure silver and average 25 nm in diameter, were acquired from NovaCentrix Inc. (Austin, TX) and further characterized as previously described (Chapter III, Figure 1). NovaCentrix particles were used for every experiment unless otherwise noted. Prior to use, NovaCentrix AgNPs were suspended in ultrapure water and sonicated for 30 seconds via Misonix S-4000 ultrasonic liquid processor equipped with a 419 microtip probe (Misonix Inc., Farmingdale, NY). AgNPs were then diluted, in complete growth medium, to their desired concentrations for each assay. Tangential flow ultrafiltered AgNPs were prepared and characterized as previously described and diluted in complete growth medium (47). Vaccinia immune globulin (NR-2632) was acquired from BEI Rescourses (Manassas, VA). Rabbit-anti-Pak1 monoclonal antibody (2602S) was acquired from Cell Signaling Technology (Beverly, VA) and used according to manufacturer specifications. Rabbit-anti-β-actin monoclonal antibody (#4970S) was acquired from Cell Signaling Technology and used as per manufacturer instructions. Donkey-anti-rabbit polyclonal secondary antibody conjugated to horseradish peroxidase was acquired from Thermo-Fisher-Pierce (#SA1200, Pittsburgh, PA) and used according to manufacturer specifications. Rabbit-anti-G9 polyclonal antibody was acquired from AbCam (#ab93828, Cambridge, UK) and used according to company specifications. vSC56, a genetically engineered Western Reserve strain of VACV

expressing β-galactosidase (β-gal) under the control of a constitutively active early/late promoter in place of the TK gene, was a generous gift from Dr. Hanna Golding at The Food and Drug Administration (24). WR-A4-GFP, a Western Reserve strain of VACV genetically engineered with its A4 core protein fused to GFP, was a generous gift of Dr. Bernard Moss at the National Institute for Allergy and Infectious Disease (3).

Viral stock preparation.

All viruses used in this study were propagated by infecting HeLa monolayers grown to confluence in T-150 flasks (CLS430825-50EA, Sigma-Aldrich Corp., St. Louis, MO). Monolayers were harvested after reaching >90 % cytopathic effects then detached with sterile glass beads. The supernatant was then collected with the culture medium in 50 cc conical tubes and centrifuged for 5 minutes at 514 x g. The supernatant was discarded and the cell pellet was resuspended in 5 mL of PBS and subjected to three rounds of rapid freeze-thaw via dry ice/ethanol bath and 37°C water bath to free MVs trapped within the cells and to disrupt the outer membrane of extracellular virions. Cell debris was then cleared from the lysates by centrifugation for 5 minutes at 514 x g. The supernatant was then collected and syringe filtered through a 0.45 μm filter. The viral suspension was then aliqouted and stored at –70°C until use.

Viral titering.

All viral titering experiments were performed on the BS-C-1 cell line in 6-well plates seeded at 5 $x10^5$ cells per well 24 hours prior to infection. On the day of infection the virus to be titered was diluted in 10-fold serial dilutions in serum free medium and 500 μL of each dilution used to infect the monolayer for 2 hours. After two hours, the infection mix was aspirated and the monolayers overlaid with 2 mL of 1.25 % SeaPlaque

agarose (Lonza Rockland Inc., Rockland, MD) in complete growth medium. Once the overlay solidified at room temperature the plates were incubated at 37°C for 2 days at which time 200 μL of a 1.66 mg mL^{-1} solution of 3-(4,5-dimethylthiazol-2-yl)-2,5-diphenyltetrazolium bromide (MTT) was then dropped on top of the agarose overlay to stain live cells purple and provide contrast for the identification of plaques. Plates were then further incubated at 37°C for 4 hours to let the stain develop and then plaques were counted.

Plaque assay for virion absorption.

Vero76 and BS-C-1 cells were plated at 5 x 10^5 cells per well in each well of a 6-well plate 24 hours prior to the day of the assay. On the day of the experiment WR-A4-GFP at 8.6 x 10^9 pfu mL^{-1} was serially diluted 10-fold and exposed to 0, 8, 32, and 128 μg mL^{-1} of AgNPs for 1 hour at 37°C. After one hour, Vero 76 cells and the AgNP/WR-A4-GFP mixtures were then cooled to 4°C on ice for 30 minutes in order to prevent viral entry. The chilled AgNP/WR-A4-GFP mixture was used to infect the Vero 76 monolayers on ice for 1 hour. After 1 hour, the monolayers were washed three times with ice cold PBS and brought to a final volume of 2 mL PBS after washing. Vero 76 monolayers were then detached from the plate by scraping and collected in 50 cc conical tubes. Cells were then lysed by rapid freeze-thaw three times in a dry ice/ethanol bath, followed by 37°C water bath. After cells were lysed, the lysates were then serially diluted 10-fold and subjected to viral titering on the BS-C-1 cells plated 24 hours previously, as described in the “viral titering” section.

Confocal virion adsorption assay.

Vero 76 cells were plated at a density of 5 x 10^5 cells per well on glass cover slips added to the bottom of 6-well plates 24 hours prior to infection. On the day of the experiment WR-A4-GFP was diluted to a multiplicity of infection (MOI) of 1,000 in complete growth medium containing 0, 8, 32, and 128 μg mL^{-1} of AgNPs and incubated at 37°C for 1 hour. After 1 hour the AgNP/WR-A4-GFP mixture was then chilled to 4°C along with the cells and culture medium for 30 mintues. Once the cells were chilled they were infected with the AgNP/WR-A4-GFP mixtures on ice for 1 hour. After one hour, the infection mixture was removed and the cover slips incubated with 5 μM CellTracker Red CMPTX (Invitrogen, Carlsbad, CA) for 20 minutes on ice then aspirated and washed with ice cold PBS prior to 30 minutes of fixation with ice cold 3.7% formaldehyde in PBS. Cover slips were then mounted and examined as described in "Confocal entry assay for fluorescent VACV."

β-galactosidase entry assay.

The β-gal entry assay was based on a protocol developed by the FDA to measure VACV neutralization after vaccination but modified to make it specific for detecting VACV entry (24). All aspects of the β-gal entry assay were identical to those described previously, except the following which made the assay specific for VACV entry (24): Vero 76 cells were plated at 2.5 x 10^5 cells per well in a 12-well plate 24 hours prior to initiating the assay. On the day of the assay, vSC56 was diluted to an MOI of 10 in complete medium and incubated with various AgNP concentrations for 1 hour prior to use for the virucidal condition. For the cytoprotective condition, cells were treated with AgNP concentrations, at 2-fold incriments from 2 to 256 μg mL^{-1}, for 1 hour then

aspirated prior to infection with untreated vSC56. The AgNP/VACV mixture was then added to the cells for the virucidal condition or untreated vSC56 was added to previously AgNP treated cells for the cytoprotective condition. The infection was then carried out for 4 hours, at which time each well was aspirated then trypsinized with 0.25% trypsin in Hank's Balanced Salt Solution. The trypsin was inactivated by the addition of an equal volume of complete medium and the detached cell suspension was collected in a 1.5 mL tube then centrifuged at 0.3 x g for 5 minutes. The supernatant was discarded and the cell pellet was then lysed with 4 % IGEPAL CA-630 in complete growth medium for a period of 1 hour at 37°C. Optical Densities collected at 570 nm on a Dynex MRX^{e} Revelation plate reader (Dynex Inc., Chantilly, VA) were then used to calculate the percent of untreated control for each sample. For β-gal assays accompanied by a knockdown of Pak1, cells were plated out at 2.5 x 10^5 cells per well two days prior to infection and transfected with siRNA 24 hours prior to infection with vSC56.

β-galactosidase entry assay validation.

As described previously, β-gal standards were used to ensure that the assay was operating within a measurable linear range and VIG was used as a positive control for inhibition of vSC56 entry (24). Briefly, 7 standard concentrations of β-gal were serially diluted from a 1,500 U mL^{-1} stock solution (#10105031001, Roche Diagnostics, Indianapolis, IN) to 0.6, 1.2, 2.3, 4.7, 9.4, 18.6, and 37.5 mU mL^{-1} in 4:1 Z-buffer:PBS. The series of β-gal standards was then incubated with AgNPs at 4, 8, 16, 32, 64, 128, 256, 512, and 1024 μg mL^{-1} for 1 hour at 37°C. After one hour 20 μL of a 4 mg mL^{-1} chlorophenol red β-D-galactopyranoside (CPRG) substrate (#10884308001, Roche Diagnostics, Indianapolis, IN) in 0.1 M sodium phosphate (pH = 7.0) was added to each

standard and incubated at room temperature for 30 minutes. At 30 minutes the OD at 570 nm was read as described in the previous section. The OD values were normalized to AgNP only wells to account for any OD readings brought about by the AgNPs themselves. The standard/AgNP OD values were then plotted against the β-gal concentrations to generate an XY scatter plot from which a linear trend line could be established. The linear trend line was then subjected to R^2 analysis (Microsoft Excel 2003, Microsoft Inc., Redmond, WA). R^2 values less than 0.99 were considered unacceptable, as the standard enzyme did not catalyze the substrate properly. β-gal standards were run in parallel for each β-gal assay to determine if the results were in the linear range and acceptable. VIG was used as a positive control to determine if the assay was capable of detecting vSC56 entry inhibition. The VIG was serially diluted 2-fold and incubated with vSC56 at an MOI of 10 for 1 hour at 37°C. After the one-hour incubation the infections with the VIG/vSC56 mixture were carried out and ODs collected as detailed in the previous section.

Confocal microscopy entry assay with fluorescent VACV.

Vero 76 cells were plated onto glass cover slips in the bottom of 6-well plates 24 hours prior to infection at 5 x 10^5 cells per well. Fluorescent virus WR-A4-GFP was then diluted to an MOI of 1,000 in complete medium containing various concentrations of AgNPs and incubated for 1 hour at 37°C. The AgNP/WR-A4-GFP mixture was then added to cells after the 1-hour incubation for the virucidal condition. For the cytoprotective condition, cells were incubated with various concentrations of AgNPs in complete medium for 1 hour prior to aspiration and addition of untreated WR-A4-GFP at an MOI of 1,000 in complete growth medium. Infections for both the virucidal and

cytoprotective conditions were carried out for 1 hour at 37°C when each well was aspirated. A solution of 1 μM CellTracker Red CMPTX (C34552, Invitrogen, Carlsbad, CA) in serum free medium was then added to each well and incubated at 37°C for 20 minutes. After 20 minutes the CellTracker solution was removed via aspiration and the cover slips were washed with PBS twice. The cover slips were then fixed with 3.7% formaldehyde in PBS for 30 minutes. Cover slips were then removed from their respective wells and mounted on glass microscope slides for viewing on an Olympus FV-300 confocal microscope equipped with both 488 and 568 nm argon and krypton laser excitation lines, respectively. Scans were acquired every 0.4 μm starting below the monolayer and proceeding past the top of the monolayer to encompass each cell in the viewing area. Green and red channels were acquired separately then merged via Fluoview 5.0 software. Each z-stack was then analyzed frame by frame with Image-Pro 6.2 software (Media Cybernetics, Inc., Bethesda, MD) to manually tag each green core within the cytoplasm, stained red by CellTracker Red CMPTX. A total of n = 3 experiments were conducted for each condition and for each experiment a minimum of 150 cells were counted for each condition. Core counts were normalized to the number of cells per condition per experiment. Percentages of untreated controls were then calculated for each experiment and averaged together. For confocal entry assays involving the knockdown of Pak1, cells were plated 48 hours prior to infection. At 24 hours prior to infection the cells were transfected with siRNA specific for Pak1.

Pak1 knockdown via siRNA.

The knockdown of Pak1 was accomplished by transfecting 50 pmol of each of three separate 27-mer siRNAs with Lipofectamine 2000 (Invitrogren) per 5 x10^5 cells, 24

hours prior to use in experiments, according to manufacturers protocols. The siRNA was designed to target regions of high homology for Pak1 between *Homo sapiens* (NCBI Gene ID # 5058), *Mus musculus* (NCBI Gene ID # 18479, *Macaca mulatta* (NCBI Gene ID # 698585) and *Callithrix jacchus* (NCBI Gene ID # 100392970). The target sequence of siRNA1 is UUAGCUUGACAGAGCCAUCCAUUCCCA. The target sequence of siRNA2 is AGUCUCAGACACAGCCUUCACAUUCAA. The target sequence of siRNA3 is AUUAUAAUCCUCAGCUGACUUAUCUGU. All siRNAs were synthesized by Integrated DNA Technologies (IDT, Coralville, IA).

Western blotting.

Cellular lysates were created by pelleting cells at 0.3 x g after trypsinization then adding lysis buffer containing phoshatase inhibitors (50 mM Tris-HCl pH 8, 120 mM NaCl, 5 mM NaPPi, 10 mM NaF, 30 mM paranitrophenylphosphate, 1 mM benzamidine, 0.1%NP-40, 1% Triton X-100, and 0.2 mM PMSF, 100 nM sodium orthovanadate) supplemented with protease inhibitors. A BCA protein content analysis kit was then used to determine the protein content of the lysates (#23221, Thermo-Fisher-Peirce, Pittsburgh, PA). Fifty micrograms of protein were then diluted and boiled for 10 minutes with a loading dye containing 0.5M dithiothreitol, 10% sodium dodecyl sulfate, 0.5M Tris (pH 6.8), 50% glycerol and 0.2% bromophenol blue. Lysates were then resolved on a 10 % SDS-PAGE gel (C = 3.3%) and then transferred to a polyvinylidene fluoride membrane (PVDF). The PVDF membrane was then probed with primary antibody specific for Pak1, β-actin, G9 or GFP according to manufacturer specifications. Secondary antibody conjugated to horseradish peroxidase were then added according to manufacturer protocol then detected via Supersignal Westpico Chemiluminescent

Substrate kit (Thermo-Fisher-Pierce, Pittsburg, PA). Chemiluminesense was detected using a Fuji LAS-4000 gel documentation center (Fujifilm, Tokyo, Japan). Densiometry readings were measured via Multiguage software (Fujifilm). For the western blot analyzing mobility shift in G9 and A4-GFP, AgNPs were added directly to WR-A4-GFP stocks at 0, 10, 100, or 1,000 ug mL^{-1}, then incubated for 1 hour at 37°C for one hour. After one hour, virus was lysed by adding 2x radio-immuno-precipitation-assay (RIPA) buffer to an equal volume of virus/AgNP mixture and the whole lystae was then resolved by SDS-PAGE and immunoblot analysis, as described above. The 2x RIPA buffer contained 300 mM sodium chloride, 2% IGEPAL CA-630, 1% sodium deoxycholate, 0.2% SDS and 100 mM Tris, pH = 8.0.

Plaque reduction assays.

Plaque reduction assays were conducted using WR-A4-GFP tittered at 8.6 $x10^9$ pfu mL^{-1} as the untreated control. For the cytoprotective condition of the plaque reduction assays, cells were incubated with various concentrations of AgNPs (one concentration per experiment) for 1 hour at 37°C prior to infection with 10-fold serial dilutions of untreated virus in complete growth medium. Virucidal plaque reduction assays were conducted by incubating the 10-fold serial dilutions of WR-A4-GFP with concentrations of AgNPs at 32 μg mL^{-1} for one hour at 37°C prior to infecting BS-C-1 monolayers. This concentration of AgNPs was used for the plaque assays as it demonstrated significant inhibition of viral entry during the β-gal for overall VACV entry. After the hour incubation of the cells with AgNPs for the cytoprotective condition or the virus with AgNPs for the virucidal condition infections were performed in a procedure identical to that detailed in the “Viral titering” section. For post-infection plaque reduction assays

infections were carried out as described in the "Viral titering" section with the addition of AgNPs at 32 μg mL^{-1} to the 1.25 % SeaPlaque agarose overlay.

Cytotoxicity of AgNPs.

Vero 76 cells were plated at 2.5 $x10^5$ cells per well in 96-well plates 24 hours prior to treatment with AgNPs. On the day of each experiment AgNPs were diluted in complete growth medium and added to corresponding wells of the plate for 1, 4, 24 and 48 hours. At the end of each time point the wells of the plate were aspirated and washed 3 times with PBS then 100 μL of complete growth medium was again added to each plate along with 30 μL of a 1.66 mg mL^{-1} solution of MTT. The plate was then incubated for 4 hours at 37°C. At the end of the 4 hours, cells and MTT were solubilized with 0.04 N HCl in 2-propanol at which point the OD at 570 nm was then read on a Dynex MRX[e] plate reader. Control conditions containing AgNPs and cells with no MTT were used to normalize the OD results for each AgNP condition and thus account for any OD reading from the AgNPs themselves.

Statistical analysis, plots and IC_{50}/LD_{50} Calculations.

SigmaPlot 11.0 software (Systat & Mystat Products, Chicago, IL) was used to create graphs and conduct One-way ANOVA statistical alalyses. Percent of control values for test conditions were compared to the 100 % untreated control groups. P-values of less than 0.05 were considered statistically significant. Inhibitory concentration 50% (IC_{50}) and lethal dose 50% (LD_{50}) values were calculated according to the Karber Method with a positive or negative reaction boundary at 50 % of the untreated control (18). Adobe Photoshop was used to crop and size graphics (Adobe Systems Inc., San Jose, CA).

RESULTS

Effect of AgNPs on adsorption of VACV to host cells.

In order to determine the point at which AgNPs inhibit VACV infection, adsorption of VACV was first investigated. The plaque assay used to measure adsorption of VACV relies on infecting cells at non-entry conditions, washing out unbound virions and then lysing cells to recover infectious virus that had adsorbed. AgNPs at 2, 8, 32, and 128 μg mL^{-1} exhibited the same titer as the untreated condition, 0 μg mL^{-1} (Figure 1A). The slight increase in viral titers observed from VACV treated with 128 μg mL^{-1} was not statistically significant by One-way ANOVA analysis. The results of the plaque assay suggest that AgNPs at all concentrations tested had no effect on the adsorption of VACV to host cells. Confocal microscopy using a Western Reserve strain of VACV expressing GFP fused to the core protein A4 was then used to corroborate the findings of the plaque assay (Figure 1B). The confocal assay demonstrated that AgNPs at concentrations of 8, 32, and 128 μg mL^{-1} had measurements within the range of the untreated control. Each of the concentrations tested was not statistically significant from the untreated control, as determined by One-way ANOVA. These results suggest that AgNPs had no affect on VACV's ability to adsorb to the host cell.

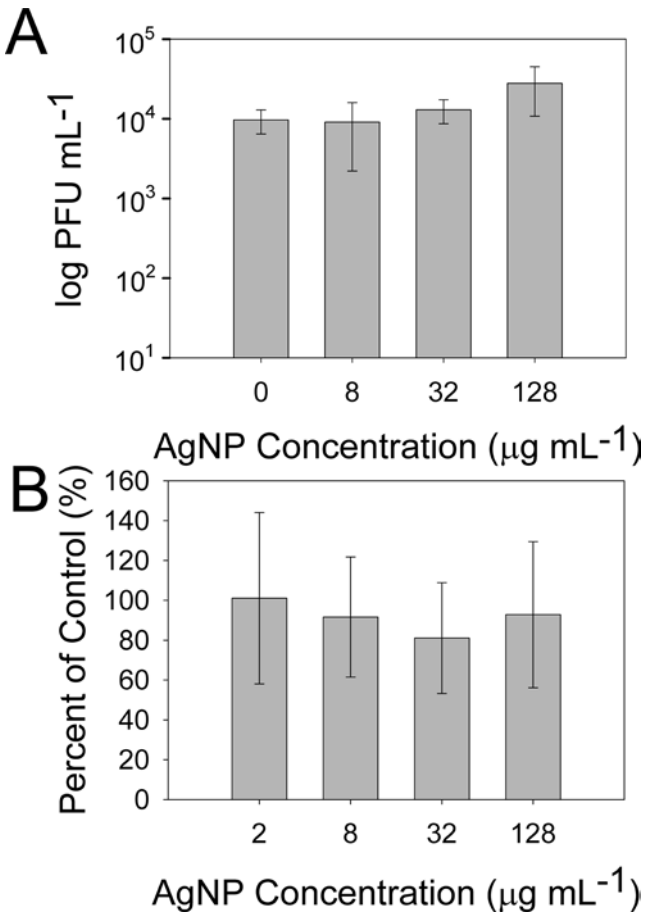

Figure 1. Effect of AgNPs on adsorption of VACV to host cells. A) Viral titers obtained from WR-A4-GFP treated with various concentrations of AgNPs then allowed to adsorb to host cells under non-entry permissive conditions. B) Confocal microscopy quantification of WR-A4-GFP bound to host cells under non-entry permissive conditions after treatment with various AgNP concentrations. Each AgNP concentration is compared to the untreated control.

Effects of AgNPs on overall VACV entry.

After adsorption, entry/fusion with the host cell is the next step in the VACV infection cycle. To monitor the effect of AgNPs on this stage of VACV infection, an assay measuring entry/fusion was developed utilizing VACV expressing β-gal under the control of a constitutively active promoter. Since the proposed assay utilized β-gal, the effect of AgNPs on the enzyme's ability to catalyze its substrate was investigated. The R^2 values obtained from every AgNP treatment condition, from 2 through 1024 ug mL^{-1}, were above the acceptability threshold of the assay indicating that the β-galactosidase enzyme activity is not altered by the presence of AgNPs ($R^2 > 0.99$, data not shown).

To further validate the β-gal assay as capable of measuring VACV entry at 4 hours post-infection, a known inhibitor of entry, VIG, was used as a positive control. A clear dose dependent decrease in β-gal expression was found, with statistically significant inhibition starting at 48 μg mL^{-1}, as determined by One-way ANOVA ($p = 0.032$, Figure 2). Uninfected cells were used as a negative control and demonstrated OD values outside of the linear range of the assay indicating that the target cell line does not endogenously express β-gal (data not shown).

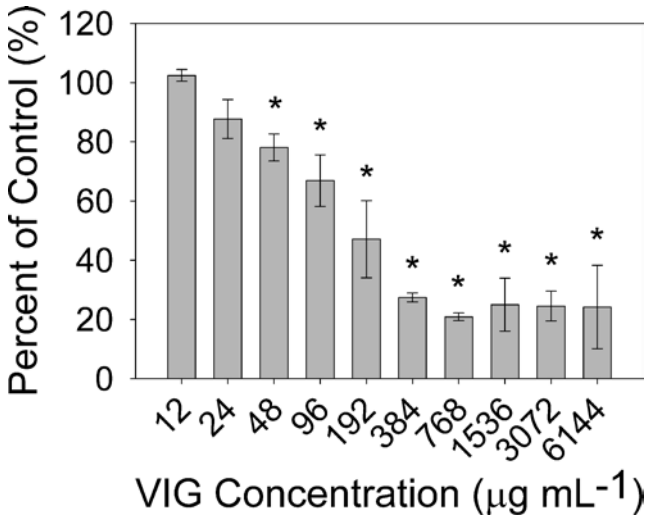

Figure 2. Validation of β-galactosidase VACV entry assay. β-galactosidase expression quantifying vSC56 entry in the presence of a known entry inhibitor, VIG. Each VIG concentration is compared to the untreated control. Asterisks above a data point indicate statistical significance, as compared to untreated control, according to One-way ANOVA ($p \leq 0.05$, $n = 3$).

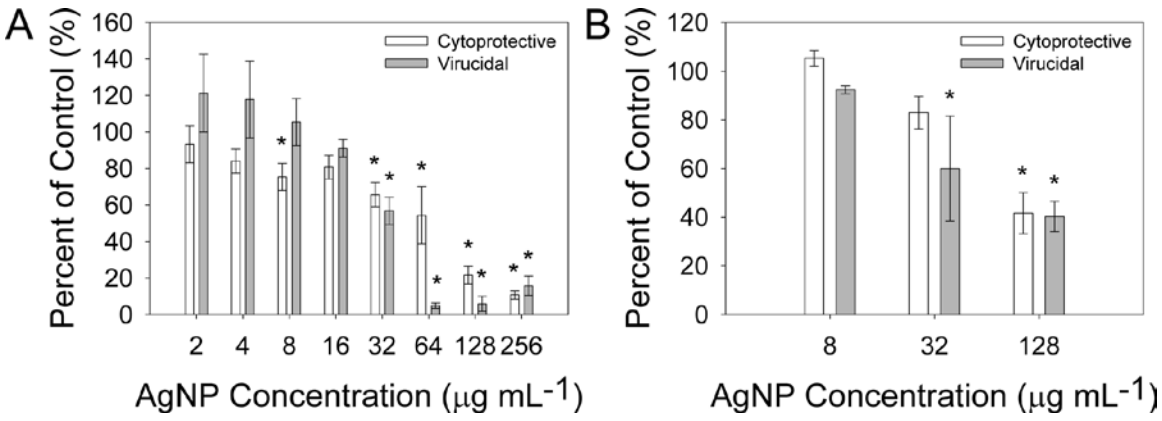

Figure 3. Effects of AgNPs on overall VACV entry. Asterisks above a data point indicate statistical significance, as compared to untreated control for each treatment condition, according to One-way ANOVA ($p \leq 0.05$, $n = 3$ for all experiments). A) β-galactosidase expression from vSC56 quantifying overall viral entry in the presence of various NovaCentrix AgNP concentrations. The cytoprotective group represents cells incubated for 1 hour with AgNPs prior to infection with untreated vSC56. The virucidal group represents vSC56 treated with AgNPs for 1 hour prior to use in infection. Each AgNP condition is compared to the untreated control. B) Confocal microscopy quantification of WR-A4-GFP entry in the presence of various AgNP concentrations. The cytoprotective group represents cells incubated for 1 hour with AgNPs prior to infection with untreated vSC56. The virucidal group represents vSC56 treated with AgNPs for 1 hour prior to use in infection. Each AgNP condition is compared to the untreated control.

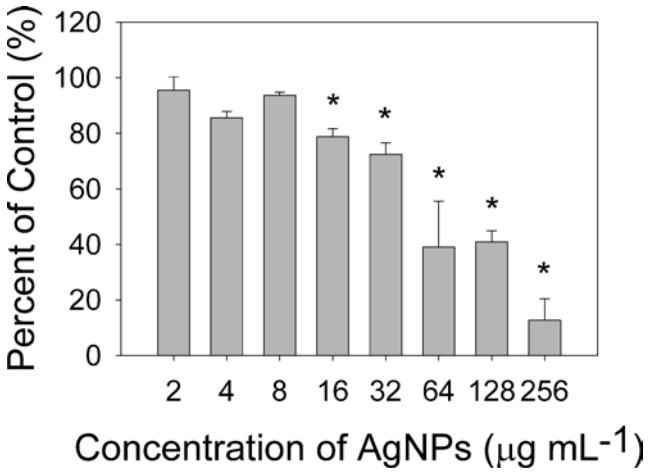

Figure 4. Tangential flow ultrafiltered AgNP virucidal effects on VACV entry. Asterisks above a data point indicate statistical significance, as compared to the untreated control, according to One-way ANOVA ($p \leq 0.05$, $n = 3$). β-galactosidase expression from vSC56 quantifying overall viral entry in the presence of various filtered AgNP concentrations.

Having established that VACV entry, and inhibition of this process, could be reliably detected, AgNPs were then evaluated for their potential virucidal and cytoprotective effects on overall VACV entry, both direct fusion and macropinocytosis-dependent fusion. The cytoprotective condition, in which cells were incubated with AgNPs prior to infection with untreated virus, demonstrated statistically significant inhibition of viral entry, as determined by One-way ANOVA, starting at 8 μg mL^{-1}, $p = 0.020$, with a break in statistical significance at 16 μg mL^{-1}, $p = 0.107$. Statistically significant inhibition resumed at 32 μg mL^{-1}($p < 0.001$), and continued through the highest dose examined, 256 μg mL^{-1} (Figure 3A). Additionally, the cytoprotective condition exhibited a dose dependent decrease in VACV entry through the highest dose examined with an IC_{50} of 90.66 μg mL^{-1}. The virucidal condition, in which VACV was treated with AgNPs prior to infection, exhibited statistically significant inhibition of

VACV entry, as determined by One-way ANOVA, starting at 32 μg mL^{-1}, p = 0.003, and continuing through the highest dose tested, 256 μg mL^{-1}. A dose dependent decrease in viral entry was also observed for the virucidal condition with a sharp drop in viral entry occurring above 32 μg mL^{-1}. The IC_{50} value for the virucidal condition was 48 μg mL^{-1}.

Confocal microscopy was used to corroborate the findings of the β-gal entry assay using WR-A4-GFP. The cytoprotective condition exhibited a dose dependent decrease in VACV entry with statistically significant inhibition at 128 μg mL^{-1}, $p < 0.001$ (Figure 3B). The IC_{50} for the cytoprotective condition was 88 μg mL^{-1}. The virucidal condition exhibited statistically significant and dose dependent inhibition of VACV entry starting at 32 μg mL^{-1}, with p = 0.010, and p = 0.001 for 32, and 128 μg mL^{-1} respectively (Figure 3B). The IC_{50} value for the virucidal condition was 88 μg mL^{-1}. Together, these data indicate that the β-gal entry assay can measure VACV entry and that AgNPs inhibit overall VACV entry at low, therapeutic level concentrations.

Tangential flow ultrafiltered AgNPs were also used in the β-gal entry assay in a virucidal capacity (Figure 4). Much like the NovaCentrix AgNP examined in Figure 3, the filtered AgNPs exhibited a dose depended decrease in β-gal expression correlating to a decrease in vial entry. Statistically significant inhibition of VACV entry, as determined by One-way ANOVA, started at 16 μg mL^{-1} and continued through the highest dose tested (p = 0.015, n = 3). The IC_{50} value from the filtered AgNPs was 128 μg mL^{-1}. The observation that two entirely different sets of AgNPs mediate an antiviral effects by preventing VACV entry suggests that AgNPs, in general, exert their antiviral effects at the entry stage of VACV infection.

Effects of AgNPs on the direct fusion entry pathway of VACV after Pak1 knockdown.

In order to determine if the effect of AgNP inhibition of viral entry was specific to the direct fusion or macropinocytotic entry pathway of VACV, Pak1, a critical mediator of macropinocytosis by functioning as a key signaling kinase to affect cytoskeleton rearrangement, was knocked down via siRNA (25). Figure 5A demonstrates the efficacy of each siRNA, individually and all together, to knockdown Pak1 expression. After normalization to β-actin, siRNA#1, siRNA#2, and siRNA#3 demonstrated a 9, 54, and 81% knockdown of Pak1, respectively. However, all three siRNAs together (All, Figure 5A) were capable of generating an 87% knockdown of Pak1 expression compared to the non-silencing control. A qualitative analysis through the uptake of a fluorescently labeled dextran was also performed and demonstrated that all three siRNAs together reduced fluid phase uptake among target cells (Supplemental Figure 1).

By knocking down Pak1 and subsequently reducing macropinocytosis in target cells the macropinocytosis-dependent entry of VACV would be largely reduced. In conjunction with Pak1 knockdown the ability of AgNPs to inhibit the direct fusion entry pathway of VACV was then examined with the β-gal entry assay. Knockdown of Pak1 significantly inhibited VACV virus entry as β-gal expression values averaged only ~60% of the non-silencing control (data not shown). The cytoprotective condition exhibited very little ability to inhibit the direct fusion entry pathway of VACV with no statistically significant inhibition of viral entry revealed after One-way ANOVA analysis.

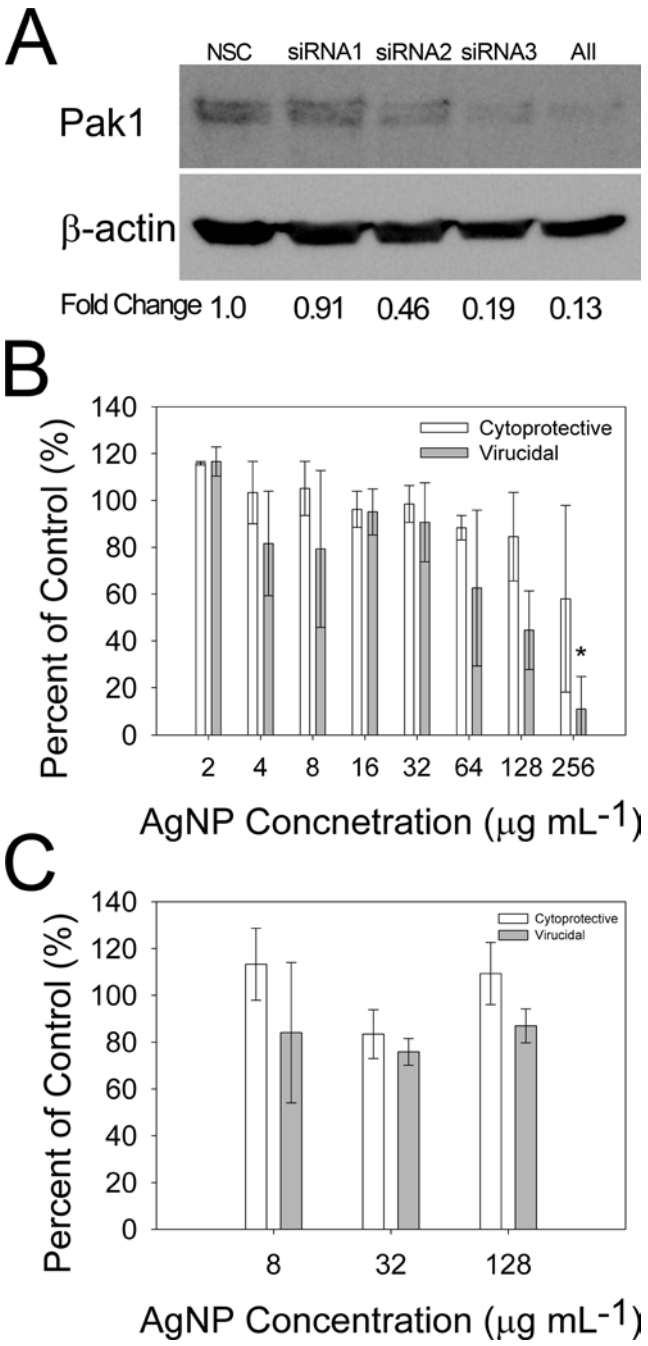

Figure 5. Effect of AgNPs on the direct fusion entry pathway of VACV after Pak1 knockdown. Asterisks above a data point indicate statistical significance, as compared to the untreated control for each condition, according to One-way ANOVA ($p \leq 0.05$, $n = 3$ for all experiments). A) Western blot quantification of Pak1 knockdown via siRNA. NSC = non-silencing control; All = all three siRNAs together. B) β-galactosidase expression from vSC56 quantifying VACV entry after Pak1 knockdown in the presence of various AgNP concentrations. Each AgNP concentration is compared to the silenced, untreated

control on the y-axis. One-way ANOVA analysis for statistical significance was performed on each AgNP treatment group compared to the silenced, untreated control. C) Confocal microscopy quantification of WR-A4-GFP entry after Pak1 knockdown in the presence of various AgNP concentrations. Each AgNP concentration is compared to the silenced, untreated control. A One-way ANOVA was performed on each AgNP treatment group compared to the silenced, untreated control.

No IC_{50} value was obtained for the cytoprotective condition. The virucidal condition exhibited a decrease in VACV direct fusion entry; however, the AgNP effect on direct fusion of VACV was less potent than that found during examination of overall VACV entry. Statistically significant inhibition of VACV direct fusion was only observed at 256 $\mu g\ mL^{-1}$, $p = 0.001$ (Figure 5B). The visible decreases in viral entry observed at 64, 128 and 256 $\mu g\ mL^{-1}$ corresponded to 23, 26, and 57% reductions in direct VACV entry compared to the Pak1 silenced, untreated control. No IC_{50} value was reached for the virucidal condition. These data indicate that AgNP anti-entry activity may largely require host cell functions dependent on Pak1 activity, such as macropinocytosis. However, a slight dose dependent decrease in viral entry was still observed for VACV treated with AgNPs prior to infection suggesting that AgNPs might prevent direct fusion in a virucidal fashion.

Confocal microscopy was again used to corroborate the results of the β-gal entry assay. Silencing Pak1 demonstrated a significant effect on the number of WR-A4-GFP cores found in the cytoplasm, with an average of ~60% of the non-silencing control (data not shown). The cytoprotective and virucidal conditions exhibited no statistically significant inhibition of the direct fusion entry pathway for VACV at any of the doses examined (Figure 5C).. No IC_{50} values were reached for either condition. These confocal

data obtained during the knockdown of macropinocytosis-dependent entry demonstrate that AgNPs may require the function of Pak1, and possibly macropinocytosis, for effective inhibition of VACV entry.

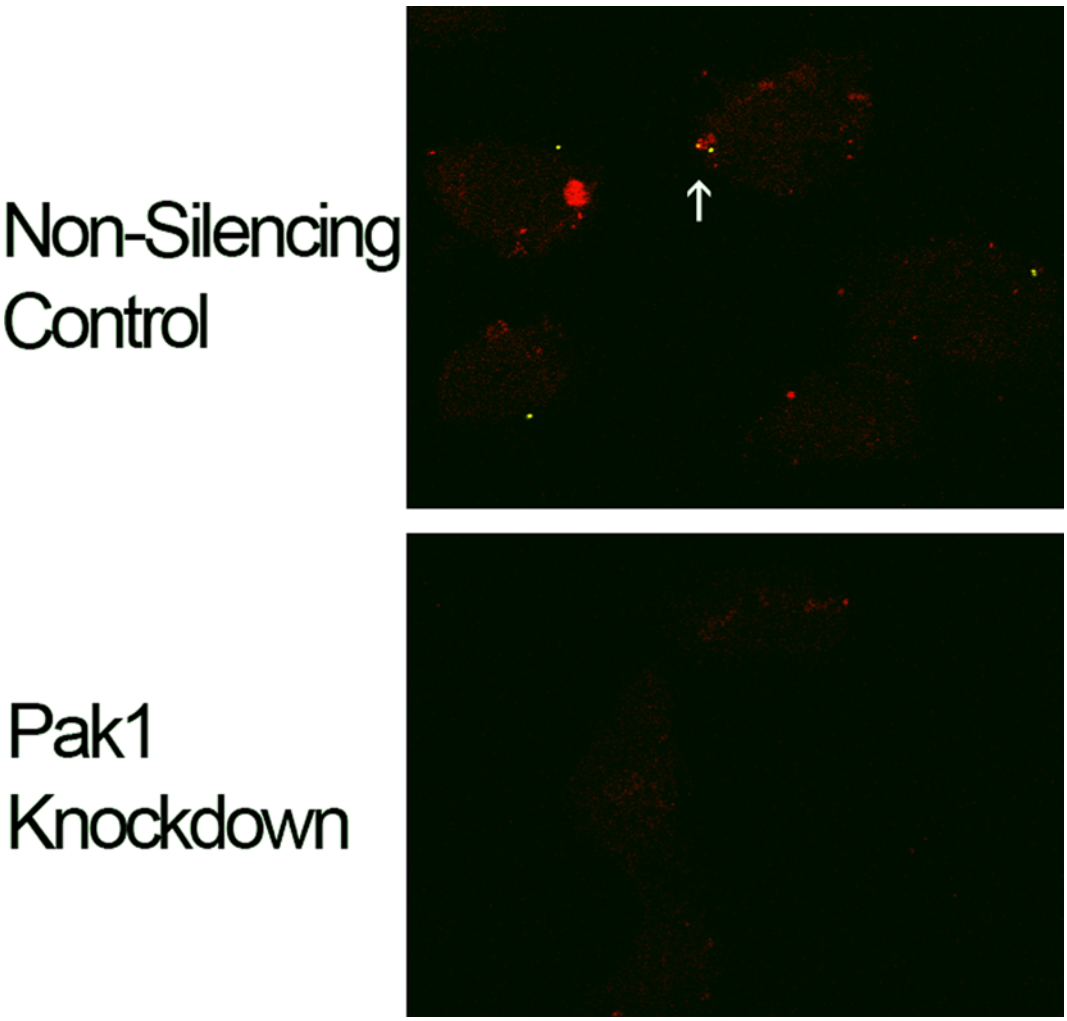

Supplemental Figure 1. Fluid Phase Uptake Before and After Pak1 Knockdown. Vero 76 cells were plated at a density of 5 x10^5 cells per glass cover slip and transfected at 24 hours with three siRNAs targeting Pak1 as outlined in the methods section. At 24 hours post-transfection cells were infected with WR-A4-GFP as described in the methods section, then pulsed for 10 minutes with a 1 mg mL^{-1} solution of Rhodamine B-isothiocyanate (RITC) labeled 10,000 molecular weight dextran (#R8881, Sigma-Aldrich, St. Louis, MO). Cells were then washed three times with PBS then fixed for 30 minutes in 3.7% formaldehyde in PBS. Confocal images were then acquired, under identical exposure conditions, as described in the methods section. Both images above are examples of one slice taken through the middle of the z-stack acquired during analysis. Arrow indicates fluid phase uptake of the RITC-labeled dextran along with WR-A4-GFP.

Effects of AgNPs on the entire replication cycle of VACV.

To determine if the inhibition of VACV by AgNPs translated to global decreases in VACV replication, a plaque reduction assay was performed. An AgNP dose of 32 μg mL-1 was chosen to perform these plaque assays because this dose demonstrated significant antiviral activity in the overall entry β-gal assay (Figure 3). Untreated VACV generated an average control titer of 8.6×10^9 pfu mL^{-1} (Figure 6, Untreated, n = 2). The virucidal condition, representing virus treated with 32 μg mL^{-1} for one hour prior to use in infection, demonstrated a titer of 1.5×10^6 pfu mL^{-1}, a 3.8-log reduction in viral titer when compared to the untreated control (Figure 6, Virucidal, n = 2). The cytoprotective condition, representing cells treated with 32 μg mL^{-1} for one hour prior to infection with untreated virus, generated a titer of 6.6×10^5 pfu mL^{-1}, a 4.1-log reduction in viral titer when compared to the untreated control (Figure 6, Cytoprotective, n = 2). The post-infection condition, representing untreated cells infected with untreated virus and then treated with 32 μg mL^{-1} AgNPs, exhibited a titer of 1.5×10^5 pfu mL^{-1}, a 4.8-log reduction in titer compared to the untreated control (Figure 6, Post-Infection, n = 2). The virucidal, cytoprotective, and post-infection treatments of 32 μg mL^{-1} AgNPs demonstrated statistically significant differences from the untreated control as determined by One-way ANOVA, p = 0.009, p = 0.009, and 0.012 respectively. Additionally, a 2-log reduction in viral titer was observed at both 8 and 16 μg mL^{-1} of virucidal treatment with AgNPs (data not shown, n = 1 for both). The inhibition of the entire VACV replication cycle suggests that AgNP inhibition of VACV entry has profound effects on viral replication kinetics whether AgNPs are administered in cytoprotective, virucidal, or post

infection fashion. Such drastic inhibition of viral replication could also be the result of an as yet unknown mechanism(s).

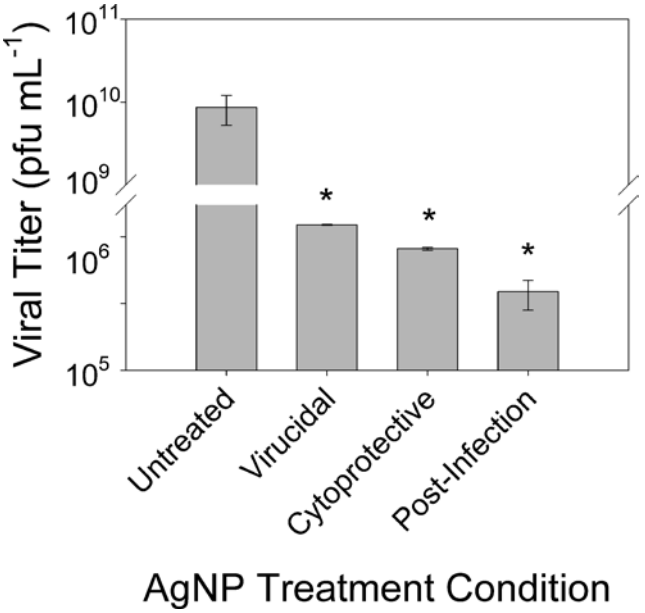

Figure 6. Effects of AgNPs on the entire replication cycle of VACV. The Untreated group represents VACV receiving no AgNP treatement. The Virucidal group represents VACV treated with 32 μg mL^{-1} AgNPs for 1 hour prior to infection. The Cytoprotective group represents cells treated with 32 μg mL^{-1} AgNPs for 1 hour prior to infection. The Post-Infection group represents untreated cells infected with untreated VACV then overlaid with a 1.25 % agarose growth medium containing 32 μg mL^{-1} of AgNPs. Asterisks above a data point represent statistical significance, as compared to the untreated control, according to One-way Anova ($p \leq 0.05$, $n = 2$ for all).

AgNPs bind to the entry fusion complex of VACV.

Western blot was used to investigate the potential of AgNPs to bind to the EFC of VACV to establish a possible mechanism of AgNP-mediated antiviral activity. A reproducible (n = 2), dose dependent decrease in the mobility of EFC complex protein G9 was observed upon treatment of whole VACV virions with AgNPs (Figure 7, top panel). Treatment of the virus at 100 and 1,000 μg mL^{-1} of AgNPs retarded the mobility of G9 equally, with 10 μg mL^{-1} showing retardation between that of the untreated control and the bands at 100 and 1,000 μg mL^{-1}. The untreated control showed a typical migration pattern of a ~39 kD protein, G9 = 38.7 kD. Since the WR-A4-GFP virus was used for these experiments, it was then possible to examine the migration of A4-GFP on the same blot to determine if AgNPs were capable of penetrating the viral membrane and binding the core fraction of the virus (Figure 7, bottom panel). The majority of the A4-GFP protein showed no mobility shift as indicated by the thicker bands in the lower panel of Figure 7; however, the 100 and 1,000 μg mL^{-1} AgNP treatment conditions had a small portion of the total A4-GFP protein demonstrating a mobility shift .The shift in A4-GFP was dose dependent with decreased mobility associated with increased AgNP dose. It is possible that the process of lysing the virions gave excess AgNPs in the solution a chance to bind the core proteins as well. These results suggest AgNPs are capable of binding to viral proteins. Since G9 is an integral member of VACV's EFC this binding may hinder function of the EFC, generating a possible mechanism for virucidal AgNP-mediated anti-entry effects.

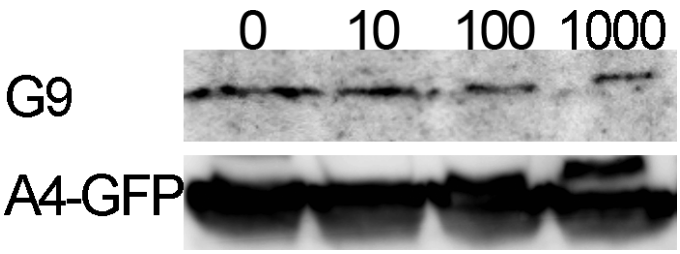

Figure 7. AgNPs bind to the entry fusion complex of VACV. WR-A4-GFP was treated with 0, 10, 100 or 1,000 μg mL^{-1} AgNPs (indicated above the blots) and then subjected to western blot with antibodies specific for the G9 protein, a member of the EFC, or GFP to detect mobility shifts in the respective proteins.

Cytotoxicity of AgNPs.

In order to determine if the inhibition of viral entry was a function of AgNP cytotoxicity and to gauge the therapeutic index of AgNPs, a standard MTT metabolic/cytotoxicity assay was performed. At one hour of AgNP exposure, mimicking the cytoprotective condition of the β-gal assays and all the confocal data, no statistically significant cytotoxic effects were detected as determined by One-way ANOVA comparing each dose to the untreated control (Figure 8, 1 hr). No LD_{50} was reached at 1 hour of AgNP exposure. At 4 hours of AgNP exposure, mimicking the virucidal condition of the β-gal assays, there was a dose dependent decrease in the metabolic function of the target cells starting at 32 μg mL^{-1} and continuing through the highest dose tested (Figure 8, 4 hr). Statistically significant metabolic decreases, attained through One-way ANOVA comparing each dose to the untreated control, were observed above 64 ug mL^{-1}, $p < 0.001$. However, the widely used trypan blue assay for detecting membrane integrity, demonstrated that at 4 hours of AgNP exposure cell membranes were intact excluding the dye. No differences in cellular morphology were detected at this

magnification for all AgNP concentrations tested in the MTT assay. These data indicate that at 4 hours of AgNP exposure the cells were intact but impaired metabolically (Supplemental Figure 2, dead cells associated with dye uptake indicated with arrows). At 24 hours of AgNP exposure there was no statistically significant cytotoxicity, as determined by One-way ANOVA comparing each dose to the untreated control, indicating that the decreased metabolic function observed at 4 hours was a temporary state and that the cells recovered (Figure 8, 24 hr).. A One-way ANOVA analysis of MTT results from cells exposed to AgNPs for 48 hours exhibited no statistically significant decrease in metabolic function when compared to the untreated control (Figure 8, 48 hr). These findings show that AgNPs exert their antiviral, anti-entry effects at non-cytotoxic concentrations and that there may be additional mechanism(s) for AgNP antiviral activity involving a decreased metabolic state around 4 hours of AgNP exposure.

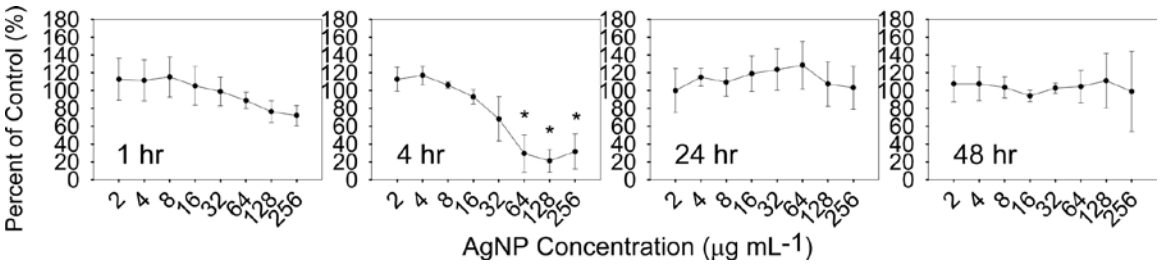

Figure 8. Cytotoxicity of AgNPs. MTT cytotoxicity data collected after 1, 4, 24 and 48 hours of exposure to various AgNP concentrations (time points indicated in the bottom left hand corner of each graph). The percent of control on the y-axis refers to the untreated control at each time point. Asterisks above a data point indicate statistical significance, as compared to the untreated control for each time point, according to One-way ANOVA ($p \leq 0.05$, $n = 3$).

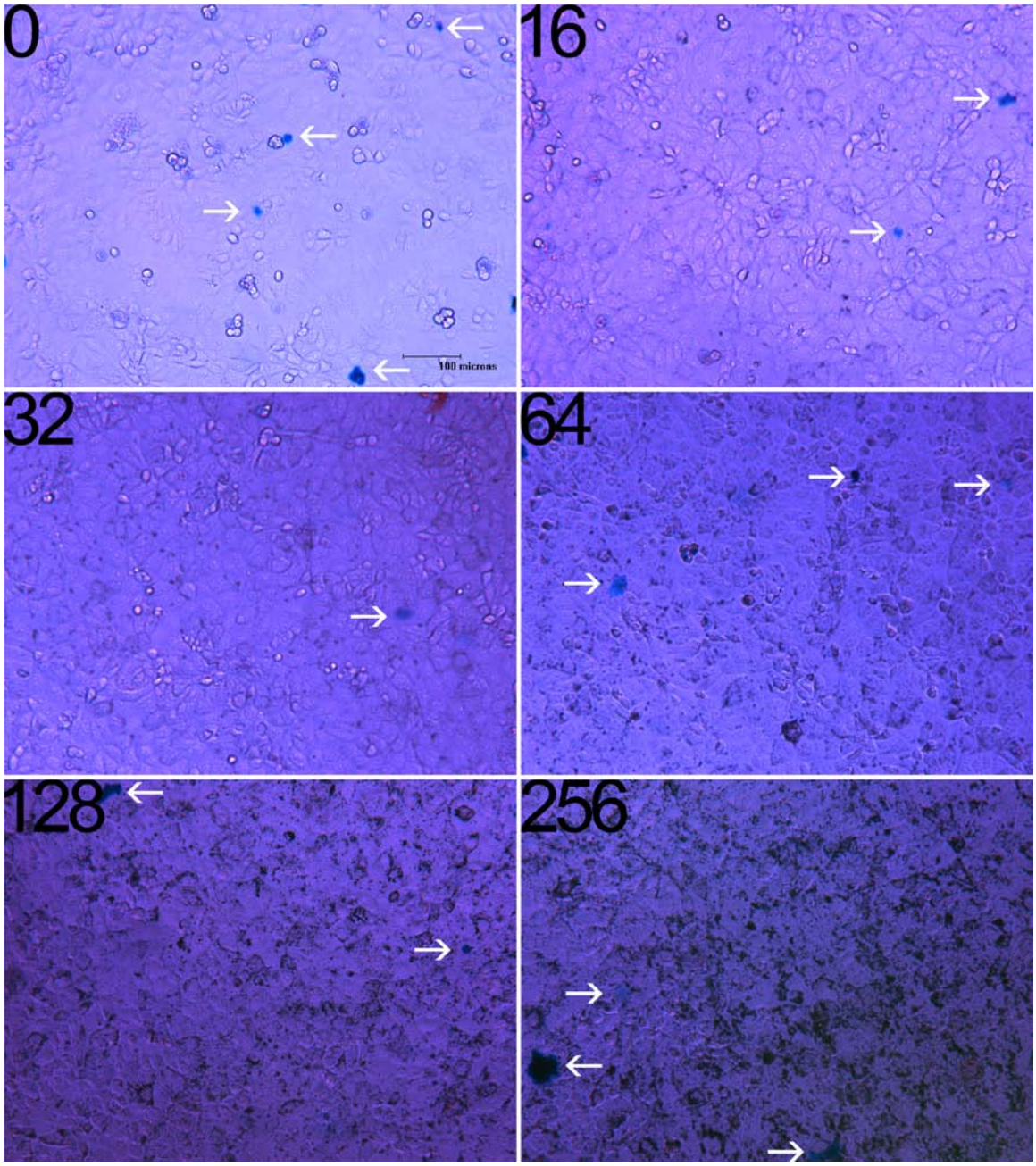

Supplemental Figure 2. Trypan Blue Exclusion Cytotoxicity Assay. Vero 76 cells were plated out at 2.5 x 10^5 cells per well in a 96-well plate 24 hours prior to exposure to AgNPs. Cells were then exposed to AgNPs, at the doses listed in the top left corner of each panel, for 4 hours. Cells were washed once with PBS then 80 µL of growth medium and 20 µL of trypan blue 0.4% were added to each well. Pictures were taken on a Leica Ctr-6000 inverted microscope with the aide of Image Pro 6.2 software. Bar = 100 µm for all panels. Arrows indicate dead cells no longer excluding the trypan blue dye.

DISCUSSION

AgNPs have been observed to inhibit the viral replication cycle; however, while the literature suggests an early time point in the viral replication process, little more is known. This study identifies a distinct step in the viral replication cycle at which AgNPs exert their antiviral effects. First, adsorption of VACV to host cells, the earliest in early VACV replication processes, was examined to determine if this step of infection was indeed the one interrupted by AgNPs to yield antiviral activity. No significant changes in VACV adsorption were found among any of the AgNPs concentrations tested suggesting that AgNPs do not interfere with the either the cellular proteins or VACV proteins responsible for binding to host cells (Figure 1). It could be that the large branched structure of the cellular factors heparan sulphate, chondroitin sulphate and laminin or their viral binding counterparts A26 A27, D8, H3, and L1 are unperturbed by the binding of AgNPs because this interaction is not dependent on a conformational change but rather an electrostatic interaction (15). The binding of AgNPs may not abolish this charge interaction or the AgNPs are capable of mimicking the charges responsible for normal virus/host interaction via their highly polarizable surfaces, thus re-establishing any abolished binding activity.

After determining that AgNPs did not affect adsorption, an assay was successfully established to measure overall VACV entry, both direct fusion and macropinocytosis-dependent fusion (Figure 2). This assay, based on the expression of β-gal driven from a constitutively active early/late promoter, demonstrated that the reporter enzyme was unaffected by the concentrations of AgNPs used in this study. Additionally, this assay was capable measuring decreased VACV in conjunction with a known VACV entry

inhibitor, VIG (Figure 2). These data demonstrated that VACV entry, or cores translocated into the cytoplasm which immediately begin to transcribe early viral mRNA resulting in early gene expression, can be accurately measured during a 4 hour, post-infection entry window. Successful reporter-based assays for VACV entry have detailed the measurement of entry as late as 6 hours post infection further suggesting that reporter assay detailed here, at 4 hours, is well within the generally accepted time frame of VACV entry (16, 52).

AgNPs were found to significantly inhibit the entry process of VACV during β-gal entry assay at 4 hours and confocal microscopic investigation at 1 hour post-infection (Figure 3). The NovaCentrix AgNPs, a "top-down," dry synthesis AgNP, had both a cytoprotective and virucidal effect on VACV measured by decreases in viral entry in both assays. Another set of AgNPs made via "bottom-up," wet synthesis methods also demonstrated clear dose dependent virucidal effects on VACV entry (Figure 4). These findings agree with the literature suggesting that AgNPs exert antiviral steps at an early stage of viral infection and add to it by pinpointing the stage of viral infection, the entry/fusion process, at which AgNP antiviral activity occurs (12, 21, 23, 34, 41). These findings also suggest that inhibition of VACV by AgNPs may not be as dependent on AgNP size as HIV-1 has demonstrated (12). This size dependence was the result of the HIV-1 entry protein gp120 being spaced at predictable intervals on the virus. The lack of size dependence for VACV might indicate that the EFC responsible for VACV entry may not have such a regimented spacing on the outside of the virion or that the virion is simply too large for the ~11 nm filtered AgNPs and 25 nm NovaCentrix AgNPs to sterically hinder themselves when binding to viral entry proteins.

Since VACV is known to enter cells via two distinct mechanisms, direct fusion and macropinocytosis-dependent fusion, Pak1 siRNA was used to inhibit macropinocytosis and permit investigation of the AgNP effect on the direct fusion entry pathway of VACV (Figure 5). Pak1 was successfully knocked down to levels similar to those found previously in the literature to inhibit macropinocytosis (Supplemental Figure 1) (25). Under these conditions, cytoprotective treatment with AgNP had almost no effect on VACV entry. These results might be explained by the AgNPs being too spaced out on the cell, at the lower concentrations, to bind to VACV or that they were exhausted by binding to cellular proteins before a chance interaction with VACV. Effective AgNP cytoprotective treatment of cells might indeed require macropinocytosis to bring AgNPs and VACV into closer proximity in order to facilitate an inhibition of entry as AgNP uptake into cells is macropinocytosis-dependent (2, 14). For example, in the tubular domains of an endosome, which are between 50-90 nm in diameter, a 25 nm particle, such as those used in this study, could occupy up to half of the luminal space (26). In the vacuolar lumen of a macropinosome, which is between 200-1,000 nm in diameter, a 25 nm AgNP would occupy 2.5-12.5% of that diameter while a VACV virion, between 250-350 nm, would occupy 25-35% of the that diameter (9, 26). While these values are considering only two dimensions, the reduction in volume of the macropinosome as it matures would increase the likelihood of VACV encountering an AgNP (9, 26). After such an encounter with an AgNP and subsequent inhibition of fusion, the virus could become trapped within the endosome and destroyed in the lysosome (19). AgNPs used in a virucidal capacity were able to exert anti-entry effects on VACV's direct fusion mechanism but at much larger doses than those observed during the overall entry assays.

The increasing doses required to inhibit entry may be a result of the incomplete inhibition of macropinocytosis and the excess AgNPs in the AgNP/VACV mixture creating cytoprotective effects. However, since the virucidal condition exhibited some anti-entry activity these results could also support the suggestion that AgNPs bind to the virus and inhibit infection at an early stage (12, 21, 23, 33).

The entry inhibition results translated to a decrease in plaque formation, indicating that the AgNPs affected the overall replication cycle of VACV whether undergoing cytoprotective, virucidal or post-infection treatment with AgNPs (Figure 6). The decrease in post-infection titer as compared to the control could be due to preventing the spread of VACV after successful infection, as AgNPs were applied in the agarose overlay, or this inhibition could be the result of an as yet unknown mechanism. AgNP treatment did not cause increased viral titer, as assessed by plaque reduction assay, in any conditions tested as was previously described with a similar Orthopoxvirus, MPV (34).

AgNPs were observed to decrease the mobility of G9 in a dose dependent fashion (Figure 7). G9 is one of the nine proteins of the EFC considered to be an integral member required for VACV entry. Furthermore, AgNPs altered the migration patter of the internal control core protein, A4-GFP. These data suggest that AgNPs bind to the viral proteins of VACV including the EFC. The shift observed in these experiments is small, ~ 1000 Da, but consistent with the findings that polyacrylamide gel pore sizes are between 21 nm, for gels with T = 10.5% and C = 5%, and 200 nm for gels with T = 4.6% and C =2 %, respectively (42). Since these experiments were conducted with T = 10% and C = 3.3%, values between those listed above, a 25 nm AgNP would likely pass through the pores, between 21 and 200 nm by the experimental conditions, and generate a small shift as seen

in Figure 7; however, precise pore sizes for these conditions are unknown. Additionally complicating issues related to G9 western blotting is the difficulty of solubilizing G9 and recovering enough protein to detect via western blot, which has been documented in the literature (28). This difficulty was overcome by increasing the detergents, reducing agents and time involved with lysate preparation; however, only low levels of the protein were detectable which results in lesser G9 blot image quality in Figure 6, (top panel vs. bottom). The observation that VACV direct fusion was mostly inhibited by virucidal AgNP treatment, and not cytoprotective treatment, in conjunction with the observations that AgNPs bind to G9, suggests that AgNPs could bind to VACV at the EFC and prevent viral entry. These observations support AgNP inactivation of viral entry proteins as one possible mechanism for AgNP antiviral activity. Additionally, these data are in agreement with previous findings in the literature demonstrating that AgNPs bind to the membrane bound proteins of viruses (12, 21). Alternatively, the shift in G9 could be a result of the stringent conditions used to solubilize the G9 protein. The literature provides no data concerning the fate of AgNPs subjected to the SDS-PAGE solubilization process, so phenomena brought about during such a procedure could also explain G9's mobility shift. In future studies, extracting the proteins from the gel and running such assays as mass spectrometry might provide a better clue as to if G9 is bound by AgNPs.

Cytotoxicity data suggest that AgNPs exert antiviral effects at non-toxic doses (Figure 8). While the MTT data support a decreased metabolic state at higher doses during a 4 hour exposure, microscopic evaluation, via the common and widely-used trypan blue staining assay for cell membrane integrity, revealed that cells at 4 hours of AgNP exposure excluded trypan blue. These results indicate that cellular membranes are

intact (Supplemental Figure 2). Furthermore, the observation that all conditions at 24 hours of exposure to AgNPs were within the range of the untreated control suggest that the cells recovered from the decreased metabolic state observed at 4 hours; if the cells had been rendered non-viable by the AgNPs it is unlikely they would recover to the same cell numbers and combined metabolic state of the untreated control as detected by the MTT cytotoxicity assay at 24 hours. Since macropinocytosis is an active, energy-dependent process, the decreased metabolic state may be creating a general antiviral-state for the target cell through the decrease in macropinocytosis brought on by decreased metabolic function within the cells (35). Further investigation into this possible mechanism of antiviral activity is warranted. Comparison of AgNPs used in this study with cytotoxicity data present in the literature is a difficult task due to the multitude of different AgNPs studied. Different AgNP characteristics such as size, shape, method of synthesis and capping/stabilizing agent can drastically alter the biological interaction of a nanomaterial (30, 47). Cytotoxicity values in the literature range from 0.7 μg mL^{-1} to greater than 449 μg mL^{-1} (1, 20). AgNPs used in this study were not toxic at antiviral concentrations suggesting they could be a potential therapeutic agent.

CONCLUSIONS

This study examined two different sets of AgNPs and is the first of its kind to establish a precise stage in viral infection at which AgNP-mediated antiviral activity occurs. In addition to defining the stage at which AgNP antiviral activity occurs, the data presented here suggest a mechanism for the observed virucidal activity. This virucidal activity was observed in multiple species of virus in the literature and would suggest that any number of virus species as yet unstudied in the context of AgNP antiviral activity would be susceptible to inhibition. Additionally, observations made within this report suggest at least one additional mechanism of AgNP antiviral activity. This additional mechanism, seemingly linked to macropinocytosis and metabolism, may also be responsible for the antibacterial properties of AgNPs. The suggested alternative mechanism(s) would also have the potential to affect the infection process of many different viral species, as there are in fact many different species that use cellular uptake mechanisms to facilitate their infection processes. The fact that AgNPs can exhibit multiple methods of antiviral activity, at non-cytotoxic concentrations, makes them attractive as potential broad-spectrum antiviral therapeutics.

AgNPs were capable of mediating a dramatic reduction in VACV entry at non-cytotoxic concentrations. The reduction in viral entry was observed in both cytoprotective and virucidal capacity and was not due to the prevention of VACV adsorption to the host cell. Furthermore, AgNPs were successful at mitigating viral entry via the direct fusion and macropinocytosis-dependent entry pathways of VACV. The observations detailed within this report suggest at least two mechanisms by which AgNP-mediated antiviral activity occur. The virucidal aspect of AgNPs could be a result of the AgNPs binding to

proteins such as the G9 subunit of the EFC and preventing their normal function to facilitate viral entry or excess AgNPs in the AgNP/VACV infection mixture creating a decreased metabolic state and reducing either VACV early gene expression or preventing viral uptake via macropinocytosis. The AgNP cytoprotective observations demonstrate that there may be an additional mechanism(s) by which AgNPs prevent viral entry and infection. These additional mechanisms likely rely on a cellular response to AgNP treatment such as concentration of AgNPs within macropinosomes during the maturation process, decreased metabolism or a decrease in viral uptake via macropinocytosis creating a general antiviral-state.

With the data collected here, *in vivo* studies of potential AgNP-mediated antiviral applications are possible and justified. Due to the multiple mechanisms at play AgNPs are uniquely suited for use as a stopgap treatment measure prior to identification of the infectious agent(s) in cases of anticipated or probable viral exposure. Currently, there are no truly broad-spectrum antiviral agents that can be used in such a manner. For airborne pathogens one might envision AgNPs administered via inhalation to prevent viral infection as they could offer virucidal effects for viruses that have not yet infected cells and cytoprotective effects for viruses that have not yet infected cells or are bound to airway tissues. There are currently no *in vivo* studies concerning AgNP antiviral activity and very few *in vivo* studies concerning AgNP toxicity. With the finding of these studies, such investigations are warranted.

AgNPs have the benefit of multiple possible methods for delivery since they are a metal and resistant to changes in temperature and pressure unlike traditional antiviral drugs. Evidence collected here and in other literature sources also suggest that AgNPs

could mediate post exposure prophylaxis as well. AgNPs could also easily be used as a disinfectant for contact spread pathogens on delicate surfaces such as sensitive equipment and the skin. Furthermore, the use of AgNPs as a powder would be advantageous over traditional liquid decontaminants, such as bleach, in the clean up of sensitive equipment that would react poorly to liquid exposure. In each case the identity of the infectious agent need not be known due to the multiple mechanisms at play, which mediate AgNP antiviral activity and offer broad-spectrum antiviral activity.

Future investigation into the mechanisms of AgNP antiviral activity is necessary. Additionally, *in vivo* investigation of potential AgNP antiviral applications is necessary. All together, these data suggest that AgNPs could be a potent broad-spectrum antiviral agent due to their multiple antiviral mechanisms.

REFERENCES

1. **Arora, S., J. Jain, J. M. Rajwade, and K. M. Paknikar.** 2009. Interactions of silver nanoparticles with primary mouse fibroblasts and liver cells. Toxicol. Appl. Pharmacol. **236:**310-318. doi: 10.1016/j.taap.2009.02.020.

2. **Asharani, P. V., M. P. Hande, and S. Valiyaveettil.** 2009. Anti-proliferative activity of silver nanoparticles. BMC Cell Biol. **10:**65. doi: 10.1186/1471-2121-10-65.

3. **Bengali, Z., A. C. Townsley, and B. Moss.** 2009. Vaccinia virus strain differences in cell attachment and entry. Virology. **389:**132-140. doi: 10.1016/j.virol.2009.04.012.

4. **Bisht, H., A. S. Weisberg, and B. Moss.** 2008. Vaccinia virus l1 protein is required for cell entry and membrane fusion. J. Virol. **82:**8687-8694. doi: 10.1128/JVI.00852-08.

5. **Bönnemann, H., and R. M. Richards.** 2001. Nanoscopic Metal Particles, Synthetic Methods and Potential Applications. Eur. J. Inorg. Chem. 2455.

6. **Brown, E., T. G. Senkevich, and B. Moss.** 2006. Vaccinia virus F9 virion membrane protein is required for entry but not virus assembly, in contrast to the related L1 protein. J. Virol. **80:**9455-9464. doi: 10.1128/JVI.01149-06.

7. **Broyles, S. S., and M. Kremer.** 2004. An *in vitro* transcription system for studying vaccinia virus early genes. Methods Mol. Biol. **269:**135-142. doi: 10.1385/1-59259-789-0:135.

8. **Carter, G. C., M. Law, M. Hollinshead, and G. L. Smith.** 2005. Entry of the vaccinia virus intracellular mature virion and its interactions with glycosaminoglycans. J. Gen. Virol. **86:**1279-1290. doi: 10.1099/vir.0.80831-0.

9. **Condit, R. C., N. Moussatche, and P. Traktman.** 2006. In a nutshell: structure and assembly of the vaccinia virion. Adv. Virus Res. **66:**31-124. doi: 10.1016/S0065-3527(06)66002-8.

10. **Dales, S., and L. Siminovitch.** 1961. The development of vaccinia virus in Earle's L strain cells as examined by electron microscopy. J. Biophys. Biochem. Cytol. **10:**475-503.

11. **De Gusseme, B., T. Hennebel, E. Christiaens, H. Saveyn, K. Verbeken, J. P. Fitts, N. Boon, and W. Verstraete.** 2011. Virus disinfection in water by biogenic silver immobilized in polyvinylidene fluoride membranes. Water Res. **45:**1856-1864. doi: 10.1016/j.watres.2010.11.046.

12. **Elechiguerra, J. L., J. L. Burt, J. R. Morones, A. Camacho-Bragado, X. Gao, H. H. Lara, and M. J. Yacaman.** 2005. Interaction of silver nanoparticles with HIV-1. J. Nanobiotechnology. **3:**6. doi: 10.1186/1477-3155-3-6.

13. **Foo, C. H., H. Lou, J. C. Whitbeck, M. Ponce-de-Leon, D. Atanasiu, R. J. Eisenberg, and G. H. Cohen.** 2009. Vaccinia virus L1 binds to cell surfaces and blocks virus entry independently of glycosaminoglycans. Virology. **385:**368-382. doi: 10.1016/j.virol.2008.12.019.

14. **Greulich, C., J. Diendorf, T. Simon, G. Eggeler, M. Epple, and M. Koller.** 2011. Uptake and intracellular distribution of silver nanoparticles in human mesenchymal stem cells. Acta Biomater. **7:**347-354. doi: 10.1016/j.actbio.2010.08.003.

15. **Hsiao, J. C., C. S. Chung, and W. Chang.** 1999. Vaccinia virus envelope D8L protein binds to cell surface chondroitin sulfate and mediates the adsorption of intracellular mature virions to cells. J. Virol. **73:**8750-8761.

16. **Izmailyan, R. A., C. Y. Huang, S. Mohammad, S. N. Isaacs, and W. Chang.** 2006. The envelope G3L protein is essential for entry of vaccinia virus into host cells. J. Virol. **80:**8402-8410. doi: 10.1128/JVI.00624-06.

17. **Jung, W. K., H. C. Koo, K. W. Kim, S. Shin, S. H. Kim, and Y. H. Park.** 2008. Antibacterial activity and mechanism of action of the silver ion in Staphylococcus aureus and Escherichia coli. Appl. Environ. Microbiol. **74:**2171-2178. doi: 10.1128/AEM.02001-07.

18. **Karber, G.** 1931. Contribution to the Collective Treatment of Pharmacological Serial Experiments. Archive for Pathology and Pharacology. . No Volume or Issue No.

19. **Kim, H. J., S. Lee, and J. U. Jung.** 2010. When autophagy meets viruses: a double-edged sword with functions in defense and offense. Semin. Immunopathol. **32:**323-341. doi: 10.1007/s00281-010-0226-8.

20. **Kim, J. S., E. Kuk, K. N. Yu, J. H. Kim, S. J. Park, H. J. Lee, S. H. Kim, Y. K. Park, Y. H. Park, C. Y. Hwang, Y. K. Kim, Y. S. Lee, D. H. Jeong, and M. H. Cho.**

2007. Antimicrobial effects of silver nanoparticles. Nanomedicine. **3:**95-101. doi: 10.1016/j.nano.2006.12.001.

21. **Lara, H. H., N. V. Ayala-Nunez, L. Ixtepan-Turrent, and C. Rodriguez-Padilla.** 2010. Mode of antiviral action of silver nanoparticles against HIV-1. J. Nanobiotechnology. **8:**1. doi: 10.1186/1477-3155-8-1.

22. **Law, M., G. C. Carter, K. L. Roberts, M. Hollinshead, and G. L. Smith.** 2006. Ligand-induced and nonfusogenic dissolution of a viral membrane. Proc. Natl. Acad. Sci. U. S. A. **103:**5989-5994. doi: 10.1073/pnas.0601025103.

23. **Lu, L., R. W. Sun, R. Chen, C. K. Hui, C. M. Ho, J. M. Luk, G. K. Lau, and C. M. Che.** 2008. Silver nanoparticles inhibit hepatitis B virus replication. Antivir Ther. **13:**253-262.

24. **Manischewitz, J., L. R. King, N. A. Bleckwenn, J. Shiloach, R. Taffs, M. Merchlinsky, N. Eller, M. G. Mikolajczyk, D. J. Clanton, T. Monath, R. A. Weltzin, D. E. Scott, and H. Golding.** 2003. Development of a novel vaccinia-neutralization assay based on reporter-gene expression. J. Infect. Dis. **188:**440-448. doi: 10.1086/376557.

25. **Mercer, J., and A. Helenius.** 2008. Vaccinia virus uses macropinocytosis and apoptotic mimicry to enter host cells. Science. **320:**531-535. doi: 10.1126/science.1155164.

26. **Mercer, J., M. Schelhaas, and A. Helenius.** 2010. Virus entry by endocytosis. Annu. Rev. Biochem. **79:**803-833. doi: 10.1146/annurev-biochem-060208-104626.

27. **Nichols, R. J., E. Stanitsa, B. Unger, and P. Traktman.** 2008. The vaccinia virus gene I2L encodes a membrane protein with an essential role in virion entry. J. Virol. **82:**10247-10261. doi: 10.1128/JVI.01035-08.

28. **Ojeda, S., A. Domi, and B. Moss.** 2006. Vaccinia virus G9 protein is an essential component of the poxvirus entry-fusion complex. J. Virol. **80:**9822-9830. doi: 10.1128/JVI.00987-06.

29. **Ojeda, S., T. G. Senkevich, and B. Moss.** 2006. Entry of vaccinia virus and cell-cell fusion require a highly conserved cysteine-rich membrane protein encoded by the A16L gene. J. Virol. **80:**51-61. doi: 10.1128/JVI.80.1.51-61.2006.

30. **Pavel, I., E. McCarney, A. Elkhaled, A. Morrill, K. Plaxco, and M. Moskovits.** 2008. Label-Free SERS Detection of Small Proteins Modified to Act as Bifunctional Linkers. J. Phys. Chem. C. Nanomater Interfaces. **112:**4880-4883. doi: 10.1021/jp710261y.

31. **Pedersen, K., E. J. Snijder, S. Schleich, N. Roos, G. Griffiths, and J. K. Locker.** 2000. Characterization of vaccinia virus intracellular cores: implications for viral uncoating and core structure. J. Virol. **74:**3525-3536.

32. **Rai, M., A. Yadav, and A. Gade.** 2009. Silver nanoparticles as a new generation of antimicrobials. Biotechnol. Adv. **27:**76-83. doi: 10.1016/j.biotechadv.2008.09.002.

33. **Roberts, K. L., and G. L. Smith.** 2008. Vaccinia virus morphogenesis and dissemination. Trends Microbiol. **16:**472-479. doi: 10.1016/j.tim.2008.07.009.

34. **Rogers, J. V., C. V. Parkinson, Y. W. Choi, J. L. Speshock, and S. M. Hussain.** 2008. A Preliminary Assessment of Silver Nanoparticle Inhibition of Monkeypox Virus Plaque Formation. Nanoscale Res Lett. **3:**129. doi: 10.1007/s11671-008-9128-2.

35. **Schelhaas, M.** 2010. Come in and take your coat off - how host cells provide endocytosis for virus entry. Cell. Microbiol. **12:**1378-1388. doi: 10.1111/j.1462-5822.2010.01510.x; 10.1111/j.1462-5822.2010.01510.x.

36. **Senkevich, T. G., and B. Moss.** 2005. Vaccinia virus H2 protein is an essential component of a complex involved in virus entry and cell-cell fusion. J. Virol. **79:**4744-4754. doi: 10.1128/JVI.79.8.4744-4754.2005.

37. **Senkevich, T. G., S. Ojeda, A. Townsley, G. E. Nelson, and B. Moss.** 2005. Poxvirus multiprotein entry-fusion complex. Proc. Natl. Acad. Sci. U. S. A. **102:**18572-18577. doi: 10.1073/pnas.0509239102.

38. **Sharma, V. K., R. A. Yngard, and Y. Lin.** 2009. Silver nanoparticles: green synthesis and their antimicrobial activities. Adv. Colloid Interface Sci. **145:**83-96. doi: 10.1016/j.cis.2008.09.002.

39. **Silver, S., T. Phung le, and G. Silver.** 2006. Silver as biocides in burn and wound dressings and bacterial resistance to silver compounds. J. Ind. Microbiol. Biotechnol. **33:**627-634. doi: 10.1007/s10295-006-0139-7.

40. **Silvestry-Rodriguez, N., E. E. Sicairos-Ruelas, C. P. Gerba, and K. R. Bright.** 2007. Silver as a disinfectant. Rev. Environ. Contam. Toxicol. **191:**23-45.

41. **Speshock, J. L., R. C. Murdock, L. K. Braydich-Stolle, A. M. Schrand, and S. M. Hussain.** 2010. Interaction of silver nanoparticles with Tacaribe virus. J. Nanobiotechnology. **8:**19. doi: 10.1186/1477-3155-8-19.

42. **Stellwagen, N. C.** 1998. Apparent pore size of polyacrylamide gels: comparison of gels cast and run in Tris-acetate-EDTA and Tris-borate-EDTA buffers. Electrophoresis. **19:**1542-1547. doi: 10.1002/elps.1150191004.

43. **Townsley, A. C., and B. Moss.** 2007. Two distinct low-pH steps promote entry of vaccinia virus. J. Virol. **81:**8613-8620. doi: 10.1128/JVI.00606-07.

44. **Townsley, A. C., T. G. Senkevich, and B. Moss.** 2005. The product of the vaccinia virus L5R gene is a fourth membrane protein encoded by all poxviruses that is required for cell entry and cell-cell fusion. J. Virol. **79:**10988-10998. doi: 10.1128/JVI.79.17.10988-10998.2005.

45. **Townsley, A. C., T. G. Senkevich, and B. Moss.** 2005. Vaccinia virus A21 virion membrane protein is required for cell entry and fusion. J. Virol. **79:**9458-9469. doi: 10.1128/JVI.79.15.9458-9469.2005.

46. **Townsley, A. C., A. S. Weisberg, T. R. Wagenaar, and B. Moss.** 2006. Vaccinia virus entry into cells via a low-pH-dependent endosomal pathway. J. Virol. **80:**8899-8908. doi: 10.1128/JVI.01053-06.

47. **Trefry, J. C., J. L. Monahan, K. M. Weaver, A. J. Meyerhoefer, M. M. Markopolous, Z. S. Arnold, D. P. Wooley, and I. E. Pavel.** 2010. Size selection and concentration of silver nanoparticles by tangential flow ultrafiltration for SERS-based biosensors. J. Am. Chem. Soc. **132:**10970-10972. doi: 10.1021/ja103809c.

48. **Turner, P. C., B. P. Dilling, C. Prins, S. G. Cresawn, R. W. Moyer, and R. C. Condit.** 2007. Vaccinia virus temperature-sensitive mutants in the A28 gene produce non-infectious virions that bind to cells but are defective in entry. Virology. **366:**62-72. doi: 10.1016/j.virol.2007.03.060.

49. **U.S. Department of Health and Human Services.** 2007. HHS Public Health Emergency Medical Countermeasure Enterprise Implementation Plan for Chemical, Biological, Radiological or Nuclear Threats.

50. **V. V. Kopeikin and E. F. Panarin.** 2001. Water-Soluble Nanocomposites of Zerovalent Metallic Silver with Enhanced Antimicrobial Activity. Doklady Chemistry. **380:**277.

51. **Wagenaar, T. R., and B. Moss.** 2007. Association of vaccinia virus fusion regulatory proteins with the multicomponent entry/fusion complex. J. Virol. **81:**6286-6293. doi: 10.1128/JVI.00274-07.

52. **Whitbeck, J. C., C. H. Foo, M. Ponce de Leon, R. J. Eisenberg, and G. H. Cohen.** 2009. Vaccinia virus exhibits cell-type-dependent entry characteristics. Virology. **385:**383-391. doi: 10.1016/j.virol.2008.12.029.

53. **White, J. M., S. E. Delos, M. Brecher, and K. Schornberg.** 2008. Structures and mechanisms of viral membrane fusion proteins: multiple variations on a common theme. Crit. Rev. Biochem. Mol. Biol. **43:**189-219. doi: 10.1080/10409230802058320.

54. **Wolfe, C. L., and B. Moss.** 2011. Interaction between the G3 and L5 proteins of the vaccinia virus entry-fusion complex. Virology. **412:**278-283. doi: 10.1016/j.virol.2011.01.014.

55. **Woodrow Wilson International Center for Scholars and the Pew Charitable Trusts.** 2011. The Project on Emerging Nanotechnologies. **2011**. http://www.nanotechproject.org/inventories/silver/

CHAPTER V:

DISCUSSION and CONCLUSION

DISCUSSION

Due to the exponential increase in biological applications for AgNPs, it is important that key gaps in knowledge surrounding their use are addressed. Chapter II of this dissertation sought to address the problems facing the manufacture of AgNPs for their use as antimicrobial agents without unwanted side effects common to contemporary AgNP synthesis and collection techniques. Developing a standard technology that is both high throughput and capable of simultaneously measuring AgNP antiviral activity and cytotoxicity is presented in Chapter III. A technology such as the one developed in Chapter III would greatly benefit the screening of nanomaterials for antiviral activity by enabling a automation of the process, standardizing the antiviral measurements and simultaneous assessing cytotoxicity. The fourth chapter addresses the unknown mechanisms involved in AgNP mediated antiviral activity by determining a stage at which antiviral activity occurs and suggesting possible antiviral mechanisms of action.

Data presented here and in the literature suggest that AgNPs can be used as a new class of broad-spectrum antiviral agents. These antiviral agents would have numerous benefits over the traditional antiviral drugs and therapies. Since AgNPs are a metal there would be no limitations on storage conditions or restrictions in their method of application. Data presented here and in the literature concerning their ability to bind to

and inhibit a number of different viral species would suggest that they are a true broad-spectrum antiviral, therefore in the instance of suspected viral exposure or at the onset of symptoms, a precise determination of the infectious agent is not necessary. Viral resistance to AgNPs would also be less prevalent than in traditional specific antiviral therapies due to the same non-specific biological interactions that grant AgNPs the ability to inhibit many different viral species. Despite all these potential benefits, many issues still surround the production of AgNPs, the screening of their antiviral potential against different viral species, and the determination of their precise time point and mechanism of antiviral activity.

In order to produce highly concentrated, biocompatible AgNPs with low aggregation and narrow size distribution from a wet synthesis procedure, a tangential flow ultrafiltration procedure was constructed and tested against the common ultracentrifugation method for AgNP concentration. This procedure, which utilizes hollow fiber modules with specific pore sizes to solutes within a solvent, was capable of separating out a specific size population of naked AgNPs through upper and lower bound filters for AgNPs synthesized via the Creighton Colloid method. Wet synthesis methods of creating naked AgNPs, such as the Creighton method, produce a broad range of sizes, which can be problematic as different size AgNPs can cause different biological reactions (3, 10, 11). These differences are undesirable for the development of an antimicrobial agent as differentiating between harming the host or the target microbe is complicated due to the unknown effects caused by polydisperse AgNPs. The tangential flow ultrafiltration procedure concentrated AgNPs to a level 13-fold higher than the original colloid. This concentration effect is significant because the use of AgNPs as antiviral

agents relies on the number of AgNPs available to bind to a target microbe, a phenomenon less likely to occur in a less concentrated sample (24, 27, 37). Also, the ability to size select and concentrate AgNPs creates a highly uniform population of AgNPs that will increase antimicrobial efficacy and decrease unwanted side effects brought on by polydispersity.

The tangential flow procedure for size selecting and concentrating AgNPs was then compared to the common AgNP harvesting method of ultracentrifugation. Tangential flow ultrafiltration was capable of concentrating AgNPs over 2.5-fold more than standard ultracentrifugation. The AgNPs collected via ultracentrifugation demonstrated a massive size distribution, high levels of aggregation and amorphous shapes when compared to the filtered AgNP. The large size distribution and introduction of various AgNP shapes would drastically affect normal biological processes which could generate cytotoxic effects that would be interpreted as antiviral activity (3, 4). Multiple reports detail the use of ultracentrifuged AgNPs for biological applications, such as the detection of cancerous versus non-cancerous cells, cytotoxicity studies, and general blood plasma screening for a variety of biomarkers (10). Any study employing ultracentrifugation to purify or concentrate nanoparticles may introduce errors into the data collected due to the different effects caused by a poly-disperse population of AgNPs, such as those generated by ultracentrifugation (11). By using AgNPs prepared by tangential flow ultrafiltration the likelihood of introducing errors based on AgNP poly-dispersity is abrogated. This method ensures that any measured antiviral activity is due to the monodisperse, naked AgNPs themselves and not a function of contaminating synthesis agents, size polydispersity, or aggregation.

The findings of Chapter II indicate that tangential flow ultrafiltration is a preferable method to the traditional method of ultracentrifugation for concentrating AgNPs for use as antimicrobial agents. In addition to concentrating AgNPs, tangential flow filtration is capable of size selecting AgNPs to generate a uniform, mono-disperse population of AgNPs, while ultracentrifugation creates large aggregates and a large size distribution of AgNPs. The large size distribution of AgNPs produced by ultracentrifugation can introduce errors into data collected in the analysis of cytotoxicity and antimicrobial activity. These variations in AgNP characteristics from different synthesis techniques and concentration technique may cause other undocumented biological reactions that occur upon exposure to AgNPs. Thus, minimizing the risk of a diverse biological reaction from an AgNP population with broad size distribution is preferable when developing an antimicrobial agent. The use of ultrafiltration to concentrate other nanoparticles would provide a reliable, standardized method to reduce variability when testing the antimicrobial of any nanoparticles In addition to size selecting and concentrating AgNPs, this technique would work for any nanomaterial in liquid phase. Because of the greater control over the physical characteristics of nanomaterials, this filtering process will significantly advance the mobilization of nanotechnology into consumer and therapeutic products as antiviral and antibacterial agents.

Chapter III presents a standard, high-throughput method of testing nanomaterials for antiviral activity to address the need for a standard antiviral screening method for nanomaterials. Because traditional plaque assays are subjective and require large amounts of time and money, a quicker high-throughput format for screening antiviral activity is

desirable. Additionally, current techniques rely on performing cytotoxicity assays separately from the antiviral testing. This separation can result in the masking of antiviral activity by cytotoxicity, as well as double the amount of work, time and money required.

A large-scale HIV-1 mutation rate assay, based on colony forming units, was chosen as the basis for developing the new high-throughput antiviral assay. This assay utilized an HIV-1-based viral vector system that infects host cells and carries with it Hyg resistance so that only infected cells will be viable after addition of selective medium (14). The vector system was scaled down to a 96-well microtiter plate for ease of automation and high-throughput antiviral screening with an endpoint measurement by the standard MTT metabolic assay, a staple in the assessment of cell viability (6, 23, 25, 26). Because this new assay employs a viral vector system, the glycoproteins incorporated into the virion are interchangeable and thus multiple different viruses can be simulated and screened via the same standard assay simply by interchanging the target virus's entry glycoprotein (8, 14). Standardization of antiviral screening was also established through the use of MTT as the endpoint measurement. Many labs are already equipped with the machinery and reagents required to conduct this assay and the National Cancer Institute's Nanotechnology Characterization Laboratory lists MTT as one of only two standard methods for screening AgNP cytotoxicity (25, 35). Tetrazolium salts, such as MTT and its chemical relatives, have different wavelengths at which they absorb and thus can be interchanged to test different types of nanomaterials. This interchangeability is essential because different nanomaterials exhibit different SPR wavelengths that might interfere with the endpoint of the MTT (9, 19). By using different tetrazolium salts the assay remains the same standard assay from nanomaterial to nanomaterial and by using the

viral vector system the same standard assay can be used from virus to virus, affording a standardization and flexibility lacking in current methods.

The new standard assay was then evaluated for its ability to accurately detect viral titers through comparison with the traditional colony forming unit assay. Changes in viral titers over three orders of magnitude were accurately measured by the new assay and confirmed via colony forming unit assay. These data indicate that the new high-throughput assay is capable of detecting decreases in viral titer brought on by inhibition of infection. To the author's knowledge this assay is the first example of a viral colony forming unit assay for antiviral activity in high-throughput, 96-well microtiter format.

Once the new assay was established to accurately measure viral titer and thus inhibition of infection, AgNPs were used to gauge the assay's ability to simultaneously measure antiviral activity and cytotoxicity. The new assay demonstrated that AgNPs clearly inhibited infection by the viral vector system. Furthermore, this antiviral activity was not accompanied by AgNP cytotoxicity. Traditional colony forming unit assays and reporter constructs are dependent on the living cells to gauge relative infectivity of a virus. If the antiviral agent being screened kills the target cells, a false positive for antiviral activity will be observed and interpreted as antiviral activity (36). The traditional assays must typically be run twice for each antiviral agent concentration tested in order to rule out possible toxicity; however, counting colonies can be a highly subjective process and thus introduces a large variation into the data collected (2, 20). Running the traditional assays in parallel to rule out possible cytotoxic effects add to the cost and time involved with each experiment thus preventing these technologies from achieving high-throughput capabilities. Additionally, variations in cell number and MOI from assay to

assay will further cloud the distinctions between antiviral activity and cytotoxicity. This new assay eliminates the variations introduced in the traditional assays by permitting the simultaneous measurement of antiviral activity and cytotoxicity in the same plate. The viral vector system employed by this assay also permits a general indication of possible antiviral mechanisms at work by limiting the infection cycle to the point of proviral gene expression. Inhibition of the viral vector system can be interpreted as affecting the early processes during infection, an ability not present in the use of wild type virus colony forming unit assays which undergo all stages of viral replication. Inhibition of the viral vector system in this new assay indicates that antiviral activity occurs at early time points in infection and that AgNPs were observed to inhibit viral vector infection, this study is in agreement with current literature that indicate viral inhibition by AgNPs occurs at an early stage of viral infection (7, 17, 18, 29, 33, 34).

In Chapter III a new high-throughput screening assay was successfully developed and found to simultaneously measure the antiviral activity and cytotoxicity of nanomaterials in a cell culture-based system. This assay represents a new system by which nanomaterials can be screened for antiviral activity in the absence of complications masking antiviral effects. Additionally, due to the parameters of this assay such as the use of MTT and interchangeable entry glycoproteins, this assay affords a level of standardization lacking in the assessment of nanomaterials as antivirals. The results of this assay can also serve as a "finger in the wind," gauge from which the direction of future mechanistic studies of nanomaterial antiviral activity. In the process of validating this new assay with a contemporary nanomaterial, AgNPs showed clear antiviral effects and low cytotoxicity. These data demonstrate a potential antiviral agent with a high

therapeutic index. The AgNPs inhibited the virus at an early stage of replication prior to assembly of new particles in the cell. Further investigation into the mechanism of nanoparticle antiviral activity is warranted to determine if the AgNPs bind to the virus, the AgNPs bind to the cell, or both, are responsible for antiviral activity.

The third objective of this manuscript, examined in Chapter IV of this manuscript, hypothesized that AgNP mediated antiviral activity was the result of AgNPs preventing viral entry. Two completely different sets of highly concentrated and uniform AgNPs were used in this objective to pinpoint the stage of viral infection at which AgNP antiviral activity occurs and illuminate possible mechanisms behind this inhibition, a vital gap in knowledge concerning AgNP antiviral activity. VACV was chosen as the viral system to examine AgNP-mediated antiviral activity and its possible mechanisms due to the call to research by various governmental agencies and the growing concern for the use of *Variola major* as a potential bioweapon.

Adsorption of VACV to host cells was examined in the first aim of objective three to determine if AgNPs interrupted this process. AgNPs did not interfere with adsorption to the host cell, indicating that either the cellular proteins or the VACV proteins responsible for binding to host cells were unaffected by AgNPs. It is possible that the large branched structure of the cellular GAGs, or their viral binding counterparts, are unperturbed by the binding of AgNPs because this interaction is not dependent on a conformational change but rather an electrostatic interaction (13). The binding of AgNPs may not abolish this charge interaction or the AgNPs are capable of mimicking the charges responsible for normal virus/host interaction, thus re-establishing any abolished binding activity.

The effects of AgNPs on overall VACV entry, both direct fusion and macropinocytosis-dependent entry, were then investigated. Two distinct sets of AgNPs were found to significantly inhibit the entry process of VACV during β-gal entry assay at 4 hours. Confocal microscopic investigation at 1 hour post-infection confirmed the findings of the β-gal entry assay. The AgNPs had both a cytoprotective and virucidal effect on VACV measured by decreases in viral entry in both assays. These findings are in agreement with the sources of literature that suggest AgNPs exert antiviral activity occurs during early stages of viral infection. This study expanded on the literature findings by pinpointing the precise stage of viral inhibition to the entry/fusion process (7, 17, 18, 29, 34). Additionally, AgNPs were observed binding the G9 protein of VACV's EFC through mobility shifts during Western blotting. The decrease in mobility supports previous observations of AgNPs binding to viral entry proteins as a mechanism for their virucidal activity (7). Inhibition of viral entry by AgNPs also translated to a decrease in plaque formation, indicating that the prevention of viral entry by AgNPs affected the overall replication cycle of VACV. This effect was observed whether undergoing cytoprotective, virucidal or post-infection treatment with AgNPs. Importantly, AgNP treatment did not cause increases in viral titer, as assessed by plaque assay, in any conditions tested as was previously described (29).

Since VACV is known to enter cells via two distinct mechanisms, direct fusion and macropinocytosis-dependent fusion, the third aim of this objective used Pak1 siRNA to inhibit macropinocytosis and permit investigation into the AgNP affect on direct fusion of VACV to the target cell. Pak1 was successfully knocked down to levels similar to those found previously in the literature, at which macropinocytosis was inhibited (21).

Under these conditions, cytoprotective treatment with AgNPs had almost no effect, which indicates that inhibition of direct fusion of VACV by AgNPs might be prevented by the AgNPs being too spaced out on the cell at the lower concentrations to adequately prevent viral entry. Importantly, the cytoprotective effects of AgNPs might require macropinocytosis to bring AgNPs and VACV into closer proximity, thus facilitating a chance encounter and an inhibition of entry since AgNP uptake into cells is macropinocytosis-dependent (1, 12). In the tubular domains of an endosome, which are between 50-90 nm in diameter, a 25 nm particle, such as those used in this objective, could occupy up to half of the macropinosome's luminal space (22). In the vacuolar lumen of a macropinosome, between 200-1,000 nm in diameter, a 25 nm AgNP would occupy 2.5-12.5% of that diameter while a VACV virion, averaging 250-350 nm in diameter, would occupy 25-35% of the that diameter (5, 22). While these values are considering only two dimensions, the reduction in volume of the macropinosome as it matures would increase the likelyhood of VACV encountering an AgNP. VACV could then become trapped within the endosome and destroyed in the lysosome as a result of a chance encounter with an AgNP during macropinosomal maturation (16). Supporting the suggestion that AgNPs bind to the virus and inhibit infection at an early stage, virucidal treatment of VACV elicited anti-entry effects on VACV's direct fusion mechanism (7, 17, 18, 28).

These anti-entry effects by AgNPs were observed at non-cytotoxic concentrations of AgNPs as demonstrated by MTT assay and trypan blue exclusion indicating that AgNPs have a high therapeutic index. While the MTT assay showed decreased metabolic function at high AgNP doses for 4 hours of exposure, microscopic evaluation revealed

that cells at 4 hours of AgNP exposure were intact, excluding trypan blue. Combining the results from the MTT assay and trypan blue assay suggests that the cells are intact though experiencing a decreased metabolic state. Furthermore, the observation that all AgNP treatments at 24 hours of exposure were within the range of the untreated control suggest that the cells recovered from the observed decreased metabolic state at 4 hours. This recovery could be the result of the AgNPs binding to their maximum amount of biological material, thus creating the decline in metabolism. After the AgNPs have bound all the biological material possible including cellular and viral proteins, the cells may then regenerate the proteins inactivated by AgNP binding and thus accounting for the rebound in metabolic status. Since macropinocytosis is an active, energy-dependent process, the decreased metabolic state may also be creating a general antiviral-state for the target cell through the decrease in macropinocytosis brought on by decreased metabolic function within the cells (31). This decrease in metabolism and possible reduction in macropinocytosis preventing viral entry may be part of a mechanism responsible for the anti-entry effects of AgNPs.

Chapter IV demonstrated that AgNPs inhibit VACV infection by preventing viral entry at non-cytotoxic concentrations. These effects were observed to occur at VACV entry in both a cytoprotective and virucidal capacity. Furthermore, observations were made that suggest multiple possible antiviral mechanisms of action. These possible mechanistic observations are significant as previous studies assessed viral systems covering more than one stage during viral infection or investigated the only the virucidal activity of AgNPs. The results presented in this dissertation suggest AgNPs can be described as viral entry inhibitors. Additionally, by examining both the virucidal and

cytoprotective capacity of AgNPs, potent cytoprotective antiviral effects were observed in Chapter IV. These cytoprotective effects could have even farther reaching potential as these effects most likely rely on active uptake by the host cells and could possibly be used to combat diseases associated with aberrant cellular uptake. These results lay down a framework upon which further investigation into the development of AgNPs as an antiviral agent and antiviral therapeutic is possible. Because AgNPs exhibited multiple mechanisms of action against VACV, which exploits multiple mechanisms for entry, AgNPs would be an ideal candidate as a new class of broad-spectrum antiviral agents.

CONCLUSIONS

Nanotechnology's presence is exponentially increasing in commercial applications. The applications of the most popular commercial nanotechnology AgNPs range from use as antiviral agents to cutting edge biosensors. However, this technology is still very young and requires better methods of generating AgNPs, better methods of studying their antiviral properties and a greater understanding of how AgNPs exert antiviral activity. The findings of these investigations suggest tangential flow ultrafiltration is capable of generating a highly uniform set of AgNPs. With this process more precise antimicrobial study is possible without the unwanted contaminants or adverse biological reactions possible when using AgNPs prepared via traditional methods. Additionally, other nanomaterials in the liquid phase can be concentrated and size selecting using this technique. These studies also proposed the use of a novel assay for screening nanomaterials for their antiviral potential. Tested with AgNPs, this assay exhibited the unique potential to measure cytotoxicity and antiviral activity simultaneously while enabling automation via its high-throughput format. AgNPs were

found to have low cytotoxicity and high antiviral activity indicating they have a high therapeutic index. This assay is also capable of screening other nanomaterials for antiviral activity and cytotoxicity simultaneously. AgNPs were found exert potent antiviral activity at non-cytotoxic concentrations with this new assay. Further investigation into the time point and mechanism of AgNP antiviral activity were also evaluated in these studies. AgNP antiviral activity was pinpointed to the entry stage of VACV infection where AgNPs were found to have both cytoprotective and virucidal effects at non-cytotoxic concentrations again suggesting that AgNPs have a high therapeutic index. This work also observed multiple mechanisms by which AgNPs may exert their antiviral properties. Because of the multiple methods of preventing viral entry, AgNPs would be ideal for further development as broad-spectrum antiviral agents.

Future investigations into the antiviral activity of AgNPs can be divided up in the three basic categories. These categories are immediate investigations to take place within the next year, intermediate investigations to take place over the next five years, and long term investigations to take place over the next ten years. The first immediate investigation would concern the knockdown of Pak1 as discussed in Chapter IV. Because the siRNA system designed against Pak1 was only capable of an 87% knockdown, some Pak1 may be functional within the target cells. This unaffected Pak1 could then mediate a low level of macropinocytosis, thus allowing some of the VACV virions to enter the target cells via macropinocytosis-dependent fusion. A quantitative assay measuring macropinocytosis via fluid phase marker, such as a fluorescent dextran or horseradish peroxidase, would account for this possibility by generating a percent knockdown of macropinocytosis in conjunction with Pak1 knockdown. Characterizing the specific

decrease in macropinocytosis will enhance the data presented within this dissertation by providing a context for the level of VACV direct fusion inhibition by AgNPs. For example, if macropinocytosis is still occurs after Pak1 knockdown, a refined mechanism for AgNP antiviral activity would be apparent because the inhibition seen in Figure 4 might be a result of AgNPs preventing fusion of virions contained within macropinocytotic vesicles. This refined mechanism would place more emphasis on the cytoprotective effect of AgNPs than on the virucidal potential of AgNPs.

The effects of AgNPs on fluid phase uptake could be determined as part of the immediate investigations. Since a metabolic decline was observed at 4 hours of incubation with AgNPs above 64 μg mL^{-1}, macropinocytosis could be decreased as well due to its dependence on the cell's active metabolism. It would be vital to know if AgNPs could mediate such an effect for the development of an antiviral agent as well as a potential therapeutic for other diseases associated with aberrant macropinocytosis. Transmission electron microscopy examination of cellular morphology and membrane ultra-structure would also be useful in determining whether or not AgNPs are capable of preventing macropinocytosis. AgNPs limiting macropinocytosis would represent yet another mechanism by which AgNPs demonstrate antiviral activity. This antiviral activity would likely be broad-spectrum as a number of different viral species gain access to their target cells via macropinocytosis (22).

The decrease in MTT values at 4 hours of AgNP exposure followed by a rebound to control levels at 24 hours of AgNP exposure suggests that AgNPs mediated a temporary decline in metabolism. A better understanding of the cytotoxic properties of AgNPs is required to understand if the decline in metabolism was beneficial to the cell by

promoting a general antiviral state or if the decreased metabolism was due to damage associated with AgNP exposure. If the AgNPs can induce a decreased metabolic state from which the cells can recover, it would represent a novel form of broad-spectrum antiviral agent. This mechanism of antiviral activity would be affective against any possible viral pathogen due to the inhibition of early viral gene expression. Inhibition at this stage of viral infection could possibly deny the virus time to establish a foothold inside the cell and provide the immune system time react and effectively combat the intruder. To further explore the potential cytotoxicity of AgNPs an assay for apoptosis, an additional metabolic assay for viability and a necrosis assay could be used to determine how AgNPs may negatively impact the target cell. These data could be collected easily with an assay kit, such as ApoTox-Glo (Promega, # G6320, Madison, WI) containing all three assays performed in the same well. Other assays could provide support to the kit assay and build on its findings. These additional assays could include a lactate dehydrogenase leakage assay to determine cellular necrosis, caspase activation assays to determine if AgNPs are causing apoptosis, ROS assays to determine if AgNPs are mediating ROS production, and ATP:ADP quantification assays to determine if mitochondrial function is impaired by AgNP exposure. Each of these assays could help to pinpoint possible negative impacts of host cell exposure to AgNPs as well as suggest if the AgNPs are capable of mediating an antiviral state due to decreased metabolism.

In combination with the above assays for possible cytotoxic effects mediated by host cell exposure to AgNPs, a TEM analysis of AgNPs effects on cellular morphology could also be conducted in the immediate investigations. Such a study would detail when and where AgNPs were interacting with cells. For example, TEM could detect possible

increased AgNP concentrations in a macropinosome or where AgNPs bound to cellular membranes. By varying the time points at which samples were prepared for TEM a chronological analysis of when AgNPs collect at various organelles within the cell is possible. AgNP effects on cellular structure could also be determined and used to gauge possible cytotoxic effects as well.

Based on the results generated by the quantitative macropinocytosis assay, cytotoxicity assays, and TEM analyses, intermediate investigations utilizing different target cells and viral strains would take place over the next five years. Different target cells could be selected for either increased or decreased basal levels of macropinocytosis. By studying viral entry in cell lines with varying levels of macropinocytosis a clearer understanding of how AgNPs exert their cytoprotective inhibition of VACV is possible. For example, in a cell line with higher levels of macropinocytosis, if VACV entry is inhibited to a greater degree after cytoprotective treatment with AgNPs, it would suggest that macropinocytosis is an active process required for AgNP-mediated anti-entry effects. Additional cell lines genetically designed without genes vital for macropinocytosis may also be a possibility for further examination of the mechanism behind AgNP effects on viral entry. Each of these scenarios would provide needed insight into the mechanism of AgNP-mediated inhibition of viral entry. These data would also shed light on possible methods of AgNP administration as an antiviral agent.

Different viral VACV strains have demonstrated varying levels of dependence on macropinocytosis for entry into the host cell (5, 28). Using a strain that primarily accomplishes entry via direct fusion, one could more accurately determine the ability of AgNPs to prevent this method of viral entry. Conversely, strains that primarily utilize

macropinocytosis for entry into the host cell could be used to expand upon the research in this dissertation and further explore factors impacting AgNP inhibition of macropinocytosis dependent fusion such as AgNP dose, size, shape, and time of exposure.

Examining other viral species' susceptibility to AgNP-mediated inhibition of entry would also be beneficial for the intermediate investigation term. A particularly interesting virus system to examine AgNP antiviral activity would be the human pathogens of the *Mastadenovirus* genus, including the respiratory pathogens of *Human adenovirus C*. Unlike, the viruses in the literature that previously demonstrated susceptibility to AgNPs, Adenoviruses do not have a lipid membrane, or envelope. A result of Adenovirus inhibition would lend support to the broad-spectrum antiviral activity of AgNPs as well as be the first such study of nanotechnology to prevent Adenoviral infection. Other viral species could also be screened via the assay described in Chapter III. By inserting the glycoproteins of other viruses into the HIV-1 vector system a broad range of viral species could be simulated in a Biosafety-Level 2 condition, such as biodefense threat viruses *Lassa virus* and *Ebola virus*, both of which have no approved antiviral treatment strategies. Each of these studies would also be the first of their kind to test a nanotechnology-based antiviral agent with each respective virus.

Further exploration into the time point of AgNP exposure, with respect to the infection time point, and resulting antiviral effects is also warranted during the intermediate investigation. In Chapter IV, AgNPs added after infection were capable of inhibiting viral replication as measured by standard plaque assay. AgNPs could possibly

mediate other antiviral activities associated with the multiple stages of viral replication post entry. These replication effects could pertain to, but are not limited to, genetic replication, viral morphogenesis and viral exit from the host cell. Finding additional mechanisms of AgNP antiviral activity during these processes would justify continued development of AgNPs as a novel broad-spectrum antiviral agent.

After examining AgNP antiviral activity in multiple viral species *in vitro*, significant data would exist to justify an *in vivo* approach to examining antiviral activity and cytotoxicity in the long term investigations. Very little data exist concerning AgNP toxicity *in vivo*. Generating a series of data concerning AgNP dose tolerance, delivery method, size effects and functionalization, such as targeting specific organs or increasing bioavailablity through surface modifications of the AgNPs, would be essential steps in exploring the potential use of AgNPs as antiviral agents. Additionally, there are no studies available concerning the antiviral potential of any nanotechnology *in vivo*. A mouse model would support a number of different viral infections and there are a numerous reagents designed specifically for such studies. Such a model would also be beneficial in determining the optimal method of AgNP delivery to prevent or treat viral infections.

Due to the antiviral activity observed here and in the literature, AgNPs represent a novel class of broad-spectrum antiviral agents. AgNPs would have many benefits compared to other antiviral agents because they are a hearty metal and because of their broad-spectrum antiviral activity. Since AgNP antiviral activity occurred at non-cytotoxic concentrations, AgNPs would be further advantageous over current, toxic broad-spectrum antivirals. With the methods for the accurate production and screening of nanomaterials

also detailed within this manuscript, other nanoparticles can be quickly and accurately screened for antiviral activity. All together this work suggests that AgNPs, and potentially other nanomaterials, have a unique potential as a broad-spectrum antiviral agents and therapeutics.

REFERENCES

1. **Asharani, P. V., M. P. Hande, and S. Valiyaveettil.** 2009. Anti-proliferative activity of silver nanoparticles. BMC Cell Biol. **10:**65. doi: 10.1186/1471-2121-10-65.

2. **Barber, P. R., B. Vojnovic, J. Kelly, C. R. Mayes, P. Boulton, M. Woodcock, and M. C. Joiner.** 2001. Automated counting of mammalian cell colonies. Phys. Med. Biol. **46:**63-76.

3. **Bhattacharya, R., and P. Mukherjee.** 2008. Biological properties of "naked" metal nanoparticles. Adv. Drug Deliv. Rev. **60:**1289-1306. doi: 10.1016/j.addr.2008.03.013.

4. **Canamares, M. V., J. V. Garcia-Ramos, S. Sanchez-Cortes, M. Castillejo, and M. Oujja.** 2008. Comparative SERS effectiveness of silver nanoparticles prepared by different methods: a study of the enhancement factor and the interfacial properties. J. Colloid Interface Sci. **326:**103-109. doi: 10.1016/j.jcis.2008.06.052.

5. **Condit, R. C., N. Moussatche, and P. Traktman.** 2006. In a nutshell: structure and assembly of the vaccinia virion. Adv. Virus Res. **66:**31-124. doi: 10.1016/S0065-3527(06)66002-8.

6. **DiStefano, D. J., S. L. Gould, S. Munshi, and D. K. Robinson.** 1995. Titration of human-bovine rotavirus reassortants using a tetrazolium-based colorimetric end-point dilution assay. J. Virol. Methods. **55:**199-208.

7. **Elechiguerra, J. L., J. L. Burt, J. R. Morones, A. Camacho-Bragado, X. Gao, H. H. Lara, and M. J. Yacaman.** 2005. Interaction of silver nanoparticles with HIV-1. J. Nanobiotechnology. **3:**6. doi: 10.1186/1477-3155-3-6.

8. **Escors, D., and K. Breckpot.** 2010. Lentiviral vectors in gene therapy: their current status and future potential. Arch. Immunol. Ther. Exp. (Warsz). **58:**107-119. doi: 10.1007/s00005-010-0063-4.

9. **Evanoff, D. D.,Jr, and G. Chumanov.** 2005. Synthesis and optical properties of silver nanoparticles and arrays. Chemphyschem. **6:**1221-1231. doi: 10.1002/cphc.200500113.

10. **Feng, S., R. Chen, J. Lin, J. Pan, G. Chen, Y. Li, M. Cheng, Z. Huang, J. Chen, and H. Zeng.** 2010. Nasopharyngeal cancer detection based on blood plasma surface-enhanced Raman spectroscopy and multivariate analysis. Biosens. Bioelectron. **25:**2414-2419. doi: 10.1016/j.bios.2010.03.033.

11. **Gorth, D. J., D. M. Rand, and T. J. Webster.** 2011. Silver nanoparticle toxicity in Drosophila: size does matter. Int. J. Nanomedicine. **6:**343-350. doi: 10.2147/IJN.S16881.

12. **Greulich, C., J. Diendorf, T. Simon, G. Eggeler, M. Epple, and M. Koller.** 2011. Uptake and intracellular distribution of silver nanoparticles in human mesenchymal stem cells. Acta Biomater. **7:**347-354. doi: 10.1016/j.actbio.2010.08.003.

13. **Hsiao, J. C., C. S. Chung, and W. Chang.** 1999. Vaccinia virus envelope D8L protein binds to cell surface chondroitin sulfate and mediates the adsorption of intracellular mature virions to cells. J. Virol. **73:**8750-8761.

14. **Huang, K. J., and D. P. Wooley.** 2005. A new cell-based assay for measuring the forward mutation rate of HIV-1. J. Virol. Methods. **124:**95-104. doi: 10.1016/j.jviromet.2004.11.010.

15. **Kahraman, M., O. Aydin, and M. Culha.** 2009. Size effect of 3D aggregates assembled from silver nanoparticles on surface-enhanced Raman scattering. Chemphyschem. **10:**537-542. doi: 10.1002/cphc.200800740.

16. **Kim, H. J., S. Lee, and J. U. Jung.** 2010. When autophagy meets viruses: a double-edged sword with functions in defense and offense. Semin. Immunopathol. **32:**323-341. doi: 10.1007/s00281-010-0226-8.

17. **Lara, H. H., N. V. Ayala-Nunez, L. Ixtepan-Turrent, and C. Rodriguez-Padilla.** 2010. Mode of antiviral action of silver nanoparticles against HIV-1. J. Nanobiotechnology. **8:**1. doi: 10.1186/1477-3155-8-1.

18. **Lu, L., R. W. Sun, R. Chen, C. K. Hui, C. M. Ho, J. M. Luk, G. K. Lau, and C. M. Che.** 2008. Silver nanoparticles inhibit hepatitis B virus replication. Antivir Ther. **13:**253-262.

19. **Lu, X., M. Rycenga, S. E. Skrabalak, B. Wiley, and Y. Xia.** 2009. Chemical synthesis of novel plasmonic nanoparticles. Annu. Rev. Phys. Chem. **60:**167-192. doi: 10.1146/annurev.physchem.040808.090434.

20. **MANSBERG, H. P.** 1957. Automatic particle and bacterial colony counter. Science. **126:**823-827.

21. **Mercer, J., and A. Helenius.** 2008. Vaccinia virus uses macropinocytosis and apoptotic mimicry to enter host cells. Science. **320:**531-535. doi: 10.1126/science.1155164.

22. **Mercer, J., M. Schelhaas, and A. Helenius.** 2010. Virus entry by endocytosis. Annu. Rev. Biochem. **79:**803-833. doi: 10.1146/annurev-biochem-060208-104626.

23. **Pabbruwe, M. B., K. Stewart, and J. B. Chaudhuri.** 2005. A comparison of colorimetric and DNA quantification assays for the assessment of meniscal fibrochondrocyte proliferation in microcarrier culture. Biotechnol. Lett. **27:**1451-1455. doi: 10.1007/s10529-005-1308-x.

24. **Pagba, C. V., S. M. Lane, H. Cho, and S. Wachsmann-Hogiu.** 2010. Direct detection of aptamer-thrombin binding via surface-enhanced Raman spectroscopy. J. Biomed. Opt. **15:**047006. doi: 10.1117/1.3465594.

25. **Pannecouque, C., D. Daelemans, and E. De Clercq.** 2008. Tetrazolium-based colorimetric assay for the detection of HIV replication inhibitors: revisited 20 years later. Nat. Protoc. **3:**427-434. doi: 10.1038/nprot.2007.517.

26. **Patel, M. I., R. Tuckerman, and Q. Dong.** 2005. A Pitfall of the 3-(4,5-dimethylthiazol-2-yl)-5(3-carboxymethonyphenol)-2-(4-sulfophenyl)-2H-tetra zolium (MTS) assay due to evaporation in wells on the edge of a 96 well plate. Biotechnol. Lett. **27:**805-808. doi: 10.1007/s10529-005-5803-x.

27. **Pavel, I., E. McCarney, A. Elkhaled, A. Morrill, K. Plaxco, and M. Moskovits.** 2008. Label-Free SERS Detection of Small Proteins Modified to Act as Bifunctional Linkers. J. Phys. Chem. C. Nanomater Interfaces. **112:**4880-4883. doi: 10.1021/jp710261y.

28. **Roberts, K. L., and G. L. Smith.** 2008. Vaccinia virus morphogenesis and dissemination. Trends Microbiol. **16:**472-479. doi: 10.1016/j.tim.2008.07.009.

29. **Rogers, J. V., C. V. Parkinson, Y. W. Choi, J. L. Speshock, and S. M. Hussain.** 2008. A Preliminary Assessment of Silver Nanoparticle Inhibition of Monkeypox Virus Plaque Formation. Nanoscale Res Lett. **3:**129. doi: 10.1007/s11671-008-9128-2.

30. **Rycenga, M., M. H. Kim, P. H. Camargo, C. Cobley, Z. Y. Li, and Y. Xia.** 2009. Surface-enhanced Raman scattering: comparison of three different molecules on single-crystal nanocubes and nanospheres of silver. J Phys Chem A. **113:**3932-3939. doi: 10.1021/jp8101817.

31. **Schelhaas, M.** 2010. Come in and take your coat off - how host cells provide endocytosis for virus entry. Cell. Microbiol. **12:**1378-1388. doi: 10.1111/j.1462-5822.2010.01510.x; 10.1111/j.1462-5822.2010.01510.x.

32. **Shen, X. S., G. Z. Wang, X. Hong, and W. Zhu.** 2009. Nanospheres of silver nanoparticles: agglomeration, surface morphology control and application as SERS substrates. Phys. Chem. Chem. Phys. **11:**7450-7454. doi: 10.1039/b904712c.

33. **Sopova, E. A., V. I. Baranov, O. A. Gankovskaia, V. F. Lavrov, and V. V. Zverev.** 2010. Effects of silver and silicon dioxide nanopowders on the development of herpesvirus infection *in vitro*. Gig. Sanit. **(4):**89-91.

34. **Speshock, J. L., R. C. Murdock, L. K. Braydich-Stolle, A. M. Schrand, and S. M. Hussain.** 2010. Interaction of silver nanoparticles with Tacaribe virus. J. Nanobiotechnology. **8:**19. doi: 10.1186/1477-3155-8-19.

35. **Stern, S. T., and T. M. Potter.** 2006. Nanotechnology Characterization Laboratory, Method GTA-1 and GTA-2, Version 1.0. Nanotechnology Characterization Laboratory, National Cancer Institute. .

36. **Tonini, T., P. P. Claudio, A. Giordano, and G. Romano.** 2004. Determination of functional viral titer by drug-resistance colony assay, expression of green fluorescent protein, and beta-galactoside staining. Methods Mol. Biol. **285:**149-153. doi: 10.1385/1-59259-822-6:149.

37. **Trefry, J. C., J. L. Monahan, K. M. Weaver, A. J. Meyerhoefer, M. M. Markopolous, Z. S. Arnold, D. P. Wooley, and I. E. Pavel.** 2010. Size selection and concentration of silver nanoparticles by tangential flow ultrafiltration for SERS-based biosensors. J. Am. Chem. Soc. **132:**10970-10972. doi: 10.1021/ja103809c.